Stress disrupts engram ensembles in lateral amygdala to generalize threat memory in mice

Lesuis, S.L.; Park, S.; Hoorn, A.; Rashid, A.J.; Mocle, A.J.; Salter, E.W.; ... ; Josselyn, S.A.

Cell

Article

Stress disrupts engram ensembles in lateral amygdala to generalize threat memory in mice

Graphical abstract

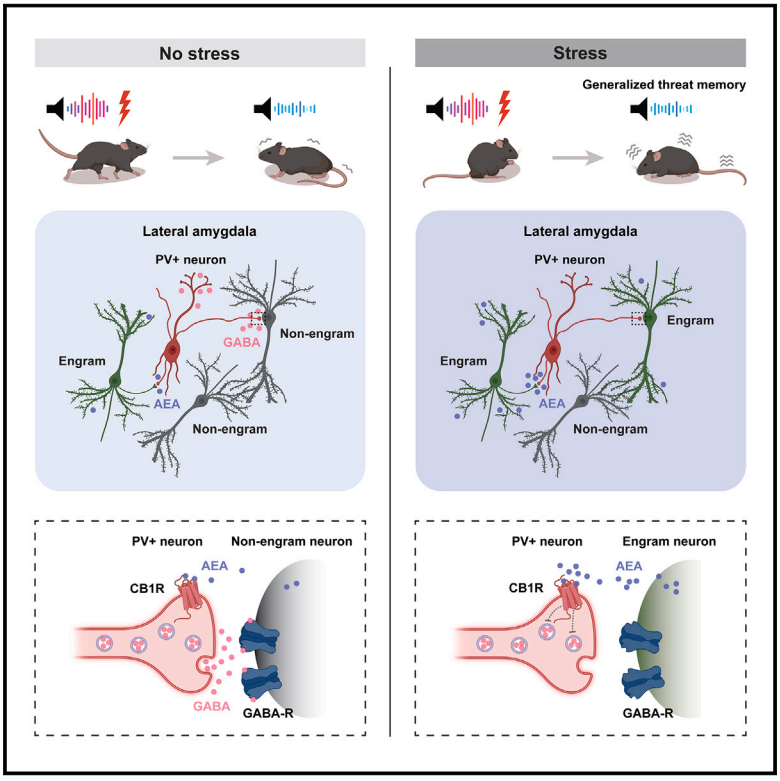

Highlights

- Stress generalizes threat memory and enlarges engram in lateral amygdala (LA)
- Memory specificity and engram sparsity restored by increasing LA PV+ activity
- Memory specificity and engram sparsity restored by CB1R KD in LA PV+ neurons
- Stress increases engram density by disrupting GABA release from PV+ neurons by eCBs

Authors

Sylvie L. Lesuis, Sungmo Park, Annelies Hoorn, ..., Paul W. Frankland, Matthew N. Hill, Sheena A. Josselyn

Correspondence

paul.frankland@sickkids.ca (P.W.F.), mnhill@ucalgary.ca (M.N.H.), sheena.josselyn@sickkids.ca (S.A.J.)

In brief

Stress induces threat memory generalization in mice by expanding the engram ensemble in the lateral amygdala via retrograde endocannabinoid signaling on parvalbumin-positive interneurons.

Lesuis et al., 2025, Cell *188*, 121–140
January 9, 2025
https://doi.org/10.1016/j.cell.2024.10.034

CellPress

Cell

CellPress

Article

Stress disrupts engram ensembles in lateral amygdala to generalize threat memory in mice

Sylvie L. Lesuis,[1,2] Sungmo Park,[1] Annelies Hoorn,[1,3] Asim J. Rashid,[1] Andrew J. Mocle,[1,3] Eric W. Salter,[3,4] Stefan Vislavski,[1] Madison T. Gray,[1,5] Angelica M. Torelli,[1] Antonietta DeCristofaro,[1] Wouter P.F. Driever,[6] Mario van der Stelt,[6] Larry S. Zweifel,[7,8] Graham L. Collingridge,[3,4] Julie L. Lefebvre,[1,5] Brandon J. Walters,[9] Paul W. Frankland,[1,3,10,*] Matthew N. Hill,[11,*] and Sheena A. Josselyn[1,3,10,12,*]

[1]Program in Neurosciences & Mental Health, Hospital for Sick Children, 555 University Ave., Toronto, ON M5G 1X8, Canada
[2]Cellular and Computational Neuroscience, Swammerdam Institute for Life Science, Amsterdam Neuroscience, University of Amsterdam, 1090 GE Amsterdam, the Netherlands
[3]Department of Physiology, University of Toronto, Toronto, ON M5S 1A8, Canada
[4]Lunenfeld-Tanenbaum Research Institute, Mount Sinai Hospital, and TANZ Centre for Research in Neurodegenerative Diseases, 600 University Avenue, Toronto, ON M5G 1X5, Canada
[5]Department of Molecular Genetics, University of Toronto, Toronto, ON, Canada
[6]Department of Molecular Physiology, Leiden Institute of Chemistry, Leiden University and Oncode Institute, Einsteinweg 55, Leiden 2333 CC, the Netherlands
[7]Department of Pharmacology, University of Washington, Seattle, WA 98195, USA
[8]Department of Psychiatry and Behavioral Sciences, University of Washington, 2815 Eastlake Ave E Suite 200, Seattle, WA 98102, USA
[9]Department of Cell and Systems Biology, University of Toronto Mississauga, 3359 Mississauga Rd, Mississauga, ON L5L 1C6, Canada
[10]Department of Psychology, University of Toronto, Toronto, ON M5S 1A8, Canada
[11]Hotchkiss Brain Institute, University of Calgary, 2500 University Drive NW, Calgary, AB T2N 1N4, Canada
[12]Lead contact
*Correspondence: paul.frankland@sickkids.ca (P.W.F.), mnhill@ucalgary.ca (M.N.H.), sheena.josselyn@sickkids.ca (S.A.J.)
https://doi.org/10.1016/j.cell.2024.10.034

SUMMARY

Stress induces aversive memory overgeneralization, a hallmark of many psychiatric disorders. Memories are encoded by a sparse ensemble of neurons active during an event (an engram ensemble). We examined the molecular and circuit processes mediating stress-induced threat memory overgeneralization in mice. Stress, acting via corticosterone, increased the density of engram ensembles supporting a threat memory in lateral amygdala, and this engram ensemble was reactivated by both specific and non-specific retrieval cues (generalized threat memory). Furthermore, we identified a critical role for endocannabinoids, acting retrogradely on parvalbumin-positive (PV+) lateral amygdala interneurons in the formation of a less-sparse engram and memory generalization induced by stress. Glucocorticoid receptor antagonists, endocannabinoid synthesis inhibitors, increasing PV+ neuronal activity, and knocking down cannabinoid receptors in lateral amygdala PV+ neurons restored threat memory specificity and a sparse engram in stressed mice. These findings offer insights into stress-induced memory alterations, providing potential therapeutic avenues for stress-related disorders.

INTRODUCTION

An animal foraging for food is attacked by a predator in a particular location. As the location of the attack could be near the predator's den, it might benefit that foraging animal to avoid that particular location, as well as any nearby, when foraging the next day. However, it would be detrimental if the animal were to stop foraging entirely. This vignette illustrates how a specific memory helps animals make effective decisions, but how overgeneralizing a specific memory might be disadvantageous. Inappropriately overgeneralized threat memories, in which there is a failure to discriminate dangerous from safe stimuli, are a hallmark of several psychiatric disorders, including post-traumatic stress disorder (PTSD) and generalized anxiety disorder.[1,2]

Stress is defined as any stimulus that presents a challenge to homeostasis and risks the well-being of an animal. Stress has been implicated in the genesis of PTSD[3,4] and induces threat memory generalization.[5,6] Therefore, understanding how stress promotes threat memory generalization remains an important, and unanswered, question.

Memories for events, including threatening events, are encoded by ensembles of principal neurons active during the event, termed a memory trace or engram ensemble.[7–10] Memory retrieval is initiated by an appropriate external sensory cue that was present at the time of the event or a relevant internal retrieval

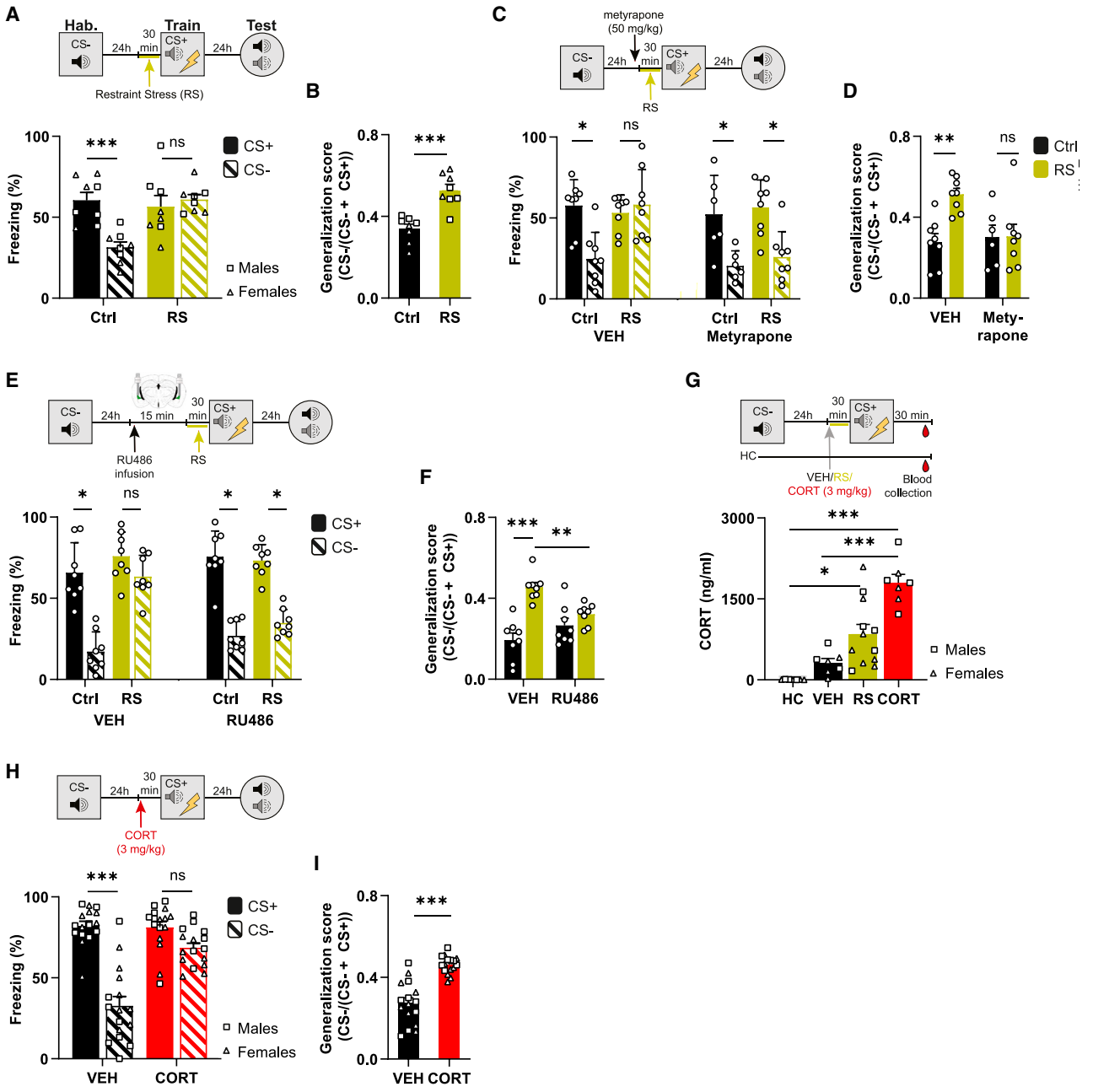

Figure 1. Threat memory generalization induced by acute RS and systemic corticosterone (CORT) administration

(A and B) (A) Threat discrimination paradigm: CS+ (7.5 kHz pips) but not CS− (2.8 kHz pure tone) paired with foot shock during training. Control mice showed specific memory (CS+ freezing > CS− freezing), while mice restraint stressed (RS) for 30 min immediately before training showed generalized memory (CS+ freezing = CS− freezing) (ANOVA, tone × RS interaction, $F[1,14] = 13.03$, $p < 0.01$) (B) and higher generalization score (CS−/[CS− + CS+]) ($F[1,14] = 26.94$, $p < 0.0001$).

(C and D) (C) Systemic injection of the corticosterone (CORT) synthesis inhibitor metyrapone (50 mg/kg, i.p.) but not vehicle (VEH) 30 min before RS restored memory specificity in RS mice (RS × metyrapone × tone interaction: $F[1,26] = 4.86$, $p = 0.03$) (D) and generalization score (RS × metyrapone interaction: $F[1,26] = 5.79$, $p = 0.02$).

(E and F) (E) Intra-lateral amygdala (LA) microinjection of glucocorticoid receptor antagonist RU486 (100 ng) but not vehicle (VEH) 30 min before RS restored memory specificity in RS mice (RS × RU486, $F[1,28] = 14.62$, $p < 0.0001$) (F) and generalization score ($F[1,28] = 12.67$, $p < 0.001$).

(G) RS and CORT (3 mg/kg, i.p.) but not vehicle (VEH) before training increased plasma CORT levels relative to home cage (HC) control mice ($F[4,38] = 22.11$, $p < 0.0001$) in both male (square) and female (circle) mice.

(legend continued on next page)

cue reactivating neurons in the engram ensemble ("engram ensemble neurons").[11–13] Consistent with computational theories,[14] an engram ensemble is sparsely encoded such that not all excitatory neurons become part of any one engram ensemble. In this way, the formation of a sparse engram ensemble requires two potentially separable processes (neuronal inclusion and neuronal exclusion[15]). First, excitatory principal neurons are allocated to an engram ensemble through a competitive process, with relatively more excitable neurons tending to "win" the competition to be included as part of the engram ensemble.[16–21] Second, engram sparsity is maintained by actively excluding "non-winning" less excitable neurons from the engram ensemble.[16,20–22]

The overall size (number of excitatory member neurons[23]) and corresponding sparsity of an engram ensemble in a given brain region is remarkably constant across types of memory[24–26] and independent of memory strength.[22,27] However, the size of an engram can be increased and sparsity correspondingly decreased by disrupting the function of inhibitory neurons, particularly parvalbumin-positive (PV+) neurons, during the training event.[16,20–23] For instance, disrupting PV+ neuronal function in the CA1 region of the dorsal hippocampus during contextual threat training induced a dense engram, likely by disrupting the neuronal exclusion process of engram ensemble formation.[23] Moreover, these mice with a dense engram ensemble showed a generalized, rather than a specific, threat memory.[23] As stress induces threat memory generalization,[28–30] and a generalized memory may be supported by dense engram ensembles, we hypothesized that stress mediates threat memory generalization by increasing the size of an engram ensemble via an unknown mechanism.

Here, we used a variety of tools and found that stress, via the recruitment of retrograde endocannabinoid (eCB) signaling at inhibitory PV+ neurons, reduced the sparsity of the engram ensemble. This occurred by disrupting the neuronal exclusion process in a key brain region, the lateral nucleus of the amygdala (LA). This denser LA engram ensemble supported a generalized threat memory. Specific threat memory and a sparse engram were restored in stressed mice by antagonizing LA glucocorticoid receptors, inhibiting LA eCB synthesis, increasing the activity of LA PV+ neurons, or knocking down cannabinoid receptors specifically on LA PV+ neurons. These effects were specific to PV+ neurons in the LA, as similar manipulation of LA somatostatin-positive (SST+) neurons did not restore memory specificity in stressed mice. The current findings agree with previous data implicating eCBs in mediating the effects of stress on rodent behavior, including enhancing aversive memory consolidation.[31,32] In addition, the current findings provide a local circuit basis for these previous observations. The present data increase our understanding of how stress, via eCBs, impacts memory at the circuit level and may provide potential avenues for therapeutic interventions in stress-related disorders.

RESULTS

Acute stress increases threat memory generalization

To examine the effects of acute stress on threat memory generalization, we restraint-stressed (RS) mice for 30 min before training in a threat discrimination task in which one tone (CS+) was paired with a foot shock, while another tone (CS−) was not. Control mice (Ctrl) showed precise threat memory, exhibiting high levels of defensive freezing to the CS+ but not the CS− stimulus during the test. By contrast, RS mice froze at equally high levels to the CS+ and CS− (Figures 1A and 1B), failing to discriminate dangerous from safe stimuli, thus showing threat memory generalization.

Acute stress induces changes throughout the body and brain, including release of glucocorticoid hormones (cortisol in humans, corticosterone [CORT] in rodents) from the adrenal cortex into circulation.[33–35] Glucocorticoids are implicated in threat memory consolidation.[36–38] To investigate whether glucocorticoid signaling also played a critical role in the observed RS-induced threat memory generalization, we systemically injected RS and Ctrl mice with the glucocorticoid synthesis inhibitor metyrapone (50 mg/kg, i.p.) 30 min before CS+-US training (immediately before RS). Metyrapone restored threat memory specificity in RS mice while having no effect in Ctrl mice (Figures 1C and 1D), indicating the involvement of glucocorticoids in RS-induced threat memory generalization. Glucocorticoid receptors are widely distributed throughout the brain[34,39–41] and are particularly abundant in the LA, a brain region crucial for threat memory.[42–45] We found that microinjecting a glucocorticoid receptor antagonist (RU 486; mifepristone; 100 ng) directly into the LA 30 min before CS+-US threat training (immediately before RS) similarly restored memory specificity in RS mice while having no effect in Ctrl mice (Figures 1E and 1F), specifically implicating LA glucocorticoid receptors in threat memory generalization.

We next examined whether RS before threat training increased circulating levels of CORT. Consistent with previous results,[38] we observed increased plasma CORT levels in both male and female threat-conditioned mice compared with home-cage (HC) controls. Moreover, both RS and systemic injection of CORT itself (3 mg/kg, i.p.) before threat conditioning further increased plasma CORT levels to a similarly high level (Figure 1G). Finally, we asked whether systemic injection of CORT alone before threat conditioning would induce threat memory generalization similar to RS. Because CORT has been reported to induce an "inverted U-shaped" dose-response curve on threat memory consolidation,[46] we first assessed the effects on threat generalization of a range of CORT doses (0.5–10 mg/kg, i.p.) administered 30 min before training. CORT-induced threat memory generalization in male and female mice at doses ranging from 1–10 mg/kg, but the dose that induced threat memory generalization most robustly and specifically was 3 mg/kg (Figures 1H, 1I, and S1A). Importantly, this dose of CORT-induced freezing in our threat memory generalization

(H and I) (H) Similar to RS, CORT (3 mg/kg, i.p.) induced threat memory generalization (tone × CORT, $F[1,30] = 30.36$, $p < 0.0001$) (I) and increased generalization score ($F[1,30] = 44.10$, $p < 0.0001$). Data are presented as mean + SEM. $^{*}p < 0.05$, $^{**}p < 0.01$, $^{***}p < 0.001$.
See also Figure S1.

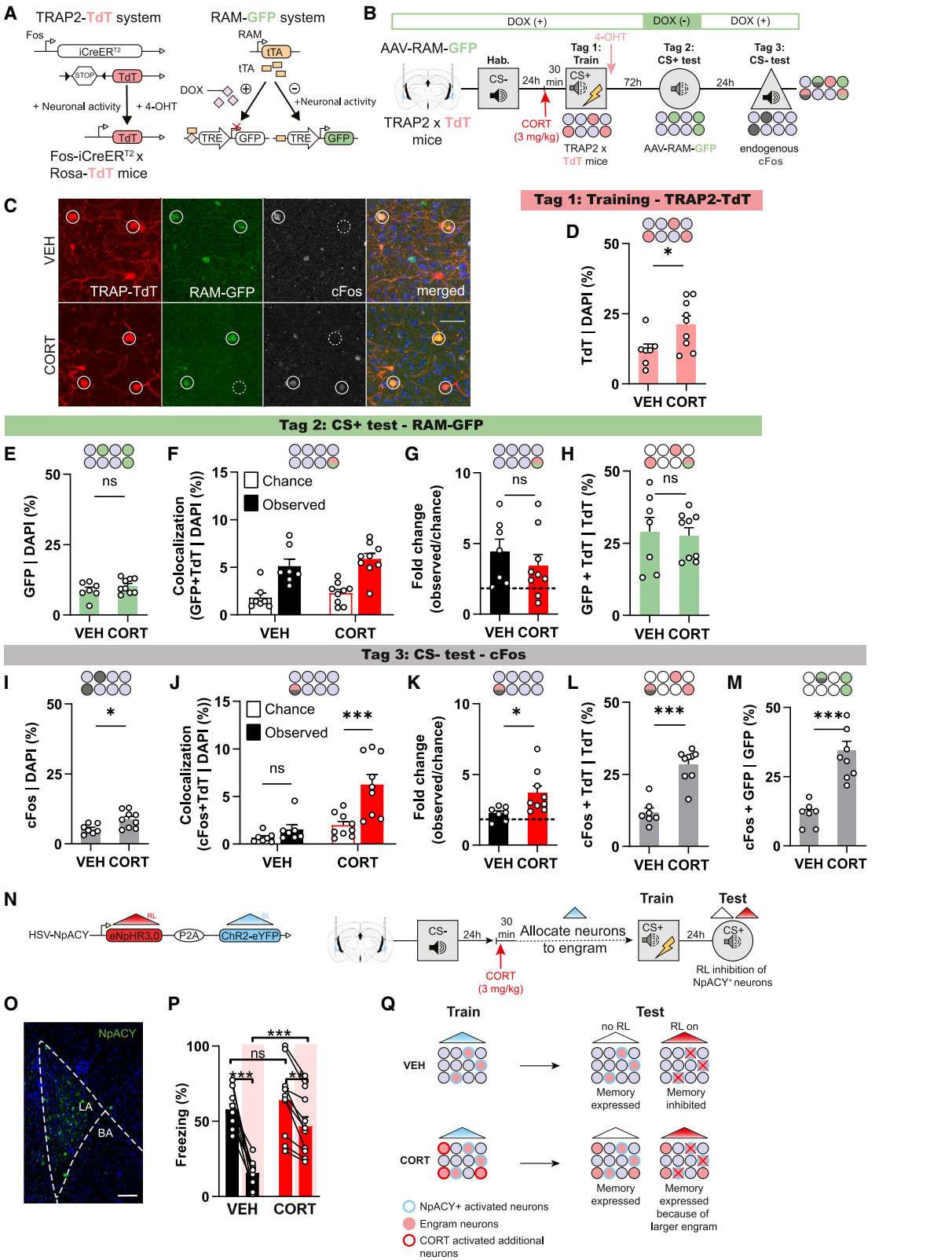

(legend on next page)

test only to CS− stimuli that were close in perceptual space to the CS+ stimulus (Figure S1B) and did not induce freezing if the foot shock was omitted during training (Figure S1C), highlighting the specificity of this finding. As these data showed that CORT is both necessary and sufficient for threat memory generalization, we used systemic CORT (3 mg/kg, i.p.) injection in further studies investigating the molecular and local circuits mediating threat memory generalization.

Systemic CORT injection increases the overall size of the LA engram ensemble, supporting a threat memory

Sparse neuronal engram ensembles are reported to support specific memories, while less-sparse engram ensembles support more generalized memories.[23] Therefore, we investigated the effects of exogenous CORT injection on the size of the LA engram ensemble formed by threat training and the reactivation of this engram ensemble by both the CS+ and CS− stimuli during memory testing. We visualized (1) the LA excitatory (principal) neurons active during training (engram ensemble), (2) neurons active during CS+ test (neurons active during specific memory test), and (3) neurons active during CS− test (neurons active during generalized memory test) in the same mouse using a triple "neuronal activity tagging" technique. Neurons active during threat training were tagged using the targeted recombination in active populations 2 (TRAP2) system[47] to express TdTomato (TdT) (Figures 2A–2C). Neurons active during the CS+ memory test were tagged using the robust activity marker (RAM) system[48] to express GFP (Figures 2A–2C), while neurons active during CS− test were visualized using an antibody against endogenous cFos protein (Figures 2B and 2C).

During training, CORT increased the number of tagged engram ensemble neurons (TdT+) relative to vehicle (VEH) (Figure 2D). By contrast, during the specific CS+ memory test, administration of CORT before training did not change the number of active neurons (GFP+) (Figure 2E) or the high level of engram ensemble reactivation (neurons active at both training and CS+ test compared with chance levels of two neurons being active given their abundance in the overall population (*observed*: [GFP+ + TdT+]/DAPI+ × 100 vs. *chance*: [GFP+/DAPI+] × [TdT+/DAPI+] × 100) (Figures 2F–2H). During the generalized CS− memory test, though, VEH mice showed very few active neurons (cFos+), low engram ensemble reactivation, and low reactivation of the CS+ ensemble. However, CORT mice showed a high number of active neurons during the CS− test, as well as high reactivation of the training engram and CS+ ensembles (Figures 2I–2M). This pattern of results was also observed in a similar experiment in which the order of the different tagging methods was varied (Figures S1D–S1G) but was not observed in an experiment in which neurons were similarly tagged but the foot shock omitted during training (Figures S1H–S1K). Together, these findings indicate that the LA engram ensemble formed in VEH-treated mice is sparse and reactivated specifically by the CS+ but not the CS− stimulus, while the LA engram ensemble formed in CORT-treated mice is larger (less sparse) and reactivated by both the specific (CS+) and the non-specific (CS−) retrieval cue. Importantly, similar to CORT, RS before threat conditioning also increased the size of the LA engram ensemble and the high level of engram ensemble reactivation by the CS− retrieval cue (Figures S1L–S1O), showing similar effects between acute stress and systemic CORT administration at the level of the LA engram.

To determine how CORT induced a larger LA engram ensemble, we next examined whether CORT impacted the two stages of engram ensemble formation (allocation and inclusion of highly excited principal neurons and exclusion of less excited principal neurons). To this end, we used an all-optical allocate-and-silence approach to visualize and manipulate neurons in an engram ensemble. This approach takes advantage of a viral vector (HSV-NpACY) to express both a blue light (BL)-sensitive excitatory opsin (ChR2(H134R)) and a red light (RL)-sensitive inhibitory

Figure 2. Systemic CORT administration induces threat memory generalization by increasing the size of an LA engram ensemble

(A) (Left) TRAP2 activity tagging system. Tdtomato (TdT) expressed in active neurons after 4-hydroxytamoxifen (4-OHT) treatment. (Right) RAM activity tagging system. GFP expressed in active neurons after doxycycline (DOX) withdrawal.

(B and C) Experimental design to examine neurons active during training (TdT, red), CS+ test (GFP, green), and CS− test (cFos, gray) in same mouse. Scale bar, 25 μm. CORT (3 mg/kg, i.p.).

(D–H) (D) CORT increased number of active neurons during training relative to vehicle (VEH) ($F[1,14] = 5.95$, $p < 0.05$) but had no effect on (E) number of neurons active during CS+ test ($F[1,14] = 1.35$, $p > 0.05$) or (F) observed percent neurons active during training (engram ensemble) reactivated during CS+ test (engram reactivation; RAM+ + TdT+|DAPI) ($F[1,28] = 0.73$, $p > 0.05$), which was higher than chance colocalization probability for RAM+ and TdT+ neurons given overall population levels of each marker (RAM+|DAPI × TdT+|DAPI) in both CORT and VEH mice, or (G) fold-change in engram reactivation ($F[1,14] = 0.74$, $p > 0.05$), or (H) likelihood that a neuron active during training is also active during CS+ test ([RAM +TdT+]/TdT+) ($F[1,14] = 0.13$, $p > 0.05$).

(I–M) (I) CORT increased number of neurons active during CS− test ($F[1,14] = 7.18$, $p < 0.05$), (J) engram reactivation as indicated by higher than chance co-localization of cFos+ and TdT+ neurons (CORT × observed interaction: $F[1,28] = 6.22$, $p < 0.05$), (K) fold-change in engram reactivation ($F[1,14] = 6.15$, $p < 0.05$), (L) likelihood that a neuron active during training is also active during CS− test ($F[1,14] = 43.16$, $p < 0.001$), (M) and likelihood that a neuron active during CS+ test is also active during CS− test ($t[1,14] = 31.47$, $p < 0.05$).

(N) Viral vector (HSV-NpACY) to excite (ChR2, blue light, BL) and inhibit (NpHR3.0, red light, RL) same small population of LA excitatory neurons. All mice received BL before training to excite NpACY+ neurons and bias their allocation and inclusion to engram ensemble. To test whether these neurons were allocated to the engram, NpACY+ neurons were inhibited with RL during CS+ test.

(O) NpACY expression in sparse population of excitatory neurons. Scale bar, 120 μm.

(P) During CS+ test, RL+ decreased freezing to a greater extent in VEH than CORT mice (CORT × RL interaction, $F[1,18] = 17.63$, $p < 0.001$).

(Q) Schematic of neuronal allocation to engram ensemble with and without CORT to examine two processes of engram formation (allocation and inclusion of highly excited neurons and exclusion of non-highly excited neurons). In both groups, RL inhibition of NpACY+ neurons excited by BL before training decreased freezing, suggesting engram inclusion process intact. However, CORT mice showed higher freezing during RL inhibition, suggesting the engram exclusion process was disrupted as additional non-NpACY+ neurons were included in the engram. Data are presented as mean + SEM. $^{*}p < 0.05$, $^{**}p < 0.01$, $^{***}p < 0.001$. See also Figure S1.

opsin (eNpHR3.0) in the same random sparse population of principal LA neurons.[49,50] Mice expressing NpACY were systemically injected with CORT or VEH 30 min before training as above. Immediately before training, we photostimulated NpACY+ neurons with BL (ChR2) to increase the excitability and bias the allocation of these NpACY+ neurons to the engram ensemble, supporting the threat memory.[23,51,52] To examine whether these highly excited principal neurons were indeed allocated to the engram ensemble, supporting this threat memory, we tested memory retrieval both in the presence and absence of RL inhibition (eNpHR3.0) of NpACY+ neurons (Figures 2N and 2O).

In the memory test, silencing NpACY+ neurons robustly decreased freezing to the CS+ in VEH mice (Figure 2P), showing that this sparse population of NpACY+ neurons experimentally excited before training became critical components of the engram ensemble supporting the threat memory. In CORT mice, silencing NpACY+ neurons also decreased CS+ freezing but did so to a much smaller extent than in VEH mice. These results suggest that (1) NpACY+ neurons experimentally excited before training did become part of the engram ensemble in CORT-treated mice but that (2) additional non-experimentally excited (NpACY−) neurons were also included in the engram ensemble and supported freezing during RL inhibition of NpACY+ neurons. This result is consistent with the above finding that CORT mice showed a larger, less-sparse engram ensemble. That inhibiting NpACY+ neurons in CORT mice produced a much smaller decrease in freezing than in VEH mice, and the larger engram observed in CORT mice suggests that CORT disrupted the second process of engram ensemble formation, that of excluding non-winning neurons (Figure 2Q).

CORT decreases the activity of LA PV+ inhibitory neurons during threat conditioning

PV+ neurons comprise roughly 17%–20% of all interneurons in the LA and play a key role in maintaining the sparsity of an engram ensemble by excluding non-winning neurons.[16,20–23] To examine whether CORT induced a larger engram ensemble by disrupting the activity of LA PV+ neurons during threat conditioning, we used fiber photometry to assess LA PV+ neuronal activity in PV-Cre mice expressing the genetically-encoded calcium indicator GCaMP7f (Figures 3A and 3B). Foot shock increased GCaMP7f fluorescence in PV+ neurons during training in VEH mice, but this response was blunted in CORT mice (Figures 3D–3F), indicating CORT indeed disrupted PV+ neuronal activity during training. In a separate group of mice expressing GCaMP7f in excitatory (αCaMKII+) LA neurons, foot shock induced a greater increase in fluorescence in CORT mice than VEH mice (Figures 3C and 3G–3I), indicating that CORT increased the activity of excitatory principal neurons. Similar findings were observed in single mice expressing two different calcium indicators (GCaMP7f and RCaMP1a) in these two neuronal populations (Figures S2A–S2H). Importantly, CORT did not change the activity of either PV+ or αCaMKII+ neurons in the absence of threat conditioning (Figures S2I–S2K). Although SST+ neurons are the second most abundant type of interneuron in the LA, comprising roughly 10%–15% of all interneurons in the LA,[53,54] CORT did not blunt the activity of SST+ neurons during training when we similarly expressed GCAMP7f in the LA of SST-Cre mice (Figure S7D). Together, these findings are consistent with the hypothesis that during threat training, CORT specifically decreased the activity of LA PV+ neurons, inducing a consequent increase in activity of LA excitatory neurons, resulting in a larger, less-sparse engram that supported a generalized threat memory.

To determine the causal role of decreased LA PV+ neuronal activity during training in mediating the effects of CORT on generalized threat memory, we expressed either Gq- or Gi-coupled designer receptor exclusively activated by designer drugs (DREADD) receptors (hM3Dq and hM4Di, respectively) in LA PV+ neurons of PV-Cre mice (Figures 3J and S3A). CORT mice expressing the excitatory DREADD receptor (hM3Dq) and injected with the DREADD ligand C21 before training showed specific, rather than generalized, threat memory (Figures 3K and S3B–S3D). Moreover, inhibiting the activity of PV+ neurons during training (activation of hM4Di by C21) produced a generalized memory in VEH mice, similar to the effects normally observed in CORT mice. This effect was specific to PV+ neurons in the LA as activating hM3Dq in SST+ LA neurons did not affect CORT-mediated threat memory generalization (Figures S3E–S3G). Together, these results indicate CORT induces threat memory generalization by inhibiting the activity of LA PV+ neurons during training to enable a larger, less-sparse LA engram ensemble that supports a generalized, rather than specific, threat memory. Through what mechanism stress and systemic CORT disrupt LA PV+ neuronal function during threat training, though, is unclear.

Effects of stress on threat memory generalization are mediated by eCBs in the LA

Based on the following lines of evidence, we next examined the role of eCBs in stress-induced threat memory generalization. First, eCBs, through their interaction with neuronal eCB CB1 receptors (CB1Rs), are known to mediate some of the effects of stress on behavior, including memory processes.[32,55,56] Second, both CORT injection and acute stress induce a rapid release of eCBs in many brain regions, including the amygdala.[57,58] Third, CB1Rs are localized on inhibitory interneurons,[59] where eCBs act as retrograde messengers to suppress γ-aminobutyric acid (GABA) release.[60–62] Moreover, eCB signaling has been shown to disrupt GABA release specifically from PV+ neurons in, e.g., the zona incerta[63] and dorsolateral striatum.[64] Therefore, although previous studies have focused on the role of eCB signaling on cholecystokinin-expressing (CCK+) interneurons in the more basal amygdala,[60] here we probed the role of eCBs in suppressing the activity of LA PV+ neurons in mediating the effects of CORT and stress on threat memory generalization.

There are two principal eCB ligands, 2-arachidonoyl glycerol (2-AG) and anandamide (AEA). We found that both levels of 2-AG and AEA in the amygdala were increased in CORT or RS mice following threat conditioning compared with HC control mice (Figures 4A, S4A, and S4B). We probed the contribution of each eCB ligand to CORT-induced threat memory generalization using a combination of pharmacological, viral, and CRISPR-mediated knockdown manipulations. First, to examine the role of 2-AG in CORT-induced threat memory generalization, we

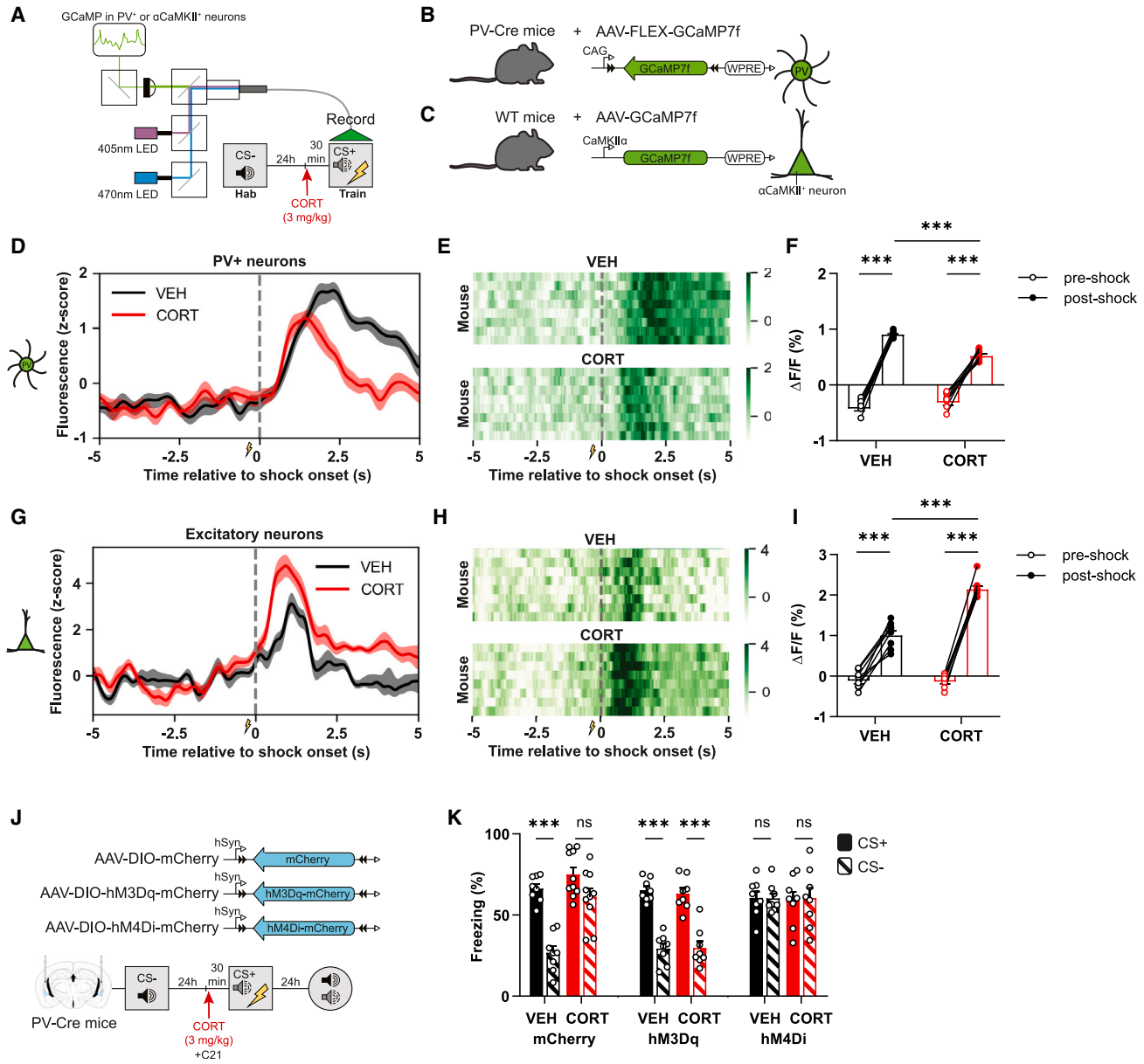

Figure 3. Systemic CORT administration induces threat memory generalization by decreasing LA PV+ neuron activity during training

(A–C) (A) Examining neuronal activity (GCaMP) during threat training via fiber photometry (B) in parvalbumin (PV+) neurons in PV-Cre mice or (C) in excitatory (αCaMKII+) neurons in wild-type (WT) mice.

(D and G) Average fluorescence (*Z* score) from (D) PV+ and (G) excitatory neurons before and after foot shock.

(E and H) Heatmaps from individual mice.

(F and I) (F) CORT blunted increase in fluorescence (Δf/f) before vs. after foot shock in PV+ neurons (CORT × pre/post-shock, $F[1,14] = 27.01$, $p < 0.0001$) (I) but potentiated increase in fluorescence in excitatory neurons (CORT × pre/post-shock, $F[1,14] = 61.38$, $p < 0.0001$).

(J and K) Activating LA PV+ neurons (hM3Dq + C21) during training restored memory specificity in CORT mice while inhibiting PV+ neurons (hM4Di + C21) during training-induced threat memory generalization in VEH mice (virus × CORT × tone, $F[2,43] = 3.22$, $p < 0.05$). Data are presented as mean + SEM. *$p < 0.05$, **$p < 0.01$, ***$p < 0.001$. CORT, corticosterone; LA, lateral amygdala; PV, parvalbumin.

See also Figures S2 and S3.

microinjected a drug to inhibit local 2-AG synthesis. 2-AG synthesis critically depends on the enzyme diacylglycerol lipase α, DAGLα.[65–67] Therefore, we microinjected the diacylglycerol lipase α inhibitor, DO34,[67] effectively decreasing 2-AG levels in the LA (Figure S4C), 15 min before administering VEH or CORT and threat conditioning mice. DO34, especially at higher doses, disrupted freezing to both CS+ and CS− in VEH and CORT mice (Figures 4C and 4D), suggesting that although LA 2-AG may be

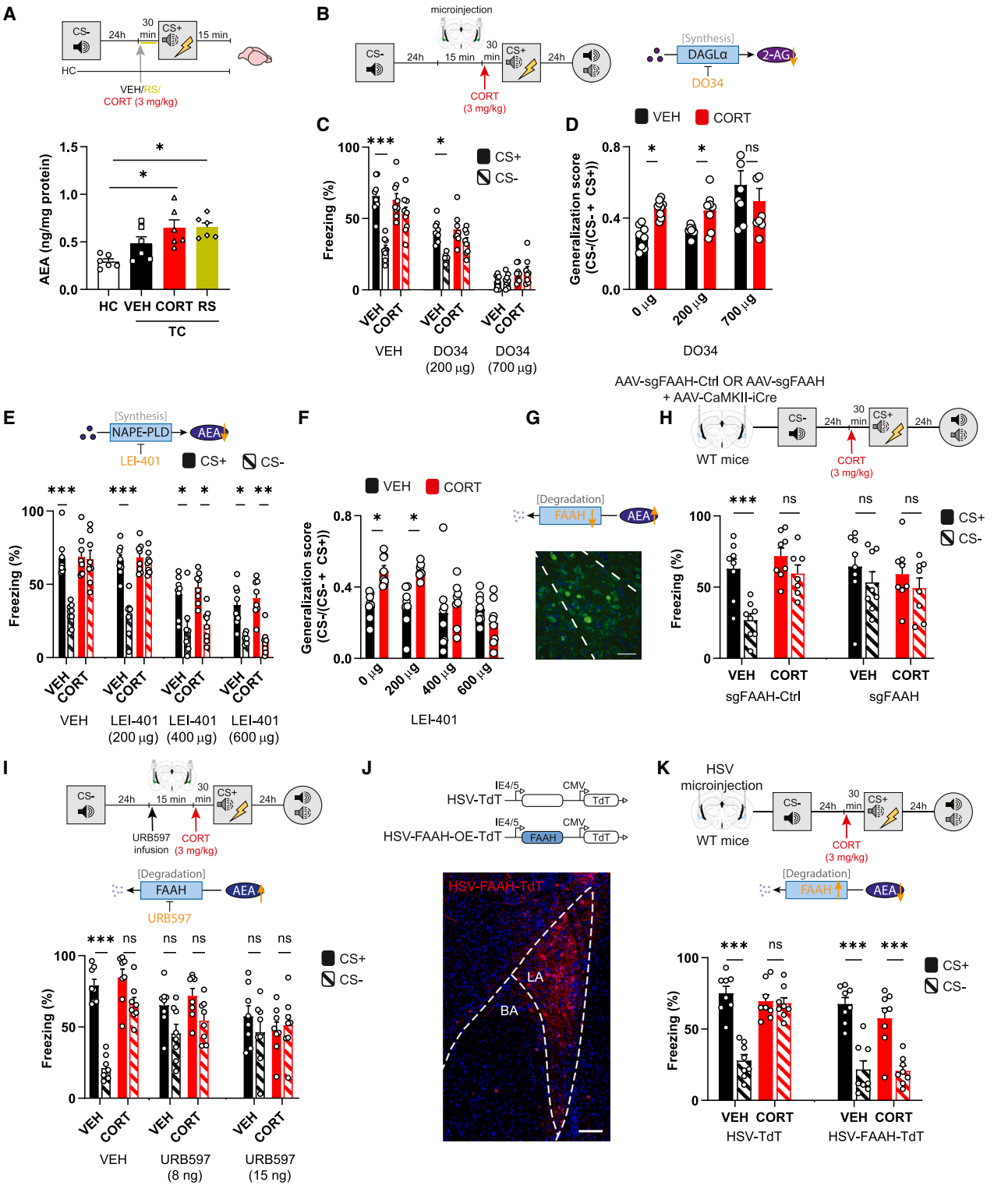

Figure 4. Restoring endocannabinoid AEA levels in the LA restores CORT-induced threat memory generalization

(A) CORT and RS increased LA AEA levels over HC controls ($F[3,20] = 7.56$, $p < 0.0001$).

(B) Examining role of LA endocannabinoid ligands, 2-AG (2-Arachidonoylglycerol) and AEA (anandamide), in mediating CORT-induced threat memory generalization.

(legend continued on next page)

important in threat memory overall, 2-AG does not play a specific role in CORT-induced threat memory generalization.

AEA synthesis depends on N-acyl phosphatidylethanolamine-specific phospholipase D (NAPE-PLD).[68] Therefore, we next decreased AEA levels in the LA by microinjecting LEI-401,[69] a drug that inhibits NAPE-PLD, thereby decreasing AEA levels (Figure S4C). LEI-401 restored memory specificity in CORT mice; CORT mice froze at high levels to the CS+ but not to the CS− (Figures 4E and 4F). Interestingly, LEI-401, microinjected into the LA or administered systemically, did not affect overall anxiety-like behavior as measured in the open field and elevated plus maze, highlighting the specificity of the effect of LEI-401 on threat memory generalization (Figures S4D–S4J).

Next, we asked whether increasing levels of AEA in the LA alone would be sufficient to induce threat memory generalization in VEH-treated mice. To functionally increase AEA levels in the LA, we disrupted the function of FAAH (fatty acid amide hydrolase[70]), an enzyme critical for AEA degradation, by using either a CRISPR-based knockdown of FAAH (AAV-SaCas9-sgFAAH[71]) or microinjecting a drug that inhibits FAAH activity (URB597[72]) (Figure S4C). Increasing LA AEA levels induced threat memory generalization in VEH mice (Figures 4G–4I) without increasing overall anxiety-like behavior as measured in the open field and elevated plus maze (Figures S4K–S4M). By contrast, viral overexpression of FAAH in excitatory neurons[19,52] to functionally decrease AEA levels in these neurons (HSV-FAAH-OE[73]), both normalized the increase in LA AEA levels observed in CORT mice after threat training (Figure S4B) and restored memory specificity (Figures 4J and 4K). Together, these data indicate that CORT-induced threat memory generalization is mediated by increased AEA levels in the LA.

Cannabinoid CB1Rs are located on LA PV+ neurons

Cannabinoid receptors 1 (CB1Rs) are the most abundant G-protein-coupled receptors in the brain[59] and are highly expressed throughout different brain areas,[74–76] including in the LA.[60] To assess whether CB1Rs are localized specifically on PV+ neurons in the LA, we used single-molecule fluorescence *in situ* hybridization (smFISH) for the gene encoding CB1Rs (*Cnr1*) (Table S1). Consistent with previous reports,[77,78] we confirmed *Cnr1* expression in several brain regions, including the basal nucleus of the amygdala, cortex, CA1, CA2, CA3, and dentate gyrus subfields of the dorsal hippocampus, as well as the LA (Figures 5A and 5B). Co-labeling of *Cnr1* with *GAD2* and *Pvalb* mRNA in the LA showed that a subset of LA *Pvalb+* and *GAD2+* neurons also expressed *Cnr1*, particularly in the anterior region of the LA (Figures 5A and 5B).

Presynaptic CB1R activation reduces the probability of neurotransmitter release from many types of neurons.[79,80] To determine whether CB1R activation similarly disrupts GABA release from LA PV+ neurons, we examined the effects of the CB1R agonist WIN55,212-2 (WIN55) on PV+ neuron synapses onto LA principal neurons using *ex vivo* slice electrophysiology. We selectively stimulated LA PV+ neurons in slices from PV-Cre mice expressing the excitatory opsin ChRmine[81] in PV+ neurons. GABA release was assessed using paired-pulse ratio (PPR) measurements from optical inhibitory postsynaptic potentials (oIPSCs) elicited by two successive optogenetic pulses (Figures 5C and 5D). In control slices (aCSF), PV+ synapses showed a low PPR, indicating a high basal probability of GABA release. By contrast, slices treated with the CB1R agonist WIN55 showed elevated PPR, suggesting that CB1R activation disrupted GABA release (Figure 5E). These results are consistent with previous research showing CB1R activation decreases the probability of neurotransmitter release[82] and extends these findings to include LA PV+ neurons. Although we did not measure the effects of stress or CORT on PV+ IPSCs, previous research shows reduced principal neuron inhibition following CORT treatment in the basolateral complex of the amygdala.[44]

We next asked whether CORT increased eCB binding on LA PV+ neurons during threat training by expressing the genetically-encoded eCB sensor GRAB_eCB2.0[83] in LA PV+ neurons and using fiber photometry (Figures 5F–5H). We simultaneously recorded the activity of LA hSyn+ neurons using a red calcium-activity sensor, RCaMP1a. Similar to our previous findings, CORT mice showed higher foot shock-induced RCaMP1a fluorescence in LA excitatory neurons than VEH mice (Figure 5I). Moreover, in the same mice, CORT also increased foot shock-induced eCB binding on LA PV+ neurons above VEH levels (Figure 5J). The lag pattern of fluorescence cross-correlation (Figures 5K and 5L) suggested that GRAB_eCB2.0 activity in PV+ neurons occurred before (and perhaps mediated) the increase in excitatory neuron activity. Importantly, this pattern of lag cross-correlation was not observed in control mice similarly

(C and D) (C) Inhibiting 2-AG synthesis with DO34 dose-dependently decreased overall freezing levels to CS+ and CS− similarly in both VEH and CORT mice (dose × CORT: $F[2,43] = 1.69$, $p > 0.05$) and (D) did not restore CORT-induced threat memory generalization ($F[2,43] = 3.78$, $p > 0.05$, VEH-700 μg vs. CORT-700 μg: $p > 0.05$).

(E and F) (E) Inhibiting AEA synthesis with LEI-401 specifically decreased CS− freezing in CORT mice (dose × CORT × tone, $F[3,56] = 6.82$, $p < 0.001$), and (F) restored memory specificity in CORT mice (dose × CORT, $F[3, 56] = 5.02$, $p < 0.01$).

(G) Expression of a short-guide RNA AAV-sgFAAH in LA excitatory (αCaMKII+) neurons to increase AEA levels by knocking down the degradation enzyme fatty acid amide hydrolase (FAAH), visualized with antibody directed against HA tag (green). DAPI, nuclei; dotted outline, LA boundary. Scale bar, 90 μm.

(H) sgFAAH (but not sgFAAH-Ctrl) induced threat memory generalization in VEH mice, similar to CORT mice with sgFAAH-Ctrl (tone × virus × CORT, $F[2,56] = 4.46$, $p < 0.05$).

(I) URB597, to inhibit FAAH and increase AEA, increased threat memory generalization in VEH mice (dose × treatment interaction: $F[2,42] = 4.36$, $p < 0.05$).

(J) Vector overexpressing FAAH (FAAH-OE) to decrease AEA levels (or control vector). Expression in LA (red). DAPI, nuclei; dotted outline, LA boundary. Scale bar, 120 μm.

(K) FAAH overexpression but not control virus restored threat memory specificity in CORT mice (CORT × virus × tone, $F[1,28] = 8.69$, $p < 0.01$). Data are presented as mean + SEM. *$p < 0.05$, **$p < 0.01$, ***$p < 0.001$. AEA, anandamide; LA, lateral amygdala; CORT, corticosterone; DO34, *; LEI-401, *; DAGLα, diacylglycerol lipase α; HC, home cage; TC, threat conditioned.

See also Figure S4.

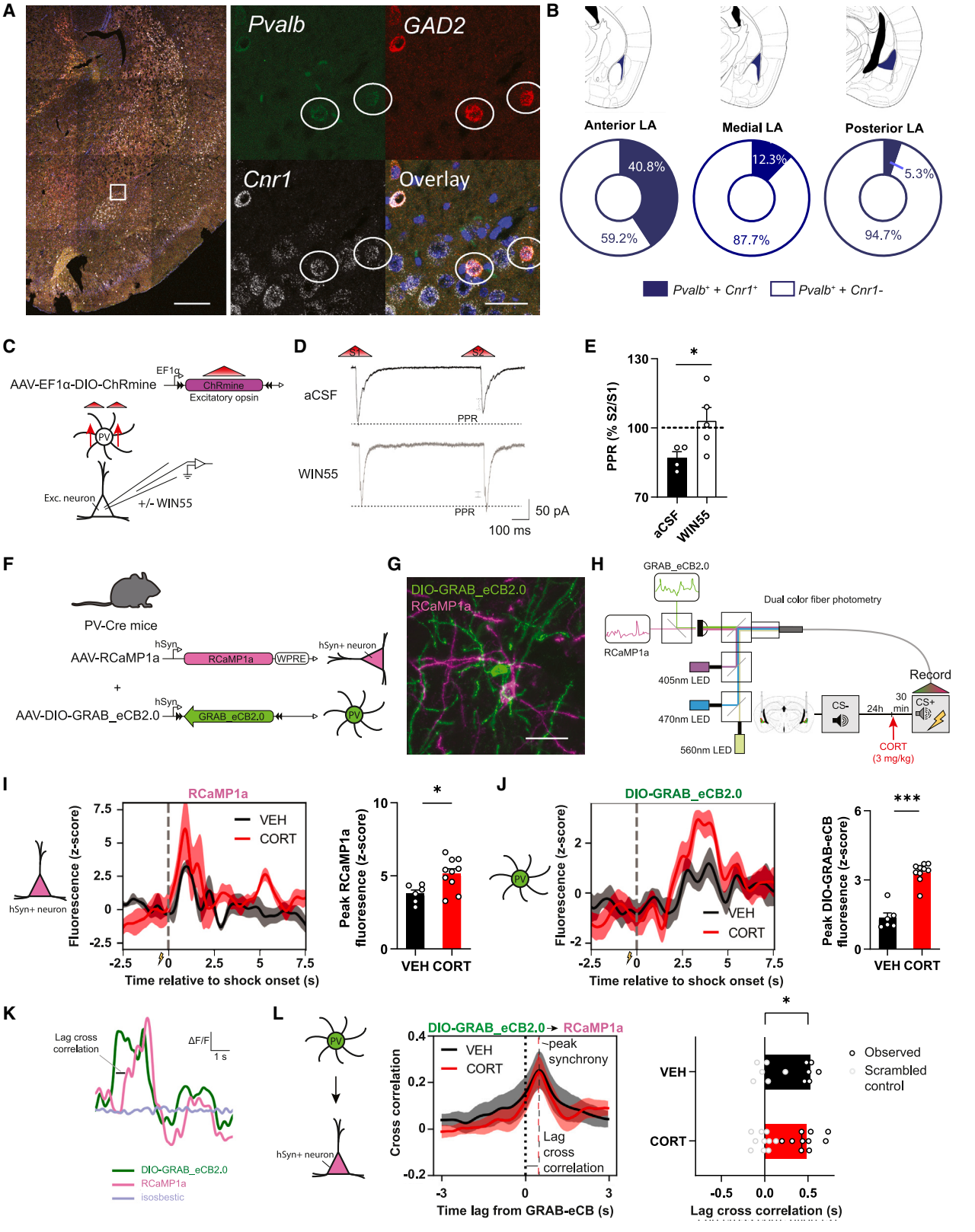

(legend on next page)

expressing a mutant form of the genetically-encoded eCB sensor (GRAB_eCBmut) that does not change fluorescence with eCB binding (Figures S5A–S5H) or in mice expressing the functional GRAB sensor (GRAB_eCB2.0) in LA excitatory neurons (Figures S5I–S5P). In additional control mice, we observed CORT alone induced a mild increase in fluorescence from the functional eCB reporter expressed in PV+ neurons (Figures S5Q–S5S), as might be expected. Together, these data are consistent with the interpretation that during threat conditioning, CORT augments eCB release in the LA, perhaps from excitatory neurons. eCBs may then retrogradely activate CB1Rs on PV+ neuronal terminals, decreasing the release of GABA onto LA principal neurons, leading to an increase in the size of the engram ensemble and threat memory generalization. In support of this hypothesis, we observed that decreasing AEA levels in LA excitatory neurons (via FAAH overexpression) failed to restore memory specificity in CORT mice when PV+ neurons were chemogenetically silenced (Figures S6A and S6B).

To directly assess whether CORT induced threat memory generalization by increasing the binding of eCB to CB1Rs on LA PV+ neurons, we developed a novel Cre-dependent CRISPR-Cas9 strategy to knockdown CB1Rs specifically in LA PV+ neurons. Our construct contained four Cre-dependent sgRNAs (DIO-sgCB1R$_{KD}$) directed against the *Cnr1* gene to knockdown CB1Rs in LA PV-Cre-expressing neurons (Figure 6A). A control construct consisted of a Cre-dependent non-targeting sgRNA (DIO-sgCB1R$_{Ctrl}$). Both knockdown and control vectors also expressed TdT. We validated this CB1R knockdown construct using several approaches. First, we assessed yellow fluorescent protein (YFP) expression from a CB1R-YFP plasmid in HEK293 cells also expressing either the knockdown or control virus along with Cas9 and iCre constructs (Figure 6B). YFP expression was observed in cells expressing the control virus but not in cells expressing the knockdown virus, along with Cas9 and iCre constructs (Figure 6C). Second, we examined postsynaptic spontaneous currents (sIPSC) in *ex vivo* slices prepared from mice expressing the knockdown or control construct in LA PV+ neurons with and without bath application of the CB1R agonist WIN55 (Figures 6D and 6E). WIN55 selectively reduced sIPSC frequency in slices expressing the control but not the knockdown construct (Figures 6F, S6C, and S6D). Third, expressing the knockdown construct in LA PV+ neurons disrupted the decrease in GABA release induced by the CB1R agonist following paired-pulse stimulation (Figures S6E and S6F). Together, these results indicate our knockdown construct decreased CB1R expression on LA PV+ neurons.

Having validated our knockdown construct, we asked whether knocking down CB1R in LA PV+ neurons was sufficient to restore memory specificity and engram ensemble sparsity in CORT mice. CORT mice expressing our CB1R knockdown construct showed a specific memory (Figure 6G) and a sparse engram (Figures 6H–6J), similar to VEH mice, whereas CORT mice expressing the control construct continued to show generalized threat memory and a larger engram (Figures 6G, 6J, and 6K). Moreover, although CORT mice with the control construct showed aberrant engram reactivation to the generalized (CS−) retrieval cue (as in Figure 2L), we found CORT mice expressing our CB1R knockdown construct did not (Figures 6K and 6L). Importantly, knocking down CB1Rs in LA PV+ neurons using our construct was also sufficient to rescue the threat memory generalization induced by RS (Figures 6M and S6G).

We conducted several control experiments to verify that knocking down CB1Rs in LA PV+ neurons normalized threat memory generalization induced by CORT or acute stress. First, we replicated the normalization of threat memory specificity in CORT mice using a different validated CRISPR construct to knockdown CB1R expression[84] in LA PV+ neurons (Figures S6H and S6I). Second, we showed that this effect was specific to PV+ neurons in the LA. Although SST+ interneurons also express CB1Rs,[78] we found that knocking down CB1Rs using our construct in SST-Cre mice did not normalize threat

Figure 5. eCBs retrogradely mediate CORT-induced threat memory generalization via CB1Rs on LA PV+ neurons

(A) Colocalization of *Pvalb*, *GAD2*, and *Cnr1* mRNA in LA. Scale bar, 800 μm. Scale bar inlay, 80 μm.

(B) Graded colocalization of *Cnr1* in *Pvalb*+ neurons across anterior/posterior (AP) extent of LA (anterior; bregma −0.82 to −1.22; medial: −1.34 to −1.82; posterior −1.94 to −2.30).

(C) Expression of excitatory opsin ChRmine in LA PV+ neurons (via AAV-DIO-ChRmine in PV-Cre mice) used to examine GABA release in slices by recording optically evoked inhibitory postsynaptic currents (oIPSCs) on excitatory (Exc.) neurons in presence and absence of CB1R agonist WIN55.

(D) Example traces from excitatory neurons after two light pulses delivered in close succession. In control (aCSF) slices, response to the second light pulse (S2) attenuated compared with first light pulse (S1) (paired-pulse depression). In WIN55 slices responses to first and second pulses roughly equal.

(E) PPR (S2/S1) of oIPSCs recorded from excitatory neurons was higher in WIN55-treated slices than control slices ($F[1,3] = 10.89$, $p < 0.05$). n = 4–5 mice, 2–5 cells/mouse.

(F and G) (F) Strategy to examine endocannabinoid binding (GRAB_eCB2.0) in PV+ neurons and activity (RCaMP1a) of excitatory neurons in same mouse during threat conditioning (G) using dual-color fiber photometry.

(H) PV-Cre mice microinjected with AAV-DIO-GRAB_eCB2.0 (green) and AAV-hSyn-RCaMP1a (pink). Scale bar, 20 μm.

(I) (Left) CORT increased foot shock-induced RCaMP1a fluorescence in excitatory neurons and (right) higher peak fluorescence than VEH ($F[1,14] = 7.67$, $p < 0.05$).

(J) (Left) CORT increased foot shock-induced GRAB_eCB2.0 fluorescence in PV+ neurons and (right) higher peak fluorescence than VEH ($F[1,30] = 49.98$, $p < 0.0001$).

(K) Example of GRAB_eCB2.0 (green), RCaMP1a (pink), and isosbestic (violet) trace showing GRAB_eCB2.0 peak occurs before RCaMP1a peak.

(L) (Left) Peak synchrony of cross-correlation between GRAB_eCB2.0 and RCaMP1a signals for VEH and CORT mice. (Right) In both VEH and CORT mice, peak correlation of RCaMP signal occurred after GRAB_eCB2.0 signal (observed vs. scrambled control main effect, $F[1,14] = 156.2$, $p < 0.0001$), but peak synchrony was similar between VEH and CORT mice (main CORT effect: $F[1,14] = 0.56$, $p > 0.05$). Data are presented as mean + SEM. $^*p < 0.05$, $^{**}p < 0.01$, $^{***}p < 0.001$. CORT, corticosterone; eCB, endocannabinoids; LA, lateral amygdala; PV, parvalbumin; VEH, vehicle.

See also Figure S5.

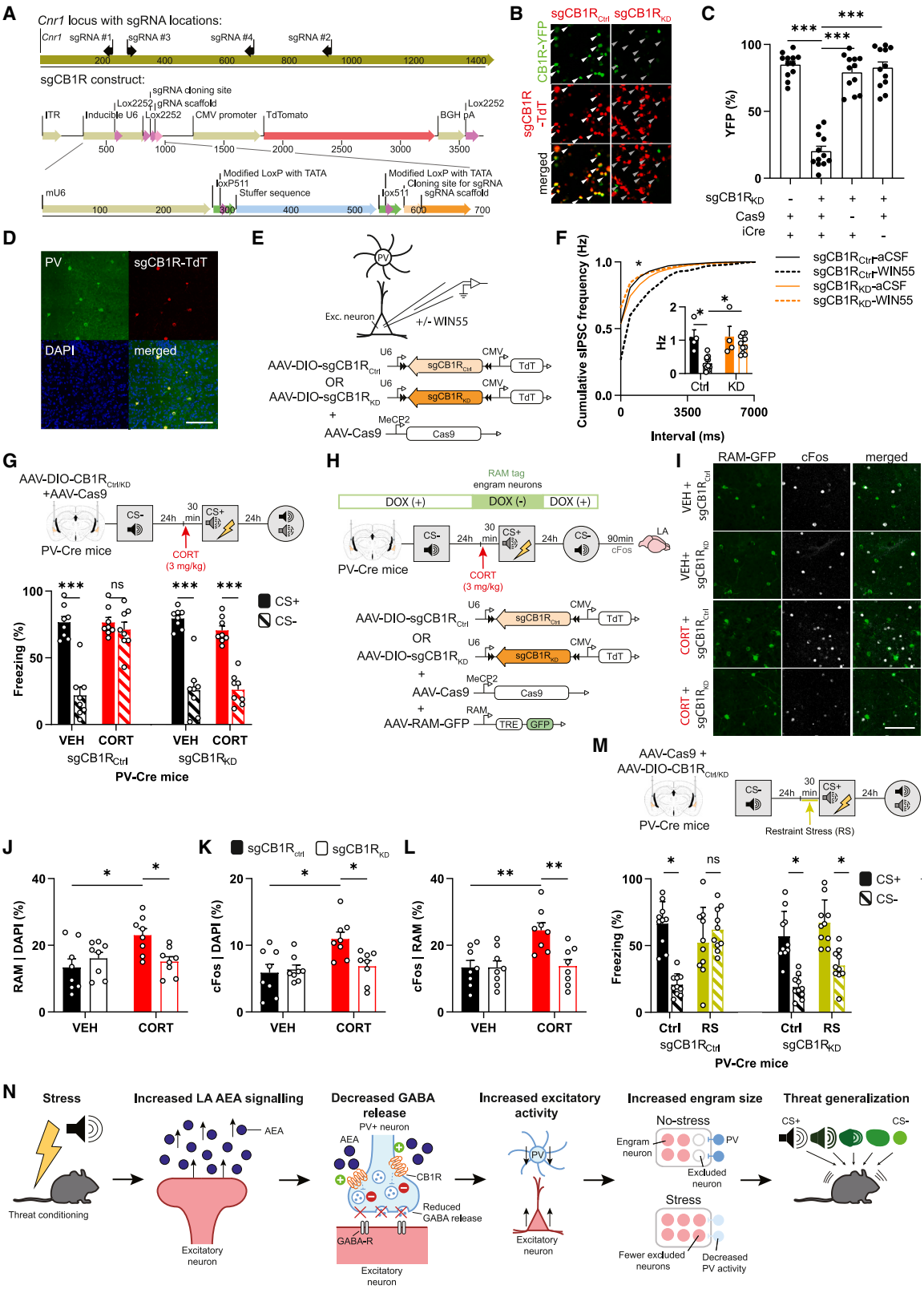

(legend on next page)

memory generalization in CORT mice (Figures S7A–S7L). Together, these findings support a cascade model in which acute stress, via CORT, increases AEA release from excitatory neurons in the LA, which results in increased AEA binding on CB1Rs on PV+ neurons, which decreases GABA release and promotes the formation of a larger engram ensemble during threat training (Figure 6N). This larger engram is reactivated by both specific and non-specific retrieval cues, mediating threat memory generalization.

Above, we found the effects of acute stress and CORT administration on threat memory generalization were largely restored by disrupting either glucocorticoid signaling directly in the LA or eCB binding on LA PV+ neurons. However, to be useful in normalizing stress-induced threat memory generalization in humans, it would be important that the route of administration of a treatment, ideally an FDA-approved treatment, be less invasive. Therefore, we assessed the effects of systemically administering an FDA-approved glucocorticoid receptor antagonist (RU486, 50 mg/kg, i.p.) or an AEA synthesis inhibitor (LEI-401, 30 mg/kg, i.p.) on restraint stress-induced threat memory generalization in mice. Both treatments restored threat memory specificity in RS mice (Figures 7A–7D), highlighting the therapeutic potential of this pathway.

DISCUSSION

Stress has previously been observed to induce the generalization of threat/aversive memories,[1] but the neurobiological processes mediating this effect have been elusive. Here we used a combination of tools to examine both the molecular and local circuit processes mediating this observation. We found that acute stress drives threat memory generalization at the level of the engram ensemble in the LA. Acute stress, via increases in CORT, promoted the release of the eCB AEA in the LA during threat training. Increased AEA retrogradely binds to CB1Rs on PV+ neurons, leading to a decrease in GABA release onto LA principal neurons during threat conditioning. The decreased GABAergic inhibition disrupts the process of neuronal exclusion from an engram ensemble, resulting in the formation of a larger and less-sparse engram ensemble. This larger ensemble is subsequently reactivated by both specific and non-specific retrieval cues, resulting in generalized threat memory (Figure 6N). Previous data show that increasing neuronal excitability of principal LA neurons[85] or disrupting the function of GABAergic neurons in the amygdala[86,87] induces threat memory generalization in the absence of CORT. The present results agree with these previous findings and, moreover, extend these findings by identifying an underlying molecular and circuit process.

Stress and memory generalization

The present findings add to the literature examining the role of stress and/or glucocorticoids in modulating different types of memory. It is generally accepted that stressful events are well remembered. Rodent studies, using pharmacological and genetic tools, show that under some circumstances stress and administration of CORT facilitate and might even be indispensable for several types of robust learning and memory.[4,36,38,88–92] Data from human research suggest that the more salient an experience, the stronger the memory of this experience.[93–98] Such robust memory retention may be highly adaptive but also may incur a cost if these memories lose their specificity. Threat memories formed under stressful circumstances can result in overgeneralization to safe situations in the absence of predictive threat cues,[28,29,99] as might also occur with PTSD.[3,100,101] Stress, particularly highly traumatic stress, is a necessary factor in the development of PTSD, and stress-induced alterations in memory processing may be an important contributor to the onset and/or progression of this disorder.[1,2]

Figure 6. Knockdown of CB1R in LA PV+ neurons restores threat memory specificity and engram ensemble size in CORT mice

(A) *Cnr1* locus and constructs used to knockdown CB1R in a Cre-dependent manner. Mixture of 4 sgRNAs used to make DIO-sgCB1R$_{KD}$-TdT. Control construct (DIO-sgCR1R$_{Ctrl}$-TdT) expressed non-targeting sgRNA.

(B) Validation of DIO-sgCB1R$_{KD}$-TdT in HEK293 cells expressing CB1R-eYFP (green). YFP decreased in Cas9+, iCre+ cells with DIO-sgCB1R$_{KD}$-TdT (red) but not DIO-sgCB1R$_{Ctrl}$-TdT (red).

(C) Quantification of CB1R-eYFP in sgCB1R$_{KD}$-TdT+ expression in HEK293 cells with or without Cas9 and iCre constructs showed necessity of all components to decrease CB1R expression ($F[3,44] = 72.24$, $p < 0.0001$).

(D) sgCB1R$_{KD}$-TdT (red) colocalized with PV (green) in LA. Scale bar, 50 μm.

(E) Functional validation of DIO-sgCB1R$_{KD}$-TdT in PV+ neurons from LA slices. sIPSCs recorded from excitatory neurons with or without CB1R agonist WIN55 in PV-Cre mice microinjected with sgCB1R$_{Ctrl}$ or sgCB1R$_{KD}$ and Cas9.

(F) WIN55 decreased sIPSC frequency recorded from excitatory LA neurons in sgCB1R$_{Ctrl}$ but not sgCB1R$_{KD}$ mice (virus x WIN, $F[1,26] = 4.54$, $p < 0.05$).

(G) CB1R knockdown in PV+ neurons (AAV-DIO-sgCB1R$_{KD}$ (but not AAV-DIO-sgCB1R$_{Ctrl}$) + AAV-Cas9 in PV-Cre mice) restored threat memory specificity in CORT mice (CORT × virus × tone, $F[1,28] = 12.92$, $p < 0.01$).

(H) Examining whether CB1R knockdown restored CORT-induced larger, less-sparse engram ensemble, and inappropriate engram reactivation during CS− test. Engram ensemble identified using AAV-RAM-GFP with mice removed from DOX during training. Neurons active during CS− memory test identified with cFos immunohistochemistry.

(I–L) (I) RAM-GFP + cFos expression in different groups. Scale bar, 50 μm. Knocking down CB1Rs in LA PV+ neurons in CORT mice restored (J) number of neurons active during training (RAM+) (CORT × CB1R, $F[1,28] = 7.02$, $p < 0.01$), (K) number of neurons active during CS− test (cFos+) (CORT × CB1R, $F[1,28] = 5.54$, $p < 0.05$), and (L) engram reactivation during CS− test (cFos+| RAM) (CORT × CB1R, $F[1,28] = 8.10$, $p < 0.01$).

(M) Similarly, knocking down CB1Rs in PV+ LA neurons restored memory specificity in RS mice (RS × KD × tone interaction: $F[1,36] = 9.20$, $p < 0.01$).

(N) Summary of findings. During threat learning, stress increases AEA release from LA excitatory neurons, which bind to CB1R on PV+ neurons and inhibit GABA release onto excitatory neurons. Rather than normally constraining the size of the LA engram, decreased PV inhibition induces formation of larger LA engram ensemble, resulting in generalized threat memory. Data are presented as mean + SEM. *$p < 0.05$, **$p < 0.01$, ***$p < 0.001$. CB1R, cannabinoid receptor 1; CORT, corticosterone; RS, restraint stress; WIN55, WIN55,212-2.

See also Figure S6.

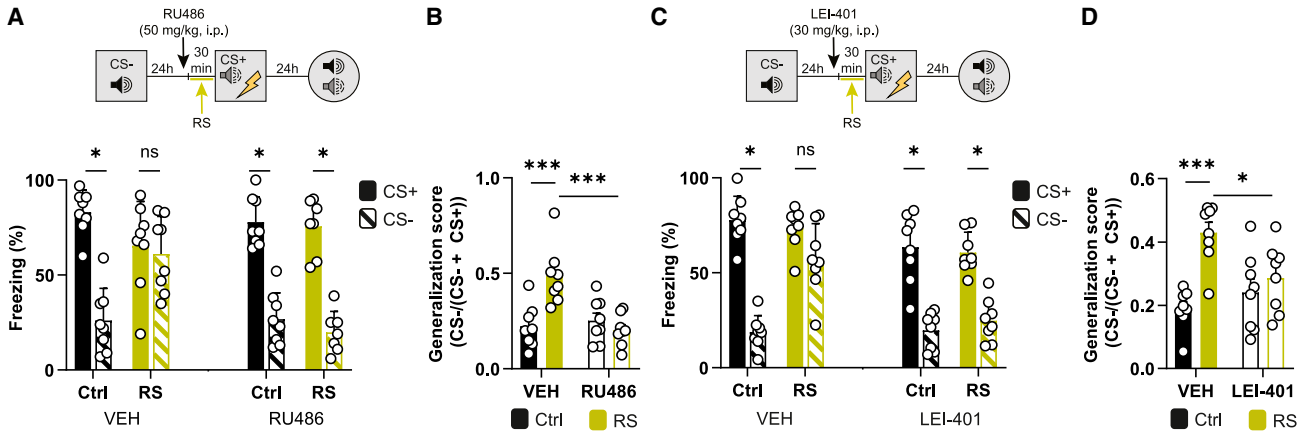

Figure 7. Systemically administering drugs that target glucocorticoid or AEA levels restores threat memory specificity in restraint-stressed mice

(A and B) Systemically administering glucocorticoid receptor antagonist RU486 (40 mg/kg, i.p.) restored (A) threat memory specificity in RS mice (stress × RU486 × tone interaction, $F[1,27] = 10.31$, $p < 0.01$), and (B) generalization score ($F[1,27] = 13.14$, $p < 0.001$).

(C and D) Systemically administering AEA synthesis inhibitor LEI-401 (30 mg/kg, i.p.) restored (C) threat memory specificity in RS mice (stress × LEI-401 × tone, $F[1,28] = 7.61$, $p < 0.01$), and (D) generalization score ($F[1,28] = 7.71$, $p < 0.01$). Data are presented as mean + SEM. $^{*}p < 0.05$, $^{**}p < 0.01$, $^{***}p < 0.001$. CORT, corticosterone; RS, restraint stress.

Although CORT exerts an inverted U-shaped dose-response curve on memory consolidation,[46] the present data are consistent with several previous reports that CORT, in the present dose range, enhances threat memory generalization.[28,29] Here we showed that pre-treatment with a moderate dose of CORT (3 mg/kg) induced threat memory generalization similar to the effects we observed with RS. In the present results, we observed that lower doses of CORT did not induce threat memory generalization, suggesting sufficient levels of CORT are required to induce threat memory generalization. These findings are consistent with human data suggesting only traumatic events perceived as highly stressful become generalized. People with PTSD show overgeneralization of threat memories characterized by an inability to inhibit threat responses in safe situations.[102–105] Interestingly, our results show that threat memory generalization occurs shortly after training rather than requiring an incubation period as suggested by some previous findings.[106,107]

eCBs and stress, anxiety, and threat

The current findings add to the rich literature on the role of eCBs in many brain regions in modulating and mediating the effects of stress on threat and anxiety, in addition to other behavioral and physiological responses to stress.[32,108,109] First, consistent with previous reports, we find that aversive learning mobilizes eCB signaling in the amygdala,[58] and extend these findings by showing that this effect is augmented by pre-exposure to systemic administration of CORT or stress. These elevations in AEA signaling were found to augment activity within excitatory principal neurons of the LA through disinhibition of PV+ interneurons, thus resulting in a less-sparse engram ensemble via decreased exclusion of non-winning excitatory neurons. Recent human work has similarly shown that threat conditioning can mobilize AEA and that the magnitude of AEA increases correlates with increased neural activity in the amygdala during learning itself.[110] As such, the current data provide a cellular mechanism to explain how elevated AEA during threat conditioning can increase neural activity within the amygdala.

Second, we show that AEA signaling in the LA is a key mediator of stress-induced threat memory generalization. This builds on previous work showing that AEA signaling within the amygdala contributes to the enhanced consolidation of aversive memories that occurs following increased intensity of the stressful stimulus,[58,111] but extends this work by showing that in addition to enhanced consolidation, AEA signaling in the LA drives overgeneralization of threat memories by disrupting engram ensemble sparsity. These data are particularly intriguing in light of recent human clinical work reporting that high circulating AEA at the time of a traumatic event is associated with increased risk of PTSD development.[112] The current data, in tandem with previously published work, provide a potential mechanism for this finding by suggesting that elevated AEA during trauma exposure may both facilitate hyper-consolidation and produce overgeneralization of the traumatic memory.

Engram ensemble sparsity

It has long been theorized that information is sparsely encoded in the brain.[113–116] This notion is backed by experimental findings showing sparse population coding schemes in a number of species, including *Drosophila*,[117] song birds,[118] primates,[119] and rodents.[120] Various machine learning/AI models also use sparse coding,[121,122] suggesting this type of information coding is a design principle across many systems. Sparse coding is thought to increase storage capacity and resource efficiency of a system, be robust to noise, and allow distinct memories to be represented simultaneously with little interference (pattern

separation).[123–126] We therefore investigated whether the generalized threat memory observed following stress was mediated by disrupting the sparsity of an engram ensemble, supporting a threat memory. Both computational theories and experimental data indicate sparse coding in cortical networks is mediated by inhibition.[127–129] Consistent with this, here we show the importance of LA PV+ inhibitory neurons in forming a sparse engram ensemble and how disrupting the function of PV+ neurons produced threat memory generalization. Although research from many labs over the past decade has shown that different types of memories are encoded in a sparse population of neurons in an engram ensemble,[7–9] how different environmental or genetic manipulations impact the formation of an engram ensemble and its subsequent accessibility to impact memory is only beginning to be explored.

Limitations of the study

Here, we examined the effects of systemic injections of CORT or acute RS on threat memory generalization and size of the engram ensemble in LA of mice. Whether other types of acute stressor or stressors applied more chronically induce similar generalization of an aversive memory or a similar increase in the size of the engram ensemble in the LA or other brain regions is unknown. We also examined only aversive threat memories. It would be interesting to examine whether stress similarly increases the generalization of a rewarding or motivationally neutral memory.

In conclusion, this study provides insights into how acute stress induces threat memory generalization in mice at both the molecular and circuit level. We show the critical involvement of glucocorticoid signaling, retrograde eCB signaling, and engram ensemble dynamics. These findings offer potential avenues for therapeutic interventions aimed at ameliorating stress-induced memory alterations and may have implications for stress-related psychiatric conditions.

RESOURCE AVAILABILITY

Lead contact

Further information and requests for resources should be directed to and will be fulfilled by the lead contact, Sheena A. Josselyn (sheena.josselyn@sickkids.ca).

Materials availability

All unique/stable reagents generated in this study are available from the lead contact (Dr. Sheena A. Josselyn; sheena.josselyn@sickkids.ca) upon request with a completed Materials Transfer Agreement.

Data and code availability

- All data reported in this paper will be shared by the lead contact upon request.
- This paper does not report original code.
- Any additional information required to reanalyze the data reported in this paper is available from the lead contact upon request.

ACKNOWLEDGMENTS

We thank D. Lin and M. Yamamoto for technical support and the entire Josselyn and Frankland labs for advice, technical support, and discussion. This work was supported by grants from the Dutch Research Council (NWO Rubicon—019.191EN.012), Niels Stensen Fellowship, ZonMw Memorabel (10510022110011), CIHR (MFA—181868), Alzheimer Nederland (WE.03-2023-01), and Toronto Cannabis and Cannabinoid Research Consortium to S.L.L.; NIMH (R01 MH119421-01) and Brain Canada Foundation to S.A.J. and P.W.F.; CIHR (FDN—159919) to S.A.J.; CIHR (FDN-143227) to P.W.F.; and NSERC CGS-D and CIHR (PJT-426504) to M.N.H.

AUTHOR CONTRIBUTIONS

Conceptualization, S.L.L., M.N.H., P.W.F., and S.A.J.; investigation, S.L.L., S.P., A.H., S.V., E.W.S., A.M.T., and A.D.; formal analysis, S.L.L., A.J.M., and E.W.S.; methodology, S.L.L., M.T.G., J.L.L., B.J.W., P.W.F., and S.A.J.; visualization, S.L.L. and S.A.J.; resources, J.L.L., L.S.Z., B.J.W., M.v.d.S., G.L.C., and J.L.L.; supervision for electrophysiology experiments, G.L.C.; supervision for smFISH experiments, J.L.L.; funding acquisition, S.L.L., M.N.H., P.W.F., and S.A.J.; writing—original draft, S.L.L. and S.A.J.; writing—review and editing, all authors.

DECLARATION OF INTERESTS

S.A.J. is a member of the Editorial Board of *Cell*.

STAR★METHODS

Detailed methods are provided in the online version of this paper and include the following:

- KEY RESOURCES TABLE
- EXPERIMENTAL MODEL AND STUDY PARTICIPANT DETAILS
  - Mice
- METHOD DETAILS
  - Viruses
  - HSV
  - AAV
  - Stress manipulations
  - Experimental design
  - Drug administration
  - Surgery
  - Histology
  - Plasma CORT measurements
  - Fiber photometry
  - AEA and 2-AG measurement
  - Single-molecule fluorescence in situ hybridization
  - Electrophysiology
  - HEK cells
- QUANTIFICATION AND STATISTICAL ANALYSIS

SUPPLEMENTAL INFORMATION

Supplemental information can be found online at https://doi.org/10.1016/j.cell.2024.10.034.

Received: January 16, 2024
Revised: August 25, 2024
Accepted: October 17, 2024
Published: November 15, 2024

REFERENCES

1. Lissek, S., and van Meurs, B. (2015). Learning models of PTSD: Theoretical accounts and psychobiological evidence. Int. J. Psychophysiol. *98*, 594–605. https://doi.org/10.1016/J.IJPSYCHO.2014.11.006.
2. Lis, S., Thome, J., Kleindienst, N., Mueller-Engelmann, M., Steil, R., Priebe, K., Schmahl, C., Hermans, D., and Bohus, M. (2020). Generalization of fear in post-traumatic stress disorder. Psychophysiology *57*, e13422. https://doi.org/10.1111/PSYP.13422.

3. Dunsmoor, J.E., Otto, A.R., and Phelps, E.A. (2017). Stress promotes generalization of older but not recent threat memories. Proc. Natl. Acad. Sci. USA *114*, 9218–9223. https://doi.org/10.1073/pnas.1704428114.

4. De Quervain, D., Schwabe, L., and Roozendaal, B. (2017). Stress, glucocorticoids and memory: implications for treating fear-related disorders. Nat. Rev. Neurosci. *18*, 7–19. https://doi.org/10.1038/NRN.2016.155.

5. Bahtiyar, S., Gulmez Karaca, K., Henckens, M.J.A.G., and Roozendaal, B. (2020). Norepinephrine and glucocorticoid effects on the brain mechanisms underlying memory accuracy and generalization. Mol. Cell. Neurosci. *108*, 103537. https://doi.org/10.1016/J.MCN.2020.103537.

6. Roozendaal, B., and Mirone, G. (2020). Opposite effects of noradrenergic and glucocorticoid activation on accuracy of an episodic-like memory. Psychoneuroendocrinology *114*, 104588. https://doi.org/10.1016/J.PSYNEUEN.2020.104588.

7. Josselyn, S.A., Köhler, S., and Frankland, P.W. (2015). Finding the engram. Nat. Rev. Neurosci. *16*, 521–534. https://doi.org/10.1038/NRN4000.

8. Tonegawa, S., Liu, X., Ramirez, S., and Redondo, R. (2015). Memory Engram Cells Have Come of Age. Neuron *87*, 918–931. https://doi.org/10.1016/J.NEURON.2015.08.002.

9. Denny, C.A., Lebois, E., and Ramirez, S. (2017). From Engrams to Pathologies of the Brain. Front. Neural Circuits *11*, 23. https://doi.org/10.3389/FNCIR.2017.00023.

10. Josselyn, S.A., and Tonegawa, S. (2020). Memory engrams: Recalling the past and imagining the future. Preprint at American Association for the Advancement of Science. https://doi.org/10.1126/science.aaw4325.

11. Frankland, P.W., Josselyn, S.A., and Köhler, S. (2019). The neurobiological foundation of memory retrieval. Nat. Neurosci. *22*, 1576–1585. https://doi.org/10.1038/S41593-019-0493-1.

12. Denny, C.A., Kheirbek, M.A., Alba, E.L., Tanaka, K.F., Brachman, R.A., Laughman, K.B., Tomm, N.K., Turi, G.F., Losonczy, A., and Hen, R. (2014). Hippocampal memory traces are differentially modulated by experience, time, and adult neurogenesis. Neuron *83*, 189–201. https://doi.org/10.1016/J.NEURON.2014.05.018.

13. Vetere, G., Tran, L.M., Moberg, S., Steadman, P.E., Restivo, L., Morrison, F.G., Ressler, K.J., Josselyn, S.A., and Frankland, P.W. (2019). Memory formation in the absence of experience. Nat. Neurosci. *22*, 933–940. https://doi.org/10.1038/S41593-019-0389-0.

14. Kanerva, P. (1988). Sparse Distributed Memory*155* (MIT Press).

15. Josselyn, S.A., and Frankland, P.W. (2018). Memory allocation: mechanisms and function. Annu. Rev. Neurosci. *41*, 389–413. https://doi.org/10.1146/annurev-neuro-080317-061956.

16. Kim, J., Kwon, J.T., Kim, H.S., and Han, J.H. (2013). CREB and neuronal selection for memory trace. Front. Neural Circuits *7*, 44. https://doi.org/10.3389/FNCIR.2013.00044.

17. Han, J.H., Kushner, S.A., Yiu, A.P., Hsiang, H.L.L., Buch, T., Waisman, A., Bontempi, B., Neve, R.L., Frankland, P.W., and Josselyn, S.A. (2009). Selective erasure of a fear memory. Science *323*, 1492–1496. https://doi.org/10.1126/SCIENCE.1164139.

18. Zhou, Y., Won, J., Karlsson, M.G., Zhou, M., Rogerson, T., Balaji, J., Neve, R., Poirazi, P., and Silva, A.J. (2009). CREB regulates excitability and the allocation of memory to subsets of neurons in the amygdala. Nat. Neurosci. *12*, 1438–1443. https://doi.org/10.1038/NN.2405.

19. Yiu, A.P., Mercaldo, V., Yan, C., Richards, B., Rashid, A.J., Hsiang, H.L.L., Pressey, J., Mahadevan, V., Tran, M.M., Kushner, S.A., et al. (2014). Neurons are recruited to a memory trace based on relative neuronal excitability immediately before training. Neuron *83*, 722–735. https://doi.org/10.1016/J.NEURON.2014.07.017.

20. Feng, F., Samarth, P., Paré, D., and Nair, S.S. (2016). Mechanisms underlying the formation of the amygdalar fear memory trace: A computational perspective. Neuroscience *322*, 370–376. https://doi.org/10.1016/J.NEUROSCIENCE.2016.02.059.

21. Kim, D., Samarth, P., Feng, F., Pare, D., and Nair, S.S. (2016). Synaptic competition in the lateral amygdala and the stimulus specificity of conditioned fear: a biophysical modeling study. Brain Struct. Funct. *221*, 2163–2182. https://doi.org/10.1007/S00429-015-1037-4.

22. Morrison, D.J., Rashid, A.J., Yiu, A.P., Yan, C., Frankland, P.W., and Josselyn, S.A. (2016). Parvalbumin interneurons constrain the size of the lateral amygdala engram. Neurobiol. Learn. Mem. *135*, 91–99. https://doi.org/10.1016/J.NLM.2016.07.007.

23. Ramsaran, A.I., Wang, Y., Golbabaei, A., Aleshin, S., de Snoo, M.L., Yeung, B.A., Rashid, A.J., Awasthi, A., Lau, J., Tran, L.M., et al. (2023). A shift in the mechanisms controlling hippocampal engram formation during brain maturation. Science *380*, 543–551. https://doi.org/10.1126/SCIENCE.ADE6530.

24. Zhang, X., Kim, J., and Tonegawa, S. (2020). Amygdala Reward Neurons Form and Store Fear Extinction Memory. Neuron *105*, 1077–1093.e7. https://doi.org/10.1016/J.NEURON.2019.12.025.

25. Gouty-Colomer, L.A., Hosseini, B., Marcelo, I.M., Schreiber, J., Slump, D.E., Yamaguchi, S., Houweling, A.R., Jaarsma, D., Elgersma, Y., and Kushner, S.A. (2016). Arc expression identifies the lateral amygdala fear memory trace. Mol. Psychiatry *21*, 364–375. https://doi.org/10.1038/mp.2015.18.

26. Hsiang, H.L.L., Epp, J.R., van den Oever, M.C., Yan, C., Rashid, A.J., Insel, N., Ye, L., Niibori, Y., Deisseroth, K., Frankland, P.W., et al. (2014). Manipulating a "Cocaine Engram" in Mice. J. Neurosci. *34*, 14115–14127. https://doi.org/10.1523/JNEUROSCI.3327-14.2014.

27. Choi, J.H., Sim, S.E., Kim, J.I., Choi, D.I., Oh, J., Ye, S., Lee, J., Kim, T.H., Ko, H.G., Lim, C.S., et al. (2018). Interregional synaptic maps among engram cells underlie memory formation. Science *360*, 430–435. https://doi.org/10.1126/SCIENCE.AAS9204.

28. Kaouane, N., Porte, Y., Vallée, M., Brayda-Bruno, L., Mons, N., Calandreau, L., Marighetto, A., Piazza, P.V., and Desmedt, A. (2012). Glucocorticoids can induce PTSD-like memory impairments in mice. Science *335*, 1510–1513. https://doi.org/10.1126/SCIENCE.1207615/SUPPL_FILE/KAOUANE.SOM.PDF.

29. Lesuis, S.L., Brosens, N., Immerzeel, N., van der Loo, R.J., Mitrić, M., Bielefeld, P., Fitzsimons, C.P., Lucassen, P.J., Kushner, S.A., van den Oever, M.C., et al. (2021). Glucocorticoids Promote Fear Generalization by Increasing the Size of a Dentate Gyrus Engram Cell Population. Biol. Psychiatry *90*, 494–504. https://doi.org/10.1016/J.BIOPSYCH.2021.04.010.

30. van Ast, V.A., Cornelisse, S., Meeter, M., Joëls, M., and Kindt, M. (2013). Time-dependent effects of cortisol on the contextualization of emotional memories. Biol. Psychiatry *74*, 809–816. https://doi.org/10.1016/j.biopsych.2013.06.022.

31. Morena, M., and Campolongo, P. (2014). The endocannabinoid system: an emotional buffer in the modulation of memory function. Neurobiol. Learn. Mem. *112*, 30–43. https://doi.org/10.1016/J.NLM.2013.12.010.

32. Morena, M., Patel, S., Bains, J.S., and Hill, M.N. (2016). Neurobiological Interactions Between Stress and the Endocannabinoid System. Neuropsychopharmacology *41*, 80–102. https://doi.org/10.1038/NPP.2015.166.

33. Joëls, M., and Baram, T.Z. (2009). The neuro-symphony of stress. Nat. Rev. Neurosci. *10*, 459–466. https://doi.org/10.1038/NRN2632.

34. de Kloet, E.R., Joëls, M., and Holsboer, F. (2005). Stress and the brain: from adaptation to disease. Nat. Rev. Neurosci. *6*, 463–475. https://doi.org/10.1038/nrn1683.

35. Roozendaal, B., McEwen, B.S., and Chattarji, S. (2009). Stress, memory and the amygdala. Nat. Rev. Neurosci. *10*, 423–433. https://doi.org/10.1038/NRN2651.

36. Cordero, M.I., Kruyt, N.D., Merino, J.J., and Sandi, C. (2002). Glucocorticoid involvement in memory formation in a rat model for traumatic memory. Stress *5*, 73–79. https://doi.org/10.1080/1025389029000124404.

37. Cordero, M.I., Venero, C., Kruyt, N.D., and Sandi, C. (2003). Prior exposure to a single stress session facilitates subsequent contextual fear conditioning in rats: Evidence for a role of corticosterone. Horm. Behav. *44*, 338–345. https://doi.org/10.1016/S0018-506X(03)00160-0.

38. Cordero, M.I., Merino, J.J., and Sandi, C. (1998). Correlational relationship between shock intensity and corticosterone secretion on the establishment and subsequent expression of contextual fear conditioning. Behav. Neurosci. *112*, 885–891. https://doi.org/10.1037/0735-7044.112.4.885.

39. Ahima, R.S., and Harlan, R.E. (1991). Differential corticosteroid regulation of type II glucocorticoid receptor-like immunoreactivity in the rat central nervous system: topography and implications. Endocrinology *129*, 226–236. https://doi.org/10.1210/ENDO-129-1-226.

40. Johnson, L.R., Farb, C., Morrison, J.H., McEwen, B.S., and LeDoux, J.E. (2005). Localization of glucocorticoid receptors at postsynaptic membranes in the lateral amygdala. Neuroscience *136*, 289–299. https://doi.org/10.1016/J.NEUROSCIENCE.2005.06.050.

41. Inoue, R., Abdou, K., Hayashi-Tanaka, A., Muramatsu, S.I., Mino, K., Inokuchi, K., and Mori, H. (2018). Glucocorticoid receptor-mediated amygdalar metaplasticity underlies adaptive modulation of fear memory by stress. eLife *7*, e34135. https://doi.org/10.7554/eLife.34135.

42. LeDoux, J. (2003). The emotional brain, fear, and the amygdala. Cell Mol Neurobiol *23*, 727–738. https://doi.org/10.1023/A:1025048802629.

43. Maren, S. (2003). The amygdala, synaptic plasticity, and fear memory. Ann. N. Y. Acad. Sci. *985*, 106–113. https://doi.org/10.1111/J.1749-6632.2003.TB07075.X.

44. Duvarci, S., and Pare, D. (2014). Amygdala microcircuits controlling learned fear. Neuron *82*, 966–980. https://doi.org/10.1016/J.NEURON.2014.04.042.

45. Choi, D.Il, Kim, J., Lee, H., Kim, J.il, Sung, Y., Choi, J.E., Venkat, S.J., Park, P., Jung, H., and Kaang, B.K. (2021). Synaptic correlates of associative fear memory in the lateral amygdala. Neuron *109*, 2717–2726.e3. https://doi.org/10.1016/J.NEURON.2021.07.003.

46. Salehi, B., Cordero, M.I., and Sandi, C. (2010). Learning under stress: the inverted-U-shape function revisited. Learn. Mem. *17*, 522–530. https://doi.org/10.1101/LM.1914110.

47. DeNardo, L.A., Liu, C.D., Allen, W.E., Adams, E.L., Friedmann, D., Fu, L., Guenthner, C.J., Tessier-Lavigne, M., and Luo, L. (2019). Temporal evolution of cortical ensembles promoting remote memory retrieval. Nat. Neurosci. *22*, 460–469. https://doi.org/10.1038/S41593-018-0318-7.

48. Sørensen, A.T., Cooper, Y.A., Baratta, M.V., Weng, F.J., Zhang, Y., Ramamoorthi, K., Fropf, R., Laverriere, E., Xue, J., Young, A., et al. (2016). A robust activity marking system for exploring active neuronal ensembles. eLife *5*, e13918. https://doi.org/10.7554/eLife.13918.

49. Gradinaru, V., Zhang, F., Ramakrishnan, C., Mattis, J., Prakash, R., Diester, I., Goshen, I., Thompson, K.R., and Deisseroth, K. (2010). Molecular and cellular approaches for diversifying and extending optogenetics. Cell *141*, 154–165. https://doi.org/10.1016/J.CELL.2010.02.037.

50. Mei, Y., and Zhang, F. (2012). Molecular tools and approaches for optogenetics. Biol. Psychiatry *71*, 1033–1038. https://doi.org/10.1016/J.BIOPSYCH.2012.02.019.

51. Rashid, A.J., Yan, C., Mercaldo, V., Hsiang, H.-L.L., Park, S., Cole, C.J., De Cristofaro, A., Yu, J., Ramakrishnan, C., Lee, S.Y., et al. (2016). Competition between engrams influences fear memory formation and recall. Science *353*, 383–387. https://doi.org/10.1126/science.aaf0594.

52. Lau, J.M.H., Rashid, A.J., Jacob, A.D., Frankland, P.W., Schacter, D.L., and Josselyn, S.A. (2020). The role of neuronal excitability, allocation to an engram and memory linking in the behavioral generation of a false memory in mice. Neurobiol. Learn. Mem. *174*, 107284. https://doi.org/10.1016/J.NLM.2020.107284.

53. Hájos, N. (2021). Interneuron Types and Their Circuits in the Basolateral Amygdala. Front. Neural Circuits *15*, 687257. https://doi.org/10.3389/FNCIR.2021.687257.

54. Vereczki, V.K., Müller, K., Krizsán, É., Máté, Z., Fekete, Z., Rovira-Esteban, L., Veres, J.M., Erdélyi, F., and Hájos, N. (2021). Total Number and Ratio of GABAergic Neuron Types in the Mouse Lateral and Basal Amygdala. J. Neurosci. *41*, 4575–4595. https://doi.org/10.1523/JNEUROSCI.2700-20.2021.

55. deRoon-Cassini, T.A., Stollenwerk, T.M., Beatka, M., and Hillard, C.J. (2020). Meet Your Stress Management Professionals: The Endocannabinoids. Trends Mol. Med. *26*, 953–968. https://doi.org/10.1016/J.MOLMED.2020.07.002.

56. Granja-Galeano, G., Dominguez-Rubio, A.P., Zappia, C.D., Wolfson, M., Sanz-Blasco, S., Aisemberg, J., Zorrilla-Zubilete, M., Fernandez, N., Franchi, A., Fitzsimons, C.P., et al. (2023). CB1 receptor expression and signaling are required for dexamethasone-induced aversive memory consolidation. Neuropharmacology *239*, 109674. https://doi.org/10.1016/J.NEUROPHARM.2023.109674.

57. Hill, M.N., Karatsoreos, I.N., Hillard, C.J., and McEwen, B.S. (2010). Rapid elevations in limbic endocannabinoid content by glucocorticoid hormones in vivo. Psychoneuroendocrinology *35*, 1333–1338. https://doi.org/10.1016/J.PSYNEUEN.2010.03.005.

58. Morena, M., Roozendaal, B., Trezza, V., Ratano, P., Peloso, A., Hauer, D., Atsak, P., Trabace, L., Cuomo, V., McGaugh, J.L., et al. (2014). Endogenous cannabinoid release within prefrontal-limbic pathways affects memory consolidation of emotional training. Proc. Natl. Acad. Sci. USA *111*, 18333–18338. https://doi.org/10.1073/PNAS.1420285111.

59. Marsicano, G., and Lutz, B. (1999). Expression of the cannabinoid receptor CB1 in distinct neuronal subpopulations in the adult mouse forebrain. Eur. J. Neurosci. *11*, 4213–4225. https://doi.org/10.1046/J.1460-9568.1999.00847.X.

60. Katona, I., Rancz, E.A., Acsády, L., Ledent, C., Mackie, K., Hájos, N., and Freund, T.F. (2001). Distribution of CB1 cannabinoid receptors in the amygdala and their role in the control of GABAergic transmission. J. Neurosci. *21*, 9506–9518. https://doi.org/10.1523/JNEUROSCI.21-23-09506.2001.

61. Ohno-Shosaku, T., Maejima, T., and Kano, M. (2001). Endogenous cannabinoids mediate retrograde signals from depolarized postsynaptic neurons to presynaptic terminals. Neuron *29*, 729–738. https://doi.org/10.1016/S0896-6273(01)00247-1.

62. Dudok, B., Fan, L.Z., Farrell, J.S., Malhotra, S., Homidan, J., Kim, D.K., Wenardy, C., Ramakrishnan, C., Li, Y., Deisseroth, K., et al. (2024). Retrograde endocannabinoid signaling at inhibitory synapses in vivo. Science *383*, 967–970. https://doi.org/10.1126/SCIENCE.ADK3863.

63. Wang, H., Dong, P., He, C., Feng, X.Y., Huang, Y., Yang, W.W., Gao, H.J., Shen, X.F., Lin, S., Cao, S.X., et al. (2020). Incerta-thalamic Circuit Controls Nocifensive Behavior via Cannabinoid Type 1 Receptors. Neuron *107*, 538–551.e7. https://doi.org/10.1016/J.NEURON.2020.04.027.

64. Cuzon Carlson, V.C., Gremel, C.M., and Lovinger, D.M. (2020). Gestational alcohol exposure disrupts cognitive function and striatal circuits in adult offspring. Nat. Commun. *11*, 2555. https://doi.org/10.1038/S41467-020-16385-4.

65. Bisogno, T., Howell, F., Williams, G., Minassi, A., Cascio, M.G., Ligresti, A., Matias, I., Schiano-Moriello, A., Paul, P., Williams, E.J., et al. (2003). Cloning of the first sn1-DAG lipases points to the spatial and temporal regulation of endocannabinoid signaling in the brain. J. Cell Biol. *163*, 463–468. https://doi.org/10.1083/JCB.200305129.

66. Ogasawara, D., Deng, H., Viader, A., Baggelaar, M.P., Breman, A., Den Dulk, H., Van Den Nieuwendijk, A.M.C.H., Soethoudt, M., Van Der Wel, T., Zhou, J., et al. (2016). Rapid and profound rewiring of brain lipid signaling networks by acute diacylglycerol lipase inhibition. Proc. Natl. Acad. Sci. USA *113*, 26–33. https://doi.org/10.1073/PNAS.1522364112.

67. Deng, H., Kooijman, S., Van Den Nieuwendijk, A.M.C.H., Ogasawara, D., Van der Wel, T., Van Dalen, F., Baggelaar, M.P., Janssen, F.J., Van Den Berg, R.J.B.H.N., Den Dulk, H., et al. (2017). Triazole Ureas Act as Diacylglycerol Lipase Inhibitors and Prevent Fasting-Induced Refeeding.

J. Med. Chem. *60*, 428–440. https://doi.org/10.1021/ACS.JMEDCHEM.6B01482.

68. Okamoto, Y., Morishita, J., Tsuboi, K., Tonai, T., and Ueda, N. (2004). Molecular Characterization of a Phospholipase D Generating Anandamide and Its Congeners. J. Biol. Chem. *279*, 5298–5305. https://doi.org/10.1074/jbc.M306642200.
69. Mock, E.D., Mustafa, M., Gunduz-Cinar, O., Cinar, R., Petrie, G.N., Kantae, V., Di, X., Ogasawara, D., Varga, Z.V., Paloczi, J., et al. (2020). Discovery of a NAPE-PLD inhibitor that modulates emotional behavior in mice. Nat. Chem. Biol. *16*, 667–675. https://doi.org/10.1038/S41589-020-0528-7.
70. Cravatt, B.F., Demarest, K., Patricelli, M.P., Bracey, M.H., Giang, D.K., Martin, B.R., and Lichtman, A.H. (2001). Supersensitivity to anandamide and enhanced endogenous cannabinoid signaling in mice lacking fatty acid amide hydrolase. Proc. Natl. Acad. Sci. USA *98*, 9371–9376. https://doi.org/10.1073/PNAS.161191698.
71. Balsevich, G., Petrie, G.N., Heinz, D.E., Singh, A., Aukema, R.J., Hunker, A.C., Vecchiarelli, H.A., Yau, H., Sticht, M., Thompson, R.J., et al. (2023). A genetic variant of fatty acid amide hydrolase (FAAH) exacerbates hormone-mediated orexigenic feeding in mice. eLife *12*, e81919. https://doi.org/10.7554/eLife.81919.
72. Kathuria, S., Gaetani, S., Fegley, D., Valiño, F., Duranti, A., Tontini, A., Mor, M., Tarzia, G., La Rana, G., Calignano, A., et al. (2003). Modulation of anxiety through blockade of anandamide hydrolysis. Nat. Med. *9*, 76–81. https://doi.org/10.1038/NM803.
73. Morena, M., Aukema, R.J., Leitl, K.D., Rashid, A.J., Vecchiarelli, H.A., Josselyn, S.A., and Hill, M.N. (2019). Upregulation of Anandamide Hydrolysis in the Basolateral Complex of Amygdala Reduces Fear Memory Expression and Indices of Stress and Anxiety. J. Neurosci. *39*, 1275–1292. https://doi.org/10.1523/JNEUROSCI.2251-18.2018.
74. Kano, M., Ohno-Shosaku, T., Hashimotodani, Y., Uchigashima, M., and Watanabe, M. (2009). Endocannabinoid-mediated control of synaptic transmission. Physiol. Rev. *89*, 309–380. https://doi.org/10.1152/PHYSREV.00019.2008.
75. Katona, I., and Freund, T.F. (2008). Endocannabinoid signaling as a synaptic circuit breaker in neurological disease. Nat. Med. *14*, 923–930. https://doi.org/10.1038/NM.F.1869.
76. Soltesz, I., Alger, B.E., Kano, M., Lee, S.H., Lovinger, D.M., Ohno-Shosaku, T., and Watanabe, M. (2015). Weeding out bad waves: towards selective cannabinoid circuit control in epilepsy. Nat. Rev. Neurosci. *16*, 264–277. https://doi.org/10.1038/NRN3937.
77. McDonald, A.J., and Mascagni, F. (2001). Localization of the CB1 type cannabinoid receptor in the rat basolateral amygdala: High concentrations in a subpopulation of cholecystokinin-containing interneurons. Neuroscience *107*, 641–652. https://doi.org/10.1016/S0306-4522(01)00380-3.
78. Hochgerner, H., Singh, S., Tibi, M., Lin, Z., Skarbianskis, N., Admati, I., Ophir, O., Reinhardt, N., Netser, S., Wagner, S., et al. (2023). Neuronal types in the mouse amygdala and their transcriptional response to fear conditioning. Nat. Neurosci. *26*, 2237–2249. https://doi.org/10.1038/s41593-023-01469-3.
79. Oliet, S.H.R., Baimoukhametova, D.V., Piet, R., and Bains, J.S. (2007). Retrograde Regulation of GABA Transmission by the Tonic Release of Oxytocin and Endocannabinoids Governs Postsynaptic Firing. J. Neurosci. *27*, 1325–1333. https://doi.org/10.1523/JNEUROSCI.2676-06.2007.
80. Hentges, S.T., Low, M.J., and Williams, J.T. (2005). Differential regulation of synaptic inputs by constitutively released endocannabinoids and exogenous cannabinoids. J. Neurosci. *25*, 9746–9751. https://doi.org/10.1523/JNEUROSCI.2769-05.2005.
81. Marshel, J.H., Kim, Y.S., Machado, T.A., Quirin, S., Benson, B., Kadmon, J., Raja, C., Chibukhchyan, A., Ramakrishnan, C., Inoue, M., et al. (2019). Cortical layer-specific critical dynamics triggering perception. Science *365*. https://doi.org/10.1126/SCIENCE.AAW5202.
82. Lauckner, J.E., Hille, B., and Mackie, K. (2005). The cannabinoid agonist WIN55,212-2 increases intracellular calcium via CB1 receptor coupling to Gq/11 G proteins. Proc. Natl. Acad. Sci. USA *102*, 19144–19149. https://doi.org/10.1073/pnas.0509588102.
83. Dong, A., He, K., Dudok, B., Farrell, J.S., Guan, W., Liput, D.J., Puhl, H.L., Cai, R., Wang, H., Duan, J., et al. (2022). A fluorescent sensor for spatiotemporally resolved imaging of endocannabinoid dynamics in vivo. Nat. Biotechnol. *40*, 787–798. https://doi.org/10.1038/S41587-021-01074-4.
84. Gunduz-Cinar, O., Castillo, L.I., Xia, M., Van Leer, E., Brockway, E.T., Pollack, G.A., Yasmin, F., Bukalo, O., Limoges, A., Oreizi-Esfahani, S., et al. (2023). A cortico-amygdala neural substrate for endocannabinoid modulation of fear extinction. Neuron *111*, 3053–3067.e10. https://doi.org/10.1016/J.NEURON.2023.06.023.
85. Ghosh, S., and Chattarji, S. (2015). Neuronal encoding of the switch from specific to generalized fear. Nat. Neurosci. *18*, 112–120. https://doi.org/10.1038/NN.3888.
86. Bergado-Acosta, J.R., Sangha, S., Narayanan, R.T., Obata, K., Pape, H.C., and Stork, O. (2008). Critical role of the 65-kDa isoform of glutamic acid decarboxylase in consolidation and generalization of Pavlovian fear memory. Learn. Mem. *15*, 163–171. https://doi.org/10.1101/LM.705408.
87. Shaban, H., Humeau, Y., Herry, C., Cassasus, G., Shigemoto, R., Ciocchi, S., Barbieri, S., Van Der Putten, H., Kaupmann, K., Bettler, B., et al. (2006). Generalization of amygdala LTP and conditioned fear in the absence of presynaptic inhibition. Nat. Neurosci. *9*, 1028–1035. https://doi.org/10.1038/NN1732.
88. Sandi, C., Loscertales, M., and Guaza, C. (1997). Experience-dependent facilitating effect of corticosterone on spatial memory formation in the water maze. Eur. J. Neurosci. *9*, 637–642. https://doi.org/10.1111/j.1460-9568.1997.tb01412.x.
89. Cordero, M.I., and Sandi, C. (1998). A role for brain glucocorticoid receptors in contextual fear conditioning: dependence upon training intensity. Brain Res. *786*, 11–17. https://doi.org/10.1016/S0006-8993(97)01420-0.
90. Oitzl, M.S., and de Kloet, E.R. (1992). Selective corticosteroid antagonists modulate specific aspects of spatial orientation learning. Behav. Neurosci. *106*, 62–71. https://doi.org/10.1037//0735-7044.106.1.62.
91. Sandi, C., and Rose, S.P. (1994). Corticosteroid receptor antagonists are amnestic for passive avoidance learning in day-old chicks. Eur. J. Neurosci. *6*, 1292–1297. https://doi.org/10.1111/j.1460-9568.1994.tb00319.x.
92. Roozendaal, B., and McGaugh, J.L. (1996). The memory-modulatory effects of glucocorticoids depend on an intact stria terminalis. Brain Res. *709*, 243–250. https://doi.org/10.1016/0006-8993(95)01305-9.
93. Shors, T.J. (2006). Stressful experience and learning across the lifespan. Annu. Rev. Psychol. *57*, 55–85. https://doi.org/10.1146/ANNUREV.PSYCH.57.102904.190205.
94. McGaugh, J.L. (2004). The amygdala modulates the consolidation of memories of emotionally arousing experiences. Annu. Rev. Neurosci. *27*, 1–28. https://doi.org/10.1146/ANNUREV.NEURO.27.070203.144157.
95. Lupien, S.J., Wilkinson, C.W., Brière, S., Ménard, C., Ng Ying Kin, N.M.K., and Nair, N.P.V. (2002). The modulatory effects of corticosteroids on cognition: studies in young human populations. Psychoneuroendocrinology *27*, 401–416. https://doi.org/10.1016/S0306-4530(01)00061-0.
96. Cahill, L., Gorski, L., and Le, K. (2003). Enhanced human memory consolidation with post-learning stress: interaction with the degree of arousal at encoding. Learn. Mem. *10*, 270–274. https://doi.org/10.1101/LM.62403.
97. Schwabe, L., Hermans, E.J., Joëls, M., and Roozendaal, B. (2022). Mechanisms of memory under stress. Neuron *110*, 1450–1467. https://doi.org/10.1016/J.NEURON.2022.02.020.
98. Lupien, S.J., Fiocco, A., Wan, N., Maheu, F., Lord, C., Schramek, T., and Tu, M.T. (2005). Stress hormones and human memory function across the lifespan. Psychoneuroendocrinology *30*, 225–242. https://doi.org/10.1016/J.PSYNEUEN.2004.08.003.

99. Li, H.Q., Jiang, W., Ling, L., Pratelli, M., Chen, C., Gupta, V., Godavarthi, S.K., and Spitzer, N.C. (2024). Generalized fear after acute stress is caused by change in neuronal cotransmitter identity. Science *383*, 1252–1259. https://doi.org/10.1126/SCIENCE.ADJ5996/SUPPL_FILE/SCIENCE.ADJ5996_MDAR_REPRODUCIBILITY_CHECKLIST.PDF.

100. Cooper, S.E., Grillon, C., and Lissek, S. (2018). Impaired discriminative fear conditioning during later training trials differentiates generalized anxiety disorder, but not panic disorder, from healthy control participants. Compr. Psychiatry *85*, 84–93. https://doi.org/10.1016/J.COMPPSYCH.2018.07.001.

101. Lissek, S., Kaczkurkin, A.N., Rabin, S., Geraci, M., Pine, D.S., and Grillon, C. (2014). Generalized anxiety disorder is associated with overgeneralization of classically conditioned fear. Biol. Psychiatry *75*, 909–915. https://doi.org/10.1016/J.BIOPSYCH.2013.07.025.

102. Kaczkurkin, A.N., Burton, P.C., Chazin, S.M., Manbeck, A.B., Espensen-Sturges, T., Cooper, S.E., Sponheim, S.R., and Lissek, S. (2017). Neural Substrates of Overgeneralized Conditioned Fear in PTSD. Am. J. Psychiatry *174*, 125–134. https://doi.org/10.1176/APPI.AJP.2016.15121549.

103. Thome, J., Hauschild, S., Koppe, G., Liebke, L., Rausch, S., Herzog, J.I., Müller-Engelmann, M., Steil, R., Priebe, K., Hermans, D., et al. (2018). Generalisation of fear in PTSD related to prolonged childhood maltreatment: an experimental study. Psychol. Med. *48*, 2223–2234. https://doi.org/10.1017/S0033291717003713.

104. Keefe, J.R., Suarez-Jimenez, B., Zhu, X., Lazarov, A., Durosky, A., Such, S., Marohasy, C., Lissek, S., and Neria, Y. (2022). Elucidating behavioral and functional connectivity markers of aberrant threat discrimination in PTSD. Depress. Anxiety *39*, 891–901. https://doi.org/10.1002/DA.23295.

105. Jovanovic, T., Kazama, A., Bachevalier, J., and Davis, M. (2012). Impaired safety signal learning may be a biomarker of PTSD. Neuropharmacology *62*, 695–704. https://doi.org/10.1016/J.NEUROPHARM.2011.02.023.

106. Pamplona, F.A., Henes, K., Micale, V., Mauch, C.P., Takahashi, R.N., and Wotjak, C.T. (2011). Prolonged fear incubation leads to generalized avoidance behavior in mice. J. Psychiatr. Res. *45*, 354–360. https://doi.org/10.1016/J.JPSYCHIRES.2010.06.015.

107. Tsuda, M.C., Yeung, H.M., Kuo, J., and Usdin, T.B. (2015). Incubation of Fear Is Regulated by TIP39 Peptide Signaling in the Medial Nucleus of the Amygdala. J. Neurosci. *35*, 12152–12161. https://doi.org/10.1523/JNEUROSCI.1736-15.2015.

108. Lutz, B., Marsicano, G., Maldonado, R., and Hillard, C.J. (2015). The endocannabinoid system in guarding against fear, anxiety and stress. Nat. Rev. Neurosci. *16*, 705–718. https://doi.org/10.1038/NRN4036.

109. Petrie, G.N., Nastase, A.S., Aukema, R.J., and Hill, M.N. (2021). Endocannabinoids, cannabinoids and the regulation of anxiety. Neuropharmacology *195*, 108626. https://doi.org/10.1016/J.NEUROPHARM.2021.108626.

110. Weisser, S., Mueller, M., Rauh, J., Esser, R., Fuss, J., Lutz, B., and Haaker, J. (2022). Acquisition of threat responses are associated with elevated plasma concentration of endocannabinoids in male humans. Neuropsychopharmacology *47*, 1931–1938. https://doi.org/10.1038/S41386-022-01320-6.

111. Campolongo, P., Roozendaal, B., Trezza, V., Hauer, D., Schelling, G., McGaugh, J.L., and Cuomo, V. (2009). Endocannabinoids in the rat basolateral amygdala enhance memory consolidation and enable glucocorticoid modulation of memory. Proc. Natl. Acad. Sci. USA *106*, 4888–4893. https://doi.org/10.1073/PNAS.0900835106.

112. deRoon-Cassini, T.A., Bergner, C.L., Chesney, S.A., Schumann, N.R., Lee, T.S., Brasel, K.J., and Hillard, C.J. (2022). Circulating endocannabinoids and genetic polymorphisms as predictors of posttraumatic stress disorder symptom severity: heterogeneity in a community-based cohort. Transl. Psychiatry *12*, 48. https://doi.org/10.1038/S41398-022-01808-1.

113. Barlow, H.B. (1961). Possible Principles Underlying the Transformations of Sensory Messages (Sensory Communication).

114. Sa-Couto, L., and Wichert, A. (2020). Storing Object-Dependent Sparse Codes in a Willshaw Associative Network. Neural Comput. *32*, 136–152. https://doi.org/10.1162/NECO_A_01243.

115. Palm, G., Knoblauch, A., Hauser, F., and Schüz, A. (2014). Cell assemblies in the cerebral cortex. Biol. Cybern. *108*, 559–572. https://doi.org/10.1007/S00422-014-0596-4.

116. Olshausen, B.A., and Field, D.J. (2004). Sparse coding of sensory inputs. Curr. Opin. Neurobiol. *14*, 481–487. https://doi.org/10.1016/J.CONB.2004.07.007.

117. Lin, A.C., Bygrave, A.M., De Calignon, A., Lee, T., and Miesenböck, G. (2014). Sparse, decorrelated odor coding in the mushroom body enhances learned odor discrimination. Nat. Neurosci. *17*, 559–568. https://doi.org/10.1038/NN.3660.

118. Robotka, H., Thomas, L., Yu, K., Wood, W., Elie, J.E., Gahr, M., and Theunissen, F.E. (2023). Sparse ensemble neural code for a complete vocal repertoire. Cell Rep. *42*, 112034. https://doi.org/10.1016/J.CELREP.2023.112034.

119. Rolls, E.T., and Tovee, M.J. (1995). Sparseness of the neuronal representation of stimuli in the primate temporal visual cortex. J. Neurophysiol. *73*, 713–726. https://doi.org/10.1152/JN.1995.73.2.713.

120. Feigin, L., Tasaka, G., Maor, I., and Mizrahi, A. (2021). Sparse Coding in Temporal Association Cortex Improves Complex Sound Discriminability. J. Neurosci. *41*, 7048–7064. https://doi.org/10.1523/JNEUROSCI.3167-20.2021.

121. Alreja, A., Nemenman, I., and Rozell, C.J. (2022). Constrained brain volume in an efficient coding model explains the fraction of excitatory and inhibitory neurons in sensory cortices. PLoS Comput. Biol. *18*, e1009642. https://doi.org/10.1371/JOURNAL.PCBI.1009642.

122. Lee, H., Battle, A., Raina, R., and Ng, A. (2007). Efficient sparse coding algorithms. Adv. Neural Inf. Process. Syst.

123. Willshaw, D.J., Buneman, O.P., and Longuet-Higgins, H.C. (1969). Non-Holographic Associative Memory. Nature *222*, 960–962. https://doi.org/10.1038/222960a0.

124. Tsodyks, M.V., and Feigel'man, M.V. (1988). The Enhanced Storage Capacity in Neural Networks with Low Activity Level. Europhys. Lett. *6*, 101–105. https://doi.org/10.1209/0295-5075/6/2/002.

125. Levy, W.B., and Baxter, R.A. (1996). Energy efficient neural codes. Neural Comput. *8*, 531–543. https://doi.org/10.1162/NECO.1996.8.3.531.

126. Treves, A., and Rolls, E.T. (1991). What determines the capacity of autoassociative memories in the brain? Netw.: Comput. Neural Syst. *2*, 371–397. https://doi.org/10.1088/0954-898X_2_4_004.

127. Poo, C., and Isaacson, J.S. (2009). Odor representations in olfactory cortex: "sparse" coding, global inhibition, and oscillations. Neuron *62*, 850–861. https://doi.org/10.1016/J.NEURON.2009.05.022.

128. Olshausen, B.A., and Field, D.J. (1996). Natural image statistics and efficient coding. Network *7*, 333–339. https://doi.org/10.1088/0954-898X/7/2/014.

129. Rozell, C.J., Johnson, D.H., Baraniuk, R.G., and Olshausen, B.A. (2008). Sparse coding via thresholding and local competition in neural circuits. Neural Comput. *20*, 2526–2563. https://doi.org/10.1162/NECO.2008.03-07-486.

130. Dana, H., Sun, Y., Mohar, B., Hulse, B.K., Kerlin, A.M., Hasseman, J.P., Tsegaye, G., Tsang, A., Wong, A., Patel, R., et al. (2019). High-performance calcium sensors for imaging activity in neuronal populations and microcompartments. Nat. Methods *16*, 649–657. https://doi.org/10.1038/S41592-019-0435-6.

131. Dana, H., Mohar, B., Sun, Y., Narayan, S., Gordus, A., Hasseman, J.P., Tsegaye, G., Holt, G.T., Hu, A., Walpita, D., et al. (2016). Sensitive red protein calcium indicators for imaging neural activity. eLife *5*, e12727. https://doi.org/10.7554/eLife.12727.

132. Krashes, M.J., Koda, S., Ye, C.P., Rogan, S.C., Adams, A.C., Cusher, D.S., Maratos-Flier, E., Roth, B.L., and Lowell, B.B. (2011). Rapid,

reversible activation of AgRP neurons drives feeding behavior in mice. J. Clin. Invest. *121*, 1424–1428. https://doi.org/10.1172/JCI46229.

133. Dong, A., He, K., Dudok, B., Farrell, J.S., Guan, W., Liput, D.J., Puhl, H.L., Cai, R., Wang, H., Duan, J., et al. (2022). A fluorescent sensor for spatiotemporally resolved imaging of endocannabinoid dynamics in vivo. Nat. Biotechnol. *40*, 787–798. https://doi.org/10.1038/s41587-021-01074-4.

134. Swiech, L., Heidenreich, M., Banerjee, A., Habib, N., Li, Y., Trombetta, J., Sur, M., and Zhang, F. (2015). In vivo interrogation of gene function in the mammalian brain using CRISPR-Cas9. Nat. Biotechnol. *33*, 102–106. https://doi.org/10.1038/NBT.3055.

135. Wang, W.X., and Lefebvre, J.L. (2022). Morphological pseudotime ordering and fate mapping reveal diversification of cerebellar inhibitory interneurons. Nat. Commun. *13*, 3433. https://doi.org/10.1038/S41467-022-30977-2.

136. Madisen, L., Zwingman, T.A., Sunkin, S.M., Oh, S.W., Zariwala, H.A., Gu, H., Ng, L.L., Palmiter, R.D., Hawrylycz, M.J., Jones, A.R., et al. (2010). A robust and high-throughput Cre reporting and characterization system for the whole mouse brain. Nat. Neurosci. *13*, 133–140. https://doi.org/10.1038/NN.2467.

137. Zhang, F., Aravanis, A.M., Adamantidis, A., De Lecea, L., and Deisseroth, K. (2007). Circuit-breakers: optical technologies for probing neural signals and systems. Nat. Rev. Neurosci. *8*, 577–581. https://doi.org/10.1038/NRN2192.

138. Stahlberg, M.A., Ramakrishnan, C., Willig, K.I., Boyden, E.S., Deisseroth, K., and Dean, C. (2019). Investigating the feasibility of channelrhodopsin variants for nanoscale optogenetics. Neurophotonics *6*, 015007. https://doi.org/10.1117/1.NPh.6.1.015007.

139. Park, S., Jung, J.H., Karimi, S.A., Jacob, A.D., and Josselyn, S.A. (2022). Opto-extinction of a threat memory in mice. Brain Res. Bull. *191*, 61–68. https://doi.org/10.1016/J.BRAINRESBULL.2022.10.012.

140. Fanselow, M.S. (1980). Conditioned and unconditional components of post-shock freezing. Pavlov J. Biol. Sci. *15*, 177–182. https://doi.org/10.1007/BF03001163.

141. Chaudun, F., Python, L., Liu, Y., Hiver, A., Cand, J., Kieffer, B.L., Valjent, E., and Lüscher, C. (2024). Distinct μ-opioid ensembles trigger positive and negative fentanyl reinforcement. Nature *630*, 141–148. https://doi.org/10.1038/S41586-024-07440-X.

142. Kim, C.K., Yang, S.J., Pichamoorthy, N., Young, N.P., Kauvar, I., Jennings, J.H., Lerner, T.N., Berndt, A., Lee, S.Y., Ramakrishnan, C., et al. (2016). Simultaneous fast measurement of circuit dynamics at multiple sites across the mammalian brain. Nat. Methods *13*, 325–328. https://doi.org/10.1038/nmeth.3770.

143. Verret, L., Mann, E.O., Hang, G.B., Barth, A.M.I., Cobos, I., Ho, K., Devidze, N., Masliah, E., Kreitzer, A.C., Mody, I., et al. (2012). Inhibitory interneuron deficit links altered network activity and cognitive dysfunction in Alzheimer model. Cell *149*, 708–721. https://doi.org/10.1016/J.CELL.2012.02.046.

STAR★METHODS

KEY RESOURCES TABLE

REAGENT or RESOURCE	SOURCE	IDENTIFIER
Antibodies		
guinea pig anti-cFos	Synaptic Systems	Cat# 226 308; RRID:AB_2905595
rabbit anti-cFos	Synaptic Systems	Cat# 226 008; RRID:AB_2891278
chicken anti-GFP	Aves	Cat#: GFP-1010; RRID:AB_2307313
goat anti-RFP	Rockland Immunochemicals	Cat# 200-101-379; RRID:AB_2744552
rabbit anti-RFP	Rockland Immunochemicals	Cat# 600-401-379; RRID:AB_2209751
rabbit anti-PV	Swant	Cat# PV27; RRID:AB_2631173
guinea pig-anti-PV	Swant	Cat# GP72; RRID:AB_2665495
Mouse anti-HA-tag	BioShop	TAG002
goat anti-rabbit Alexa Fluor 568	Invitrogen	Cat# A-11011; RRID:AB_143157
goat anti-chicken Alexa Fluor 488	Invitrogen	Cat# A-11008; RRID:AB_143165
goat anti-guinea pig Alexa Fluor 647	Invitrogen	Cat# A-21450; RRID:AB_2535867
goat anti-rabbit Alexa Fluor 647	Invitrogen	Cat# A-21245; RRID:AB_2535813
goat anti-guinea pig Alexa Fluor 568	Invitrogen	Cat# A-11075; RRID:AB_2534119
goat anti-mouse Alexia Fluor 488	Invitrogen	Cat# A-11122; RRID:AB_221569
Bacterial and virus strains		
pAAV-RAM-d2TTA::TRE-EGFP-WPREpA	Sørensen et al.[48]	RRID:Addgene_84469
pHSV-NpACY	Rashid et al.[51]	N/A
pHSV-FAAH-TdT	Morena et al.[32]	N/A
pHSV-TdT	This paper	N/A
pAAV-CAG-FLEX-GCaMP7f-WPRE	Dana et al.[130]	RRID:Addgene_104496
pAAV-CaMKIIα-jGCaMP7f	This paper	N/A
pAAV-Syn-NES-jRCaMP1a-WPRE-SV40	Dana et al.[131]	RRID:Addgene_100848
pAAV-hSyn-DIO-hM4Di-mCherry	Krashes et al.[132]	RRID:Addgene #44362
pAAV-hSyn-DIO-hM3Dq-mCherry	Krashes et al.[132]	RRID:Addgene #44361
pAAV-hSyn-DIO-mCherry	http://n2t.net/addgene:50459	RRID:Addgene #50459
pAAV-FLEX-SaCas9-U6-sgFAAH	Balsevich et al.[71]	N/A
pAAV-FLEX-SaCas9-U6-sgFAAH-ctrl	Balsevich et al.[71]	N/A
pAAV-CaMKIIα-iCre	This paper	N/A
pAAV-EF1α-DIO-ChRmine-mScarlet-WPRE	Marshel et al.[81]	RRID:Addgene #130998
pAAV-GRAB_eCB2.0	Dong et al.[133]	RRID:Addgene #164604
pAAV-DIO-GRAB_eCB2.0	Dong et al.[133]	RRID:Addgene # 164606
pAAV-DIO-GRAB_eCBmut	Dong et al.[133]	RRID: Addgene #164607
pAAV-U6-DIO-sgCB1R$_{control}$-CMV-TdT	This paper	N/A
pAAV-U6-DIO-sgCB1R$_{knockdown}$-CMV-TdT	This paper	N/A
pAAV-pMecp2-SpCas9-spA	Swiech et al.[134]	RRID:Addgene_60957
pAAV-CMV-FLEX-SaCas9-U6-sgCNR1	Gunduz-Cinar et al.[84]	RRID:Addgene_209196
pAAV-CMV-FLEX-SaCas9-U6-sgRosa26	Gunduz-Cinar et al.[84]	RRID:Addgene_159914
Chemicals, peptides, and recombinant proteins		
4-hydroxytamoxifen (4-OHT)	Toronto Research Chemicals	Cat#H954725; CAS:68047-06-3
4'6'-diamidino-2-phenylindole (DAPI)	Sigma	Cat#D9542; CAS:28718-90-3
Cremaphore EL	Sigma	Cat#C5135; CAS:61791-12-6
Doxycycline (DOX)	Bio-Serv	S4159
DREADD agonist 21 (C21)	Tocris	Cat# 6422

(*Continued on next page*)

Continued		
REAGENT or RESOURCE	SOURCE	IDENTIFIER
CORT	Sigma	cat# 27840
RU486	Sigma	cat# M8046
DO34	Gift from dr. M. van der Stelt	CAS no. 1848233-58-8
LEI-401	Gift from dr. M. van der Stelt	CAS no. 2393840-15-6
URB597	Cayman Chemical	Cat# 10046, CAS no. 546141-08-6
Metyrapone	Bio-Connect	cat# HY-B1232, CAS no. 54-36-4
Critical commercial assays		
CORT ELISA	Abcam	Cat# AB108821
Experimental models: Cell lines		
HEK-293 cells	ATCC	CRL-1573
Experimental models: Organisms/strains		
Mouse: C57BL/6NTac	Taconic Bioscience	RRID:IMSR_TAC:b6
Mouse: 129S6/SvEvTac	Taconic Bioscience	RRID:IMSR_TAC:129sve
Mouse: TRAP2 ($Fos^{2A\text{-}iCreER}$)	Jackson Lab	RRID:IMSR_JAX:03032
Mouse: Ai14 (B6.Cg-Gt(ROSA)26Sor$^{tm14(CAG\text{-}TdTomato)Hze/J}$)	Jackson Lab	RRID:IMSR_JAX:007914
Mouse: 129P2-Pvalb$^{tm1(cre)Arbr}$/J	Jackson Lab	RRID:IMSR_JAX: 017320
Mouse: B6J.Cg-Ssttm3.1(flpo)Zjh/AreckJ	Jackson Lab	RRID:IMSR_JAX:031629
Oligonucleotides		
Pvalb probes (see Table S1)	This paper; Molecular Instruments	N/A
GAD2 probes	Wang and Lefebvre[135]; Molecular Instruments	N/A
Cnr1 probes (see Table S1)	This paper; Molecular Instruments	N/A
Software and algorithms		
Freeze frame	Actimetrics	http://actimetrics.com/products/freezeframe/
ImageJ	National Institutes of Health	RRID:SCR_003070
Graphpad Prism 8.4.3	GraphPad Software	RRID:SCR_002798
Python	Python Software	RRID:SCR_008394
Ethovision XT version 13.0	Noldus, The Netherlands	RRID:SCR_004074
pCLAMP with ClampFit Software	Molecular Devices v10.7	RRID:SCR_011323
Other		
Cannula	HRS Scientific	C313G/SPC + C313I/SPC

EXPERIMENTAL MODEL AND STUDY PARTICIPANT DETAILS

Mice

Adult (> 10 weeks of age) male and female F1 hybrid (C57BL/6NTac x 129S6/SvEvTac) wild-type (WT) mice were used for all experiments, unless specified otherwise. Mice were bred at the Hospital for Sick Children and group housed (4 per cage) on a 12 h light/dark cycle with food and water available *ad libitum* at an ambient temperature of 22 ± 2°C. Behavioral experiments took place during the light-phase. Cage mates of the same sex were randomly assigned to experimental groups. All procedures were conducted in accordance with policies of the Hospital for Sick Children Animal Care and Use Committee and conformed to both Canadian Council on Animal Care (CCAC) and National Institutes of Health (NIH) Guidelines on Care and Use of Laboratory Animals.

PV-Cre knockin driver transgenic mice (C57BL/6NTac; 129P2-Pvalb$^{tm1(cre)Arbr}$/J; "PV-Cre mice") that express Cre recombinase in PV^{+} neurons, without disrupting endogenous PV expression, were originally generated by Dr. Silvia Arber (FMI) and obtained from Jackson Lab (JAX stock #017320). F1 hybrids used in experiments were obtained by crossing homozygous PV-Cre mice (C57BL/6NTac background) with 129S6/SvEvTac mice. Husbandry procedures for this line were identical to those described for WT mice.

Targeted Recombination in Active Populations mice ("TRAP2" mice; Jackson Labs, stock #030323), in which 4-hydroxy-tamoxifen (4-OHT)-dependent-recombinase Cre^{ERT2} is expressed in an activity-dependent manner from the loci of the activity-dependent immediate early gene cFos, were crossed with transgenic mice expressing a floxed-stop TdT cassette (AI14 mice, Jackson Labs, stock

#007914).[47,136] In offspring expressing both transgenes (TRAP2 × TdT mice), neurons in which cFos is induced shortly after 4-OHT injection permanently express TdT.

METHOD DETAILS

Viruses

All viruses were made in-house.

HSV

We used replication-defective herpes simplex viruses (HSV) to manipulate sparse subsets of LA neurons. HSV is naturally neurotrophic and, following LA microinjection, transfects approximately 10-30% of principal (excitatory) neurons. Transgene expression peaks 3-4 days after HSV microinjection.[19] HSV titers were approximately 1.0 x 10^8 infectious units/ml. The following HSV constructs were used:

HSV-NpACY

We used HSV-NpACY to bidirectionally manipulate the activity of sparse subsets of excitatory neurons. HSV-NpACY contains both the blue-light (BL) sensitive excitatory opsin, channelrhodopsin-2 (ChR2-H134R) fused to enhanced yellow fluorescent protein (eYFP), and the red-light (RL) sensitive inhibitory opsin, halorhodopsin 3.0 (NpHR3.0). These opsins are spectrally compatible, allowing for neuronal excitation by ChR2 with BL (473 nm) and neuronal silencing by NpHR3.0 with RL (660 nm).[51] Opsin genes were connected in the viral vector using a 2A self-cleavage linker (p2A) and expression was driven by the endogenous HSV promoter IE4/5. Distinct activation of ChR2 and NpHR3.0 has been indicated in hippocampal neurons.[137] Moreover, there is minimal cross-talk between BL (488 nm), which increases, and RL (594 nm, 639 nm), which decreases the activity of neurons expressing this construct.[51,138,139]

HSV-FAAH-TdT

FAAH (fatty acid amide hydrolase) hydrolyzes anandamide (AEA), such that FAAH overexpression would decrease AEA levels. HSV-FAAH-TdT was used to overexpress FAAH in the LA, as previous.[32] Expression of FAAH was driven by the IE4/5 promoter, and TdT by the CMV promoter. A virus expressing TdT alone (HSV-p1005-TdT; HSV-TdT) was used as control.

AAV

Adeno-associated viruses (AAV) were used to label, manipulate, or record neuronal activity. Transgene expression peaks 3-4 weeks after AAV microinjection and remains relatively stable for weeks. Mice were microinjected with AAV 21d before behavioral experiments. AAVs (DJ serotype) were generated in HEK293T cells with the AAV-DJ Helper Free Packaging System (Cell Biolabs, In., cat# VPK-400-DJ) using the manufacturer-suggested protocol. Viral particles were purified using Virabind AAV Purification Kit (Cell Biolabs, Inc., cat# VPK-140). AAV titers were approximately 1.0 x 10^{11} infectious units/ml. The following AAV constructs were used:

AAV(DJ)-RAM-d2TTA::TRE-eGFP-WPREpA (AAV-RAM-GFP)

To tag highly active neurons during an experience, we used the RAM (Robust Activity Marking) viral system in which removal of doxycycline (DOX) from the diet is the inducer.[48] The RAM AAV viral vector tags active neurons (via a synthetic activity-regulated promoter, P_{RAM}, made up of minimal AP-1, Fos and Npas4 promoter sequences) in a temporally-specific fashion (via a doxycycline (DOX)-dependent modified Tet-Off system, pAAV-RAM-d2TTA::TRE-EGFP-WPREpA). pAAV-RAM-d2TTA::TRE-eGFP-WPREpA was a gift from Dr. Yingxi Lin (UT Southwestern)(Addgene plasmid # 84469; http://n2t.net/addgene:84469; RRID:Addgene_84469). Expression of GFP was prevented in the presence of DOX in the chow (40 mg/kg), but removal of DOX+ food opened the tagging window, such that active neurons expressing AAV-RAM-GFP expressed GFP.

AAV(DJ)-CAG-FLEX-GCaMP7f-WPRE (AAV-FLEX-GCaMP7f)

To record calcium activity in PV+ neurons, we expressed AAV-FLEX-GCaMP7f in PV-Cre mice. pGP-AAV-CAG-FLEX-jGCaMP7f-WPRE was a gift from Dr. Douglas Kim & GENIE Project (Addgene plasmid # 104496; http://n2t.net/addgene:104496; RRID:Addgene 104496).

AAV(DJ)-CaMKIIα-jGCaMP7f (AAV-CaMKIIα-GCaMP7f)

To record calcium activity in excitatory neurons, we used a green fluorescent calcium sensor, GCaMP7f expressed under the αCaMKII promoter. Inserts were obtained from pGP-AAV-syn-jGCaMP7f-WPRE (Addgene #104488) and cloned into pAAV-CaMKIIα, which was made from pAAV-CaMKIIα-hChR2(H134R)-eYFP (Addgene #26969) where ChR2(H134R) was removed.

AAV(DJ)-Syn-NES-jRCaMP1a-WPRE-SV40 (AAV-RCaMP1a)

To record calcium activity using a red fluorescent calcium sensor, RCaMP1 was expressed under the hSyn promoter. pAAV.Syn.NES.jRCaMP1a.WPRE.SV40 was a gift from Dr. Douglas Kim & GENIE Project (Addgene plasmid #100848; http://n2t.net/addgene:100848; RRID:Addgene_100848).[131]

AAV(DJ)-hSyn-DIO-hM4Di-mCherry (AAV-DIO-hM4Di), AAV(DJ)-hSyn-DIO-hM3Dq-mCherry (AAV-DIO-hM3Dq)

We used AAV-DIO-hM4Di to inhibit and AAV-DIO-hM3Dq to activate PV+ neurons in the LA in PV-Cre mice. As a control we used AAV(DJ)-hSyn-DIO-mCherry (AAV-DIO-mCherry). All plasmids (pAAV-DIO-hM4Di, RRID:Addgene #44362, pAAV-DIO-hM3Dq,

RRID:Addgene #4436; pAAV-DIO-mCherry, RRID:Addgene #50459) were gifts from Dr. Bryan Roth (UNC). Expression of hM4Di or hM3Dq-mCherry in Cre+ neurons was driven by the hSyn promoter.

AAV(DJ)-CMV-FLEX-SaCas9-U6-sgFAAH (AAV-sgFAAH)

AAV-sgFAAH was used to knock down FAAH in LA neurons.[71] Expression of SaCas9 and sgFAAH was driven by the U6 promoter in the presence of iCre. As a control, we expressed AAV(DJ)-CMV-FLEX-SaCas9-U6-sgFAAH-ctrl (AAV-sgFAAH-ctrl). Expression of this virus was visualized by immunohistochemical staining of the HA-tagged protein. We detected the HA tag exclusively in the LA neurons. pAAV-CMV-FLEX-SaCas9-U6-sgFAAH (Addgene plasmid # 209197; http://n2t.net/addgene:209197; RRID:Addgene_209197) and pAAV-CMV-FLEX-SaCas9-U6-sgFAAH-ctrl were gifts from Dr. Larry Zweifel (UW).

AAV(DJ)-CaMKIIα-iCre (AAV-iCre)

iCre under the αCaMKII promoter was used to express the iCre recombinase in excitatory neurons to induce recombination between LoxP sites of target constructs in a cell-type specific manner. Inserts were obtained from pAAV-CAG-iCre (Addgene #51904) and cloned into pAAV-αCaMKII, which was made from pAAV-αCaMKII-hChR2(H134R)-eYFP (Addgene #26969) where ChR2 was removed.

AAV(DJ)-EF1α-DIO-ChRmine-mScarlet-WPRE (AAV-EF1α-DIO-ChRmine)

ChRmine, a red-light sensitive excitatory opsin with large photocurrents and millisecond spike-timing fidelity,[81] was expressed in Cre+ neurons to optogenetically activate distinct neurons. pAAV-Ef1a-DIO-ChRmine-mScarlet-WPRE was a gift from Dr. Karl Deisseroth (Stanford)(Addgene #130998).

AAV(DJ)-hSyn-GRAB_eCB2.0 (AAV-GRAB_eCB2.0)

We used a GRAB_eCB2.0 biosensor, a type of GPCR activation-based fluorescent sensor that is inserted in the plasmalemma and preserves the binding site structure of the GPCRs from which they are derived. The GRAB_eCB2.0 biosensor allows lipid eCB messengers to be sensed in the same subcellular compartment where endogenous CB1Rs are expressed. This sensor changes fluorescence when bound to eCB. AAV-GRAB-eCB2.0 was used in WT mice to assess eCB binding on neurons, or AAV(DJ)-hSyn-DIO-GRAB_eCB2.0 (AAV-DIO-GRAB_eCB2.0) in PV-Cre mice to assess eCB binding on PV^+ neurons.[83] As a control, we used AAV(DJ)-DIO-GRAB_eCBmut (AAV-DIO-GRAB_eCBmut) that expresses a mutated sensor that does not change fluorescence upon eCB binding. Expression of (DIO-)GRAB-eCB2.0/mut in neurons was driven by the hSyn promoter. All plasmids (pAAV-GRAB_eCB2.0, RRID:Addgene #164604; pAAV-DIO-GRAB_eCB2.0, RRID:Addgene # 164606; pAAV-DIO-GRAB_eCBmut, RRID: Addgene #164607) were a gift from Dr. Yulong Li (Peking University).

AAV(DJ)-U6-DIO-sgCB1R$_{knockdown}$-CMV-TdT (AAV-DIO-sgCB1R$_{KD}$)

To knock down the CB1R in a cell type specific manner, we developed four short guide (sg) $CB1R_{KD}$ constructs that were driven by the U6 promoter in the presence of Cre recombinase. In combination with SpCas9 in PV-Cre mice, this mixture of sg$CB1R_{KD}$ constructs knocked down the CB1 receptor in PV^+ neurons. As a control, we expressed AAV(DJ)-U6-DIO-sg$CB1R_{control}$-CMV-TdT (AAV-DIO-sg$CB1R_{Ctrl}$), which contained a non-targeting sgRNA sequence.

AAV(DJ)-pMeCP2-SpCas9-spA (AAV-Cas9)

AAV-Cas9 expressed SpCas9 under the neuronal MeCP2 promoter. Combined with abovementioned sg$CB1R_{KD}$, these constructs form a ribonucleoprotein complex to knock down the expression of the CB1 receptor. This was a gift from Dr. Feng Zhang (MIT)(Addgene plasmid # 60957; http://n2t.net/addgene:60957; RRID:Addgene_60957.[134]

AAV1-CMV-FLEX-SaCas9-U6-sgCNR1 (AAV-FLEX-sgCNR1-KD)

AAV-sgCNR1-KD was used to knock down Cnr1 in LA neurons.[84] Expression of SaCas9 and sgCNRa-KD was driven by the U6 promoter in the presence of iCre. As a control, we expressed AAV1-CMV-FLEX-SaCas9-U6-sgRosa26 (AAV-FLEX-sgRosa26-Ctrl). Both AAV-FLEX-sgCNR1 and AAV-FLEX-sgRosa26-Ctrl were gifts from Dr. Larry Zweifel (UW) (RRID:Addgene_209196, RRID:Addgene_159914).

Stress manipulations

Restraint stress

30 min before threat training, mice were placed individually in a 50 ml falcon tube with breathing holes for 30 min. The falcon tube was well ventilated but prevented mice from turning or ambulating, without exerting pressure on their bodies. Following exposure to restraint, mice were transferred to the threat conditioning chamber. Control mice remained in their home cage until threat conditioning.

CORT treatment

Mice received systemic CORT treatment (3 mg/kg, i.p.) or VEH 30 min before threat training.

Experimental design

Discriminative threat conditioning and testing

Threat conditioning experiments were divided into three phases. In the CS- exposure phase, mice were placed in a conditioning chamber (Context A, rectangular chamber with a grid floor; Med Associates) and 2 min later presented a 30-sec auditory CS- (2.8 kHz, 82 dB, pure tone). 24 h later, mice were returned to the same conditioning chamber, and 2 min later, presented with a 30-sec auditory CS+ (7.5 kHz, 82 dB, pips) which co-terminated with a 2-sec foot shock (0.4 mA). Mice remained in the chamber for an additional 30 sec before being returned to home-cage. To test specific and generalized memory, 24 h later, mice were place in a novel context B (white, triangular chamber with white plastic floors, distinct from the conditioning chamber) and, after 2 min,

presented with a 1 min CS- or CS+ (counterbalanced, 1-min inter-tone interval). Mouse behavior was recorded with overhead cameras and FreezeFrame v.3.32 software (Actimetrics). Memory was assessed by measuring percent time spent freezing (cessation of all movement except respiration[140] during CS+ and CS- presentation via automated procedures or hand-scoring of videos (in optogenetic experiments). Videos were hand-scored by an experimenter blinded to the treatment of the mice. We observed no effects of CS presentation order during the test, therefore, groups were averaged. A generalization score was computed for each mouse ($Freezing_{CS-}$/($Freezing_{CS+}$ + $Freezing_{CS-}$).

For the sake of clarity, we did not present baseline (pre-CS) freezing scores for these experiments. Overall, mice showed low freezing when placed in a novel context and, across experiments, we observed no difference between groups in baseline freezing.

Specific details for experiments deviating from the standard protocol are described below:

Plasma CORT assessment

To assess circulating plasma CORT levels after different manipulations, mice were anesthetized using isoflurane, quickly decapitated, and trunk blood was collected 30 min after threat training. 30 min before threat training, mice were restraint stressed or injected with CORT/VEH. An untrained, home cage control group was used to assess baseline plasma CORT levels.

Triple activity tag experiment

For the triple tag experiments in which we tagged the populations of neurons active during training, CS+ testing and CS- testing, we used three tagging techniques (TRAP2 transgenic mice, AAV-RAM-GFP and cFos immunohistochemistry). TRAP2 transgenic mice were crossed with TdT-reporter mice and microinjected with AAV-RAM-GFP. Mice were maintained on a DOX containing diet, to prevent GFP expression from the RAM construct (see below for details). To tag the population of neurons active during training, mice were administered 4-OHT (i.p.) immediately following threat training. Mice remained undisturbed for 72h to ensure sufficient time for the induction of TdT to occur. To tag the population of neurons active during CS+ test, mice were removed from a DOX+ diet 24h before CS+ test. To tag the CS- active population, mice were given a CS- test, and 90 min later, mice perfused and cFos visualized by immunohistochemistry.

Allocation of threat memory

HSV-NpACY expresses both a blue light-sensitive ChR2, an excitatory opsin, and a red light-sensitive NpHR3.0, an inhibitory opsin. We excited the sparse population of NpACY+ neurons with blue light (BL+, 473 nm, 20 Hz, 5 msec pulses, 10 mW peak, 10% duty cycle) for 30 sec before onset of the auditory CS in the training session, to bias the allocation of these neurons to the engram ensemble. To examine whether these neurons were preferentially allocated to the engram ensemble supporting this thread memory, we tested mice by delivering the CS twice, once in the presence of red light (RL+, 660 nm, 7 mW square pulse for the duration of the CS) to silence NpACY+ neurons and once in the absence of red light (RL-) in a counterbalanced order. The laser (Laserglow, LRS-0473) was connected to a split optic fiber (Precision Fiber Products) and was controlled by a waveform generator (Agilent Technologies, 33500B) to provide BL and RL stimulation.

Chemogenetic modulation of threat memory

1h before threat training, mice were systemically injected with the DREADD ligand C21 (or a vehicle control for Figures S3B–S3D) to activate or inhibit DREADD-expressing neurons.

Intra-LA drug microinjection

To assess the effects of manipulating 2-AG or AEA levels in the LA, URB597, DO34 and LEI-401 were microinjected directly into the LA before threat training (1 μl bilaterally). Control mice were microinjected with the same volume of a vehicle solution.

AEA and 2-AG measurements

AEA and 2-AG levels were measured in the amygdala in mice after threat training (with and without CORT) or mice taken directly from the home cage (as a control). Mice were anesthetized with isoflurane 15 min after training, quickly decapitated, and the amygdala was dissected out, snap frozen on dry ice and stored at -80 °C until further analyses were conducted.

Fiber photometry recordings

For fiber photometry recordings, habituation, training and testing occurred as above, but mice were attached to an optic fiber during all phases of the procedure.

Drug administration

Corticosterone (CORT)

To mimic aspects of the stress response, corticosterone (CORT) was systemically administered (i.p.) 30 min before threat conditioning. CORT (Sigma-Aldrich, St. Louis, MO, USA, cat# 27840) was dissolved in EtOH (16 mg/ml) and 20x diluted in saline and administered at a dose of 3 mg/kg body weight. Injection volume was 100 μl/10 g body weight. Control mice received an equal volume of EtOH:saline ("VEH").

Metyrapone

To inhibit the synthesis of glucocorticoids, metyrapone was systemically administered (i.p.) 30 min before restraint stress. Metyrapone (Bio-Connect, The Netherlands, cat# HY-B1232) was dissolved in polyethylene glycol (PEG) (50 mg/ml), and diluted in saline, and 50 mg/kg (i/p.) was systemically administered. Control mice received an equal volume of PEG:saline.

RU486

RU486 was administered to investigate the involvement of glucocorticoid receptors in the behavioral effects of CORT. For systemic injections, RU486 (Sigma-Aldrich, St. Louis, MO, USA, cat# M8046) was dissolved in 100% EtOH, 20x diluted in saline and 40 mg/kg

(i.p.) was systemically administered, 30 min before CORT injection or restraint stress. Control mice received an equal volume of EtOH:saline. For LA microinjection, RU486 was dissolved in DMSO and then diluted 1:10 in saline. 100 ng RU486 was microinjected.

DO34

To inhibit the synthesis of 2-AG, DO34 was microinjected into the LA. A stock solution was prepared by dissolving DO34 in DMSO and then diluted 1:1 in Tween-20 to a final concentration of 20 mM. Stock solution was further diluted in saline to the desired concentrations (200-700 μg). DO34 was synthesized as previously reported.[67]

LEI-401

LEI-401 was used to inhibit the synthesis of AEA. A stock solution was prepared by dissolving LEI-401 in DMSO and then diluted 1:1 in Tween-20 to a final concentration of 20 mM. Stock solution was further diluted in saline to the desired concentrations. For systemic injections, LEI-401 was injected at a dose of 30 mg/kg body weight. For LA microinjections, 0, 200, 400, 600 μg LEI-401 was microinjected bilaterally. LEI-401 was synthesized as previously reported.[69]

URB597

URB597 was used to inhibit the hydrolysis of AEA. For URB597 microinjection (20 ng, Cayman Chemical, Cedarlane, Burlington, ON, Canada, cat# 10046), a stock solution was prepared by dissolving URB5979 in polyethylene glycol (PEG), and then diluted 1:1 in Tween-90, URB597 or a vehicle (5% polyethylene glycol, 5% Tween-90, 90% saline) were microinjected into the LA 45 min before training.

Doxycycline (DOX)

Doxycycline (DOX) chow (40 mg/kg, Bio-Serv, cat no. S4159) was provided *ad libitum* 24h before microinjection of AAV-RAM-GFP. DOX+ food was replaced by standard chow 24h before the tagging event, and DOX food was replaced immediately after the tagging event.

4-hydroxytamoxifen (4-OHT)

4-hydroxytamoxifen (4-OHT, 25 mg/kg, i.p., Toronto Research Chemicals, cat no. H954725) was injected immediately after threat conditioning to induce recombination in TRAP2 mice. 4-OHT was first mixed with 100% ethanol (40 mg/ml) and vortexed vigorously. The solution was then poured into a 50°C chamber, vortexing every 15 min for approximately 2h until fully dissolved. An equal part Cremaphore was added to create a stock solution, which was mixed at a 1:1 ratio with PBS.

DREADD agonist 21 (C12)

C21 dihydrochloride (Tocris, cat# 6422) was prepared as a stock solution of 10 mg/ml in dH_2O and stored at -20 °C. Stock solution was later thawed and diluted 1:10 in PBS. Diluted C21 was administered 1 h before threat training (1.0 mg/kg, i.p.) to activate or inhibit DREADD-expressing neurons.

Surgery

Mice were pre-treated with atropine sulfate (0.1 mg/kg, i.p.), anesthetized with isoflurane-oxygen mix (3 % isoflurane for initial induction and 1-2.5 % through nose cone thereafter), and administered the analgesic meloxicam (4 mg/kg, s.c). Mice were topically administered lidocaine around the incision site, and holes were drilled bilaterally above the LA (to target AP -1.3 mm, ML ±3.4 mm, DV -4.7 mm relative to bregma for the LA). Viral vectors were slowly microinjected (HSV; 1.5 μl, AAV; 0.5-1.5 μl, rate of 0.1 μl/min) via glass micropipettes connected to Hamilton syringes (10 μl) via polyethylene tubing. Following microinjection, micropipettes were maintained in place for an additional 10 min to ensure viral diffusion. Bilateral optical fibers, when required, were implanted at the same coordinates as used for the virus injection (for fiber photometry experiments), or 0.5 mm above virus injection site (for optogenetic experiments). Optical fibers were constructed in-house by cutting a fiber (15 mm long, 200 μm diameter, 0.39 numerical aperture, Thorlabs, FT200EMT, Newton, NJ), polishing the fiber, and fixing it into a zirconia ferrule (1.25 mm, Thorlabs, CFLC230-10) with epoxy resin. Optical fibers were secured in place using screws and dental cement.

Following both microinjections, mice were administered 0.9% saline (1.0 ml, s.c.) and placed in a clean cage on a heating pad to recover.

For cannula experiments, mice were implanted with 31 G guide cannulae (HRS scientific, Canada) above the LA and secured to the skull using screws and black dental cement. A dummy cannula extending 0.25 mm from the guide cannula (same length as the internal cannula used for microinjections) was inserted. Post-surgery procedures and care were the same as described above.

Histology

Perfusion and tissue preparation

Mice were perfused transcardially with chilled 1x PBS followed by 4% paraformaldehyde (PFA), fixed in PFA overnight at 4 °C, and transferred to 30% sucrose solution for at least 24 h. Brains were sectioned coronally using a cryostat (Leica CM1850), and a 1:4 sampling fraction was used to obtain 4 sets of 50 μm sections. Sections for immunohistochemistry were stored in 0.1% NaN_3 solution until staining.

For all experiments involving virus microinjections, only mice showing strong bilateral expression (i.e., expression limited to the LA and observable in a minimum of 3 brain sections) were included in statistical analyses. For experiments in which we microinjected multiple viruses, only mice expressing both transgenes in the same region were included in the final data set. For optogenetic and fiber photometry experiments, only mice with optic fibers placed correctly above the opsin-expressing region of interest were

included in the final data set. For experiments in which we implanted cannula, correct placement was verified by ink injection and by post-hoc identification of cannula tracks in brain slices.

Immunohistochemistry

Immunofluorescence staining was conducted as previously described.[51] Free-floating sections were blocked with PBS containing 4% normal goat serum and 0.5% Triton-X for 1 h at RT. Afterwards, sections were incubated with primary antibodies in fresh blocking solution: guinea pig anti-cFos (1:1000, Synaptic Systems, cat# 226 308), rabbit anti-cFos (1:1000, Synaptic Systems, cat# 226 008), chicken anti-GFP (1:1000, Aves, cat# GFP-1010), goat anti-RFP (1:1000, Rockland Immunochemicals, cat #200-101-379), rabbit anti-RFP (1:1000, Rockland Immunochemicals, cat #600-401-379), rabbit anti-PV (1:1000, Swant, cat# PV27), guinea pig-anti-PV (1:1000, Swant, cat# GP72), mouse anti-HA-tag (1:100, BioShop, cat# TAG002) for 24 h at 4 °C. Sections were washed three times for 5 min each with PBS containing 0.1% Tween-20 (PBS-T), then incubated with PBS-T containing secondary antibodies (1:500): goat anti-rabbit Alexa Fluor 568 (Invitrogen, cat# A-11011), goat anti-chicken Alexa Fluor 488 (Invitrogen, cat# A-11008), goat anti-guinea pig Alexa Fluor 647 (Invitrogen, cat# S-11226), goat anti-rabbit Alexa Fluor 647 (Invitrogen, cat# A-21245), goat anti-guinea pig Alexa Fluor 568 (Invitrogen, cat# A-11075), or goat anti-mouse Alexa Fluor 488 (Invitrogent, cat# A-11122) for 2 h at RT. Sections were washed with PBS, counterstained with DAPI (1:10000, ThermoFisher), mounted on gel-coated slides, and cover-slipped with Vectashield mounting medium (MJS BioLynx Inc., cat#H-1000).

Imaging

Images were obtained using a confocal laser scanning microscope (LSM 710; Zeiss). For visualization of virus expression, images were acquired with a 20x objective. For image quantification, z-stacks were acquired using a 40x objective (N.A. = 1.3; 10-40 slices with a 1 μm step size). For all experiments involving quantification of the number of cells positive for immunofluorescence, all images were acquired using identical imaging parameters (laser power, photomultiplier gain, pinhole, and detection filter settings) in a minimal number of imaging sessions (when possible, in one session). For each experiment, imaging parameters were set using a sample section from a control mouse.

Quantification

For cell counting experiments, every fourth section was assessed for the marker(s) of interest. For each mouse, cells were counted manually in Fiji (NIH) using at least 5 images from separate sections and averaged. cFos+, TRAP2+, RAM+ neurons were counted, and counts were normalized against the number of $DAPI^+$ cells in that LA. Chance of colocalization of population A and B was calculated as follows: $Coloc_{chance}$ = (# neurons population A | DAPI) x (# neurons population B | DAPI) x 100%. The observed colocalization was calculated as follows: $Coloc_{observed}$ = (# of neurons A+ + B+ | DAPI) x 100%. The fold change (observed/chance) was calculated as follows: $Coloc_{observed}/Coloc_{chance}$.

All experimenters were unaware of mouse treatment group.

Plasma CORT measurements

Trunk blood was centrifuged at 10.000 rpm for 20 min at 4 °C. Plasma was then stored at -20 °C until corticosterone analyses with an ELISA kit (Cayman Chemical Co., AnnArbor, MI, cat# 501320) was conducted according to the manufacturer's instructions. Samples were tested in duplicate and diluted between 1:4 to 1:50 to ensure that corticosterone levels fit on the linear portion of the standard curve. The detection limit of the assay was 8.2-5000 pg/ml at 80% binding. Measurements were performed by the Analytical Facility for Bioactive Molecules, The Hospital for Sick Children, Toronto, Canada.

Fiber photometry

A fiber photometry system (FP3002; Neurophotometrics; San Diego, CA) was used to assess fluorescence in freely-behaving mice. The 560 nm, 470 nm and 405 nm LEDs were used as light sources for illuminating RCaMP1a, GCaMP7f/GRAB_eCB2.0 and isosbestic activities, respectively. The intensities of the source LEDs were set to obtain ± 50 μW power at the tips of optical fibers. Alternating pulses of 405 nm, 470 nm (and, if applicable, 560 nm) light were delivered at 60 (or 90) Hz, and time-locked to behavior using a custom-built Arduino. Similarly to what has been done before,[83,141,142] for all recordings, 405, 470 (and 560) signals were deinterleaved and background fluorescence was subtracted to obtain ΔF/F values, by using the following equation: $(F_{470/560} - F_{isosbestic})/F_{isosbestic}$. We applied a lowpass filter (0.005 Hz) and a highpass filter (2 Hz) to the photometry signal. The average ΔF/F values per group were then calculated across all mice. The normalization against $F_{isosbestic}$ corrects for differences in measured GCaMP fluorescence due to fiber placement, virus expression, and motion. Each trace was z-scored around the shock onset to produce a measure of fluorescence that is normalized to its own baseline.

For the RCaMP and GRAB_eCB signal, there is no isosbestic signal to which it can be normalized (as was the case for the GCaMP recordings). Yet, RCaMP and GRAB_eCB signals were still corrected to the 405 nm channel to correct for changes in measured intensity (due to movement artefacts or differences in virus expression).

Peak photometry transients for each mouse were detected using the scipy.find_peaks() function.

For the calculation of the lag cross correlation, ΔF/F values from the entire recording were shifted ± 100 frames. Correlations for each shift were computed, and plotted as a function of their shift. Implicit in the Pearson correlation calculation is normalization to the mean and standard deviation of both fluorescence traces, thus normalizing for differences in measured intensity between sessions and mice.

AEA and 2-AG measurement

Amygdala were dissected and stored at -80°C, and total protein, AEA and 2-AG content were measured according to.[143] Brain samples were subjected to a lipid extraction process, and the AEA and 2-AG content of the lipid extracts was determined using isotope-dilution liquid chromatography-mass spectrometry. Samples were injected onto a Kinetex XB-C18 50 x 3.0 mm column (Phenomenex, Torrance, CA) on an Agilent 1290 LC system coupled to a Sciex Q-Trap 5500 mass spectrometer (AB Sciex, Concord, ON, Canada) operated in positive mode. Data was collected and analysed using SCIEX Analyst v1.7. Measurements were performed by the Analytical Facility for Bioactive Molecules, The Hospital for Sick Children, Toronto, Canada.

Single-molecule fluorescence in situ hybridization

HCR amplification-based smFISH was performed following previous protocols.[135] HCR 3.0 probes were purchased from Molecular Instruments for *Pvalb*, *Cnr1*, *GAD2*. All subsequent steps were performed under RNAse-free considerations and using buffers prepared with DEPC-treated water.

Mice were perfused and tissue collected following similar protocols as above. Postfixed brains were cryopreserved in 30% sucrose for 24h, embedded and frozen in OCT cryopreservation agent (Tissue-Tek), and coronal sections were collected at 18 μm onto slides (VWR Superfrost Plus). Tissue sections were dried on coverslips for 2h at RT, and stored at -80°C until smFISH was performed.

Coverslips were permeabilized in 70% ethanol ON at 4°C then dried before clearing with 4% SDS at RT for 30 min, 3x washes in PBS, and 3x rinses in 70% ethanol. Primary probe hybridization was performed at 2 nM probe concentration in HCR hybridization buffer (Molecular Instruments) at 37°C overnight. 3x washes were performed in wash buffer (Molecular Instruments) at 37°C, followed by 3x washes in 2x SSCT (0.1% Triton-X) at RT.

HCR hairpins were prepared by heating to 95 °C for 90 s, and allowed to cool to room temperature slowly over 30 min to form metastable hairpins. Amplification solutions were prepared by mixing 2 μL of H1 and 2 μL of H2 hairpin in 100 μL of amplification buffer for each sample (Molecular Instruments). Washed samples were pre-amplified in 100 μL of amplification buffer for 10 min, and amplified in 100 μL of hairpin solution overnight at RT in the dark. Following amplification, samples were washed 3 x in 2X SSC, stained with 1:10000 DAPI (ThermoFisher) for 10 min at RT, and mounted in Fluoromount G.

Electrophysiology

Brain slice preparation

Mice were deeply anesthetized with isoflurane, and the brain was rapidly extracted in ice-cold, dissection artificial cerebrospinal fluid (ACSF; containing, in mM: 205 sucrose, 26 $NaHCO_3$, 10 glucose, 3 KCl, 1.25 NaH_2PO_4, 0.5 $CaCl_2$, 5 $MgCl_2$), saturated with 95% O_2 / 5% CO_2. 300 μm coronal slices containing the anterior LA were sectioned on a vibratome (Leica, VT1200S) and then placed in a holding chamber in standard ACSF (containing, in mM: 124 NaCl, 24 $NaHCO_3$, 10 glucose, 3 KCl, 1.25 NaH_2PO_4, 2 $CaCl_2$, 1 $MgCl_2$) saturated with 95% O_2 / 5% CO_2. Slices were recovered initially at 33.0°C for 30 min then transferred to room temperature for a minimum of 1.0 h before recording.

Whole-cell patch clamp recordings

Following the recovery period, slices were transferred into a submersion-style recording chamber, perfused constantly with recording ACSF (28.0°C), saturated with 95% O_2/ 5% CO_2, at 3.0 mL/min. The recording ACSF contained NBQX (10 μM; HelloBio, HB0443) to block AMPARs, thereby isolating inhibitory postsynaptic currents (IPSCs). Slices were visualized under a 40x water immersion objective on an upright microscope equipped with IR-DIC optics (Nikon). LA pyramidal neurons (PNs) were identified based on soma morphology and action potential firing properties (see below). Whole-cell recordings were obtained using borosilicate glass micropipettes with a tip resistance of 2.5 – 5 MΩ. The micropipettes were filled with an internal solution containing the following (in mM): 120 K-gluconate, 10 Na_2-phosphocreatine, 20 KCl, 10 HEPES, 0.5 EGTA, 4 Mg-ATP, 0.3 Na_3-GTP, pH 7.2-7.3 (adjusted with KOH), 285-290 mOsm/L. Analog signals were amplified with a Multiclamp 700B amplifier (Molecular Devices) and subsequently digitized at 20 kHz via a BNC 2110 A/D board (National Instruments). Recordings were monitored online using WinLTP software. Following break-in, a series of 100 ms current steps of increasing intensity (100, 150, 250, 300 pA) were delivered at a 10 s interval in current clamp mode to assess firing properties. Only cells which exhibited adapting trains of action potentials, characteristic of PNs in the LA, were used for experiments. IPSCs were then recorded in voltage clamp mode. Cells were voltage-clamped at -75 mV throughout the recording (no correction for liquid junction potential). A 5 mV test pulse was delivered to the cell every 10 s to monitor series resistance (R_s). Recordings were discarded if R_s varied by more than 20% over the analyzed recording period. For optically-evoked IPSCs (oIPSCs), light pulses (0.1 ms duration) were delivered through a 40X water immersion objective (Nikon Fluor, 0.8 NA) centered on the soma of the recorded neuron. Light pulses were generated by a xenon lamp source (Sutter, Lambda XL) coupled to the microscope via a liquid light guide and filtered through a FITC filter cube (Nikon). Spontaneous IPSCs (sIPSCs) were recorded in the absence of any light stimulation for a 3 – 5 min period. oIPSC and sIPSC recordings were performed on slices bathed in either standard ACSF (control) or in ACSF containing WIN55,212-2 (5 μM; Tocris, 1038).

Analysis

Analysis of oIPSCs and sIPSCs was performed using Clampfit (Molecular Devices, v10.7). Traces were first low-pass filtered at 2 kHz using an 8-pole Bessel filter. For oIPSC analysis, a baseline period -590 to 0 ms prior to the first light pulse was subtracted from the entire 10 s sweep on a sweep-by-sweep basis. oIPSC amplitude for both pulses was then measured from the baseline-subtracted

sweeps, and the average PPR from 4 sweeps was quantified. sIPSCs were analyzed using template-matching to detect events. The template and matching threshold were kept identical for all cells. Events were then individually manually accepted or rejected, with the experimenter unaware of treatment condition.

HEK cells

HEK-293 cells were cultured in complete DMEM medium, supplemented with 10% (v/v) FBS, 100 U/ml penicillin and 0.1 mg/ml streptomycin, and maintained at 37°C (95% O_2, 5% CO_2). Cells were grown in 24-well plates containing coverslips, and 24h after plating cells, cell transfection was conducted with Lipofectamine 3000 (Thermofisher) according to the manufacturer's protocols. 12h later, 1 μl virus was added to each well. After 36h, cells were fixed using PFA, imaged, and fluorophore expression was quantified.

QUANTIFICATION AND STATISTICAL ANALYSIS

No formal statistical tests were used to predetermine sample sizes, but sample sizes were similar to those reported in previous publications.[22,23,51] Data were analyzed by t-test, one-, two- or three-way analysis of variance (ANOVA), with repeated measures when appropriate. To analyze significant interactions or main effects, ANOVAs were followed by Tukey or Sidak post-hoc comparisons. For data in Figures 1A, 1B, and 1G–1I, sex was included as an independent variable, but as there was no main or interaction effect of sex on the dependent variables, all subsequent data were analyzed without regarding sex as a factor. For experiments targeting specific brain areas (with cannula or virus), mice were included in statistical analysis only if they showed bilateral hits in the LA (of virus and/or optrode and/or cannula). No mice were excluded from statistical analysis, except when clear technical issues occurred (i.e. no protein/mRNA expression anywhere in the section). All data points in the graphs represent separate mice, except for Figure 6C, where each datapoint represents one image containing >100 cells (max. 3 images per well), and Figures 6F and S6D, where recordings from individual neurons were plotted (from 4-5 mice per group). Mice were pseudo-randomly assigned to all groups, to achieve roughly equivalent group sizes. During data collection and quantification, experimenters were blinded to group assignment. The key findings (memory generalization, increased engram size, role of PV^+ neurons, and the rescue of memory generalization by CB1R KO in PV^+ neurons) were replicated at least three times throughout the study, and different methods were used to provide converging evidence for the role CB1R in stress-induced memory generalization. Statistical analyses were performed using Graphpad Prism (version 8.0.1) and significance was set at $p < 0.05$.

CellPress

Supplemental figures

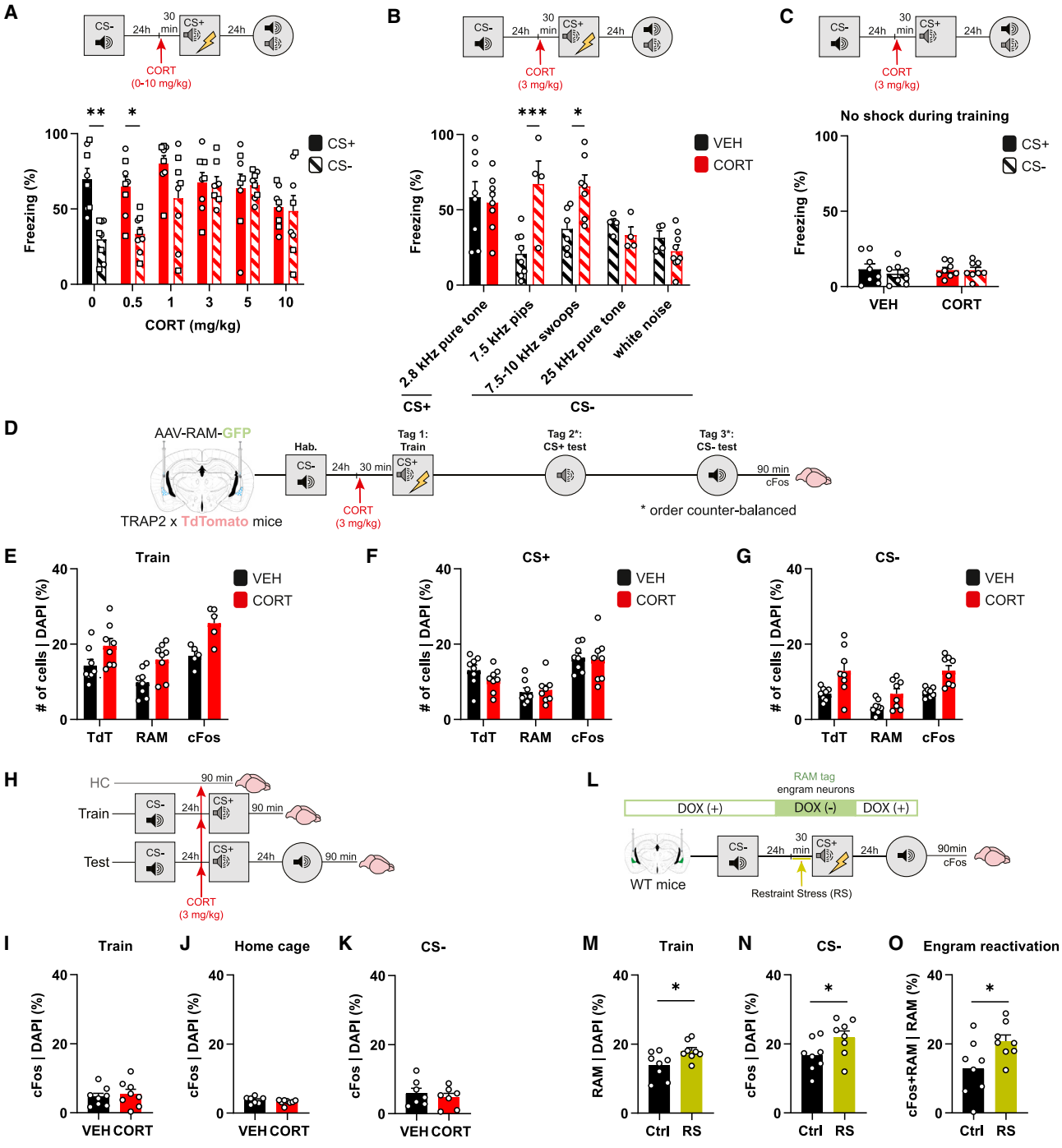

Figure S1. Systemic CORT or acute RS increase threat memory generalization and induce a larger, less-sparse engram ensemble in the LA, related to Figures 1 and 2

(A) Mice were trained in a threat discrimination paradigm in which a CS+ (7.5 kHz pips) but not the CS− (2.8 kHz pure tone) was paired with a foot shock. During memory test, mice were re-exposed to the CS− and CS+, and time spent freezing measured. Increasing doses of CORT systemically injected 30 min before training did not affect CS+ freezing at test, but higher doses of CORT (1–10 mg/kg, i.p.) increased CS− freezing (CORT dose × Tone: $F[5,42] = 2.73$, $p < 0.05$; CS+ vs. CS−: $p > 0.05$).

(legend continued on next page)

(B) VEH mice showed high freezing to CS+ (2.8 kHz pure tone), but low freezing to CS− as well as other auditory stimuli during the test. By contrast, CORT mice showed high CS+ freezing and also high freezing to CS− and other auditory stimuli that were perceptually close to the CS+ (7.5 kHz pips, 7.5–10 kHz swoops), but not to more distinct auditory stimuli (25 kHz pure tone or white noise) ($F[4,52] = 4.93$, $p < 0.01$).
(C) In the absence of a foot shock during training, VEH and CORT mice do not show freezing to either CS+ or CS− at test ($F[1,28] = 0.33$, $p > 0.05$).
(D) Experiment to assess different activity tagging strategies in the LA. TRAP2×TdT transgenic mice microinjected with AAV-RAM-GFP bilaterally in LA. Mice administered VEH or CORT 30 min before training, and neurons active during the different experimental phases (training, CS+ test, CS− test) tagged using different strategies (in a counterbalanced order). For TRAP2×TdT tag, mice injected with 4-OHT immediately after the tagging event (and then left undisturbed for subsequent 72 h). For the RAM-GFP tag, mice were removed from DOX food (DOX−) for 24 h before tagging event, and were placed back on the DOX-containing food (DOX+) immediately after event. For cFos tagging, mice were perfused 90 min after tagging event.
(E) With all tagging strategies, we observed an increase in the number of active cells after training in CORT mice (main CORT effect: $F[1,36] = 21.66$, $p < 0.0001$).
(F) Irrespective of tagging strategy or CORT treatment, no difference in number of active neurons after CS+ test (main CORT effect: $F[1,42] = 0.54$, $p > 0.05$).
(G) Irrespective of tagging strategy, CORT increased number of active neurons after CS− test (main CORT effect: $F[1,42] = 24.59$, $p < 0.0001$).
(H–K) (H) Experimental design to examine number of cFos+ neurons at different stages of above experiment but in mice that did not receive foot shock during training. No difference in the number of cFos+ neurons between VEH and CORT mice (I) in home cage ($t[13] = 1.27$; $p > 0.05$), (J) after training ($t[14] = 0.50$, $p > 0.05$), (K) or after CS+ exposure ($t[12] = 0.67$, $p > 0.05$).
(L–O) (L) Examining number of neurons active after training and CS− test in RS mice. Similar to CORT, RS increased number of (M) RAM-GFP+ (engram) neurons following training ($t[14] = 2.52$, $p < 0.05$), (N) neurons activated by CS− test ($t[14] = 2.16$, $p < 0.05$, and (O) reactivation of the training engram by the CS− test to a greater extent than in control (Ctrl) mice ([cFos+RAM]/RAM [%], $t[14] = 2.35$, $p < 0.05$).
CORT, corticosterone; CS, conditioned stimulus; DOX, doxycycline; HC, home cage; LA, lateral amygdala; RS, restraint stress; VEH, vehicle.

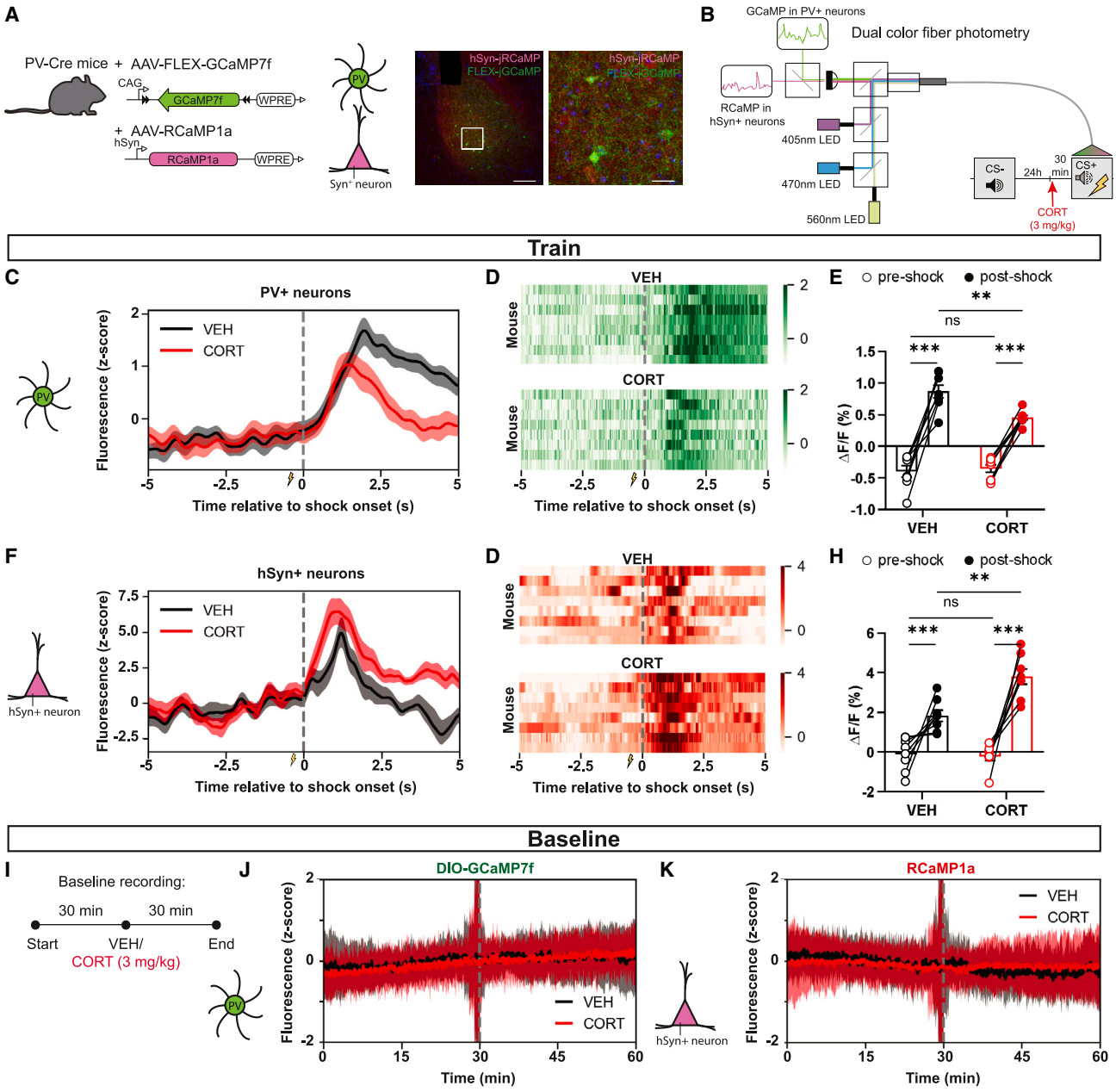

Figure S2. CORT decreases PV+ neuronal activity but increases hSyn+ neuronal activity during threat conditioning as assessed by dual-color fiber photometry, related to Figures 3A–3I

(A) (Left) PV-Cre mice microinjected with AAV-FLEX GCaMP7f and AAV-RCaMP1a to express the green and red genetically-encoded calcium indicators (GECIs) in PV+ or hSyn+ neurons, respectively. (Right) Representative viral expression and fiber placement. Scale bars, 100 μm and 15 μm.

(B) Schematic of dual-color fiber photometry in LA.

(C) Averaged fiber photometry traces from PV+ neurons during training.

(D) Heatmaps from individual mice.

(E) VEH mice showed an increase in GCaMP signal (Δf /f) before vs. after foot shock, while CORT mice showed blunted response after foot shock (and no difference before shock) (Treatment × Pre/Post-Shock: $F[1,14] = 9.90$, $p < 0.01$) (similar to the data presented in Figures 3D–3F).

(F) Averaged fiber photometry traces from hSyn+ LA neurons before and after foot shock during training.

(G) Heatmaps from individual mice.

(H) CORT potentiated RCaMP signal after foot shock (but no difference before foot shock) (Treatment × Pre/Post-Shock: $F[1,14] = 6.77$, $p < 0.05$) (similar to the data presented in Figures 3G–3I).

(I–K) (I) Baseline recording of PV-GCaMP and hSyn-RCaMP before and after VEH and CORT injection (i.p.) showed no effect on PV-GCaMP (J) or hSyn-RCaMP activity (K).

*$p < 0.05$, **$p < 0.001$, ***$p < 0.001$. CORT, corticosterone; LA, lateral amygdala; PV, parvalbumin; VEH, vehicle.

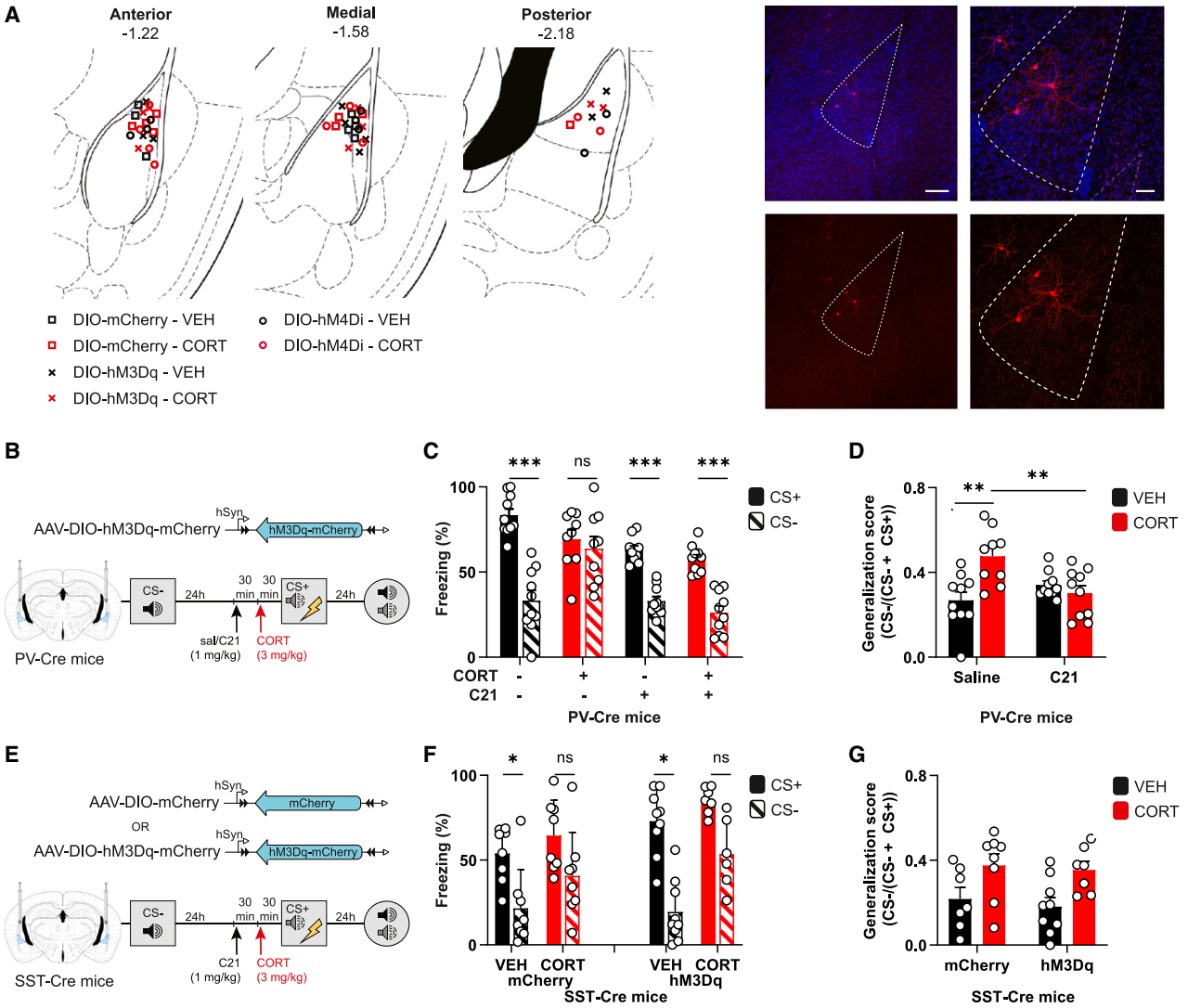

Figure S3. CORT-induced threat memory generalization; critical involvement of LA PV+ but not SST+ neurons, related to Figures 3J and 3K

(A) Schematic and histology overview of LA viral targeting, corresponding to data presented in Figure 3K. Scale bar, 250 μm (left) and 100 μm (right).

(B) Experimental design. PV-Cre mice microinjected with AAV-DIO-hM3Dq in the LA administered hM3Dq agonist C21 (1 mg/kg, i.p.) or saline (sal) 60 min before threat conditioning, and CORT or VEH 30 min before threat conditioning.

(C) CORT mice expressing hM3Dq in LA PV+ neurons treated with saline (rather than C21) showed threat memory generalization (high freezing to both CS+ and CS−) (CORT × Tone × C21 interaction test: $F[1,35] = 11.56$, $p > 0.05$). By contrast, CORT mice expressing hM3Dq in LA PV+ neurons treated with C21 to activate PV+ neurons showed a specific threat memory (greater freezing to the CS+ than CS−).

(D) Generalization scores also showed that activation of PV+ neurons by administration of C21 restored threat memory specificity in CORT mice (CORT × C21 interaction: $F[1,35] = 11.97$, $p < 0.001$).

(E) Experimental design. SST-Cre mice microinjected with AAV-DIO-hM3Dq or AAV-DIO mCherry in the LA administered C21 (1 mg/kg, i.p.) and VEH/CORT before threat conditioning.

(F and G) CORT-treated mice showed threat memory generalization, irrespective of hM3Dq expression or C21 administration (main CORT effect: $F[1,27] = 12.40$, $p < 0.001$) (F), and a higher generalization score than VEH-treated mice (main CORT effect: $F[1,27] = 11.28$, $p > 0.05$) (G), indicating LA SST neurons not critically involved in CORT-induced threat memory generalization.

*$p < 0.05$, **$p < 0.001$, ***$p < 0.001$. C21, compound 21; CORT, corticosterone; LA, lateral amygdala; PV, parvalbumin; SST, somatostatin; VEH, vehicle.

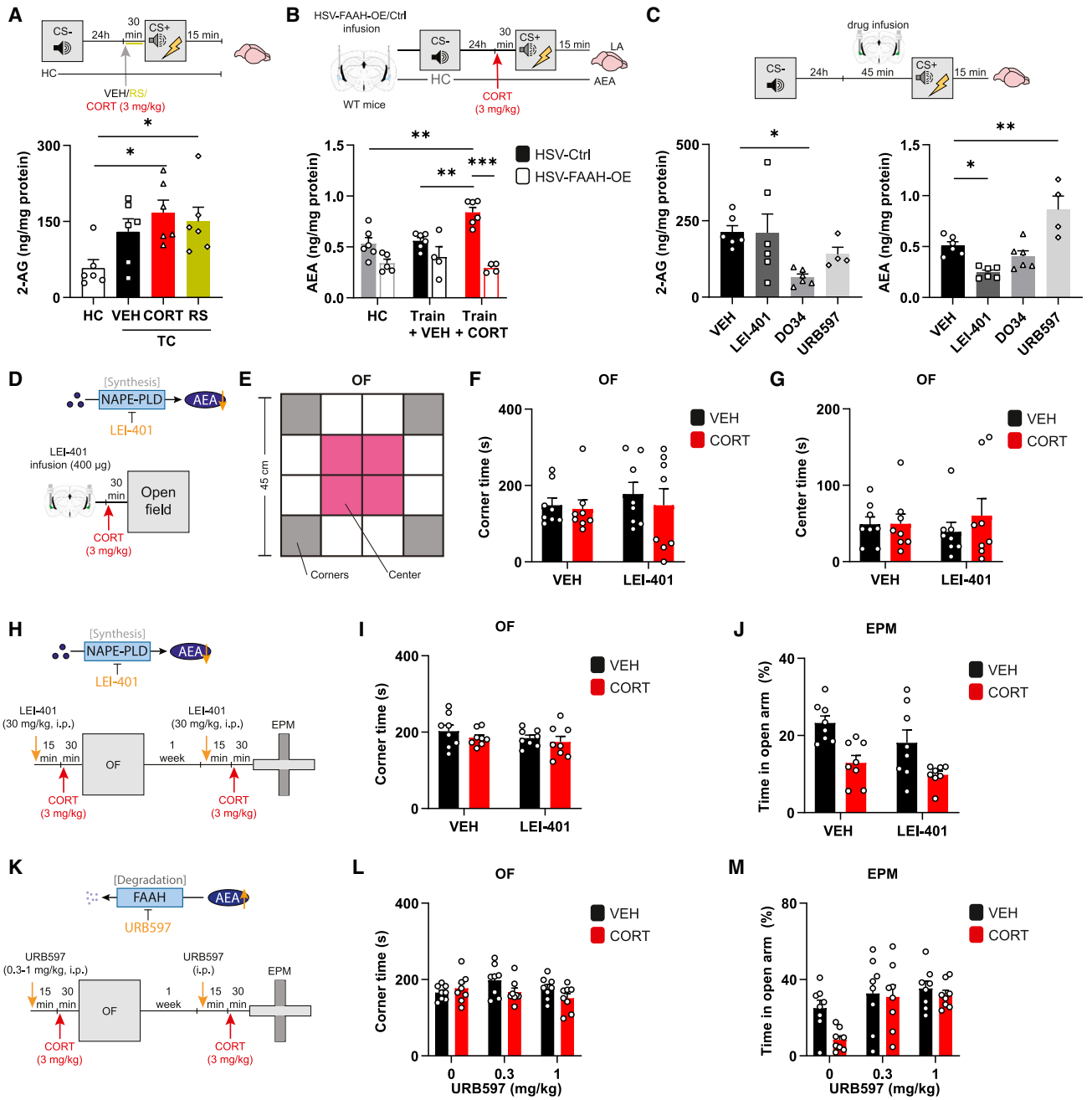

Figure S4. Validation of eCB manipulations and their effects on anxiety-like behavior in mice treated with CORT or VEH, related to Figure 4

(A) Amygdala 2-AG levels increased after threat training in mice treated with CORT or RS compared with HC mice ($F[3,20] = 3.971$, $p < 0.05$).

(B) Viral overexpression of FAAH (to decrease AEA levels in excitatory neurons) or control virus (HSV-TdT) microinjected in the LA of WT mice. Threat conditioned (TC) mice administered CORT showed increased amygdala AEA levels; restored by viral overexpression of FAAH (behavior × virus interaction: $F[2,25] = 6.87$, $p < 0.05$).

(C) Verification of agents used to manipulate eCB ligands. Amygdala 2-AG and AEA levels after mice microinjected with different agents and threat conditioned (TC). (Left) As expected, 2-AG synthesis inhibitor DO34 (200 µg) but not AEA synthesis inhibitor LEI-401 (400 µg) or AEA hydrolysis inhibitor URB597 (15 ng) decreased 2-AG levels ($F[3,18] = 3.84$, $p < 0.05$). (Right) As expected, AEA synthesis inhibitor LEI-401 before threat training decreased AEA levels, and AEA hydrolysis inhibitor URB597 increased AEA levels ($F[3,18] = 16.24$, $p < 0.0001$), while 2-AG synthesis inhibitor DO34 did not affect AEA levels.

(D) Mice were microinjected with LEI-401 (or a vehicle [VEH]) into LA, then systemically administered CORT (3 mg/kg, i.p.) or VEH and placed in the center of an open field.

(E) Open field arena, with corners and center area highlighted.

(legend continued on next page)

(F and G) (F) All groups spent similar times in corner of open field (VEH + VEH, CORT + VEH, VEH + LEI-401, CORT + LEI-401) (CORT × LEI interaction effect: $F[1,28] = 0.10$, $p > 0.05$) and (G) center (CORT × LEI interaction effect: $F[1,28] = 0.75$, $p > 0.05$).

(H) Mice were systemically injected with LEI-401 (or VEH), followed by CORT (3 mg/kg, i.p.) (or VEH), and placed in open field. 1 week later, mice were treated again, and placed in an elevated plus maze.

(I) All groups spent similar times in corners of open field (VEH + VEH, CORT + VEH, VEH + LEI-401, LEI-401 + CORT) (LEI × CORT interaction: $F[1,28] = 0.08$, $p > 0.05$).

(J) CORT reduced time in open arms in elevated plus maze (main CORT effect: $F[1,28] = 18.39$, $p < 0.001$), but this was not affected by LEI-401 (LEI × CORT interaction: $F[1,28] = 0.22$, $p > 0.05$).

(K) Mice systemically injected with URB597 (or VEH), followed by CORT (3 mg/kg, i.p.) (or VEH) injection, and placed in an open field. 1 week later, mice were injected again and placed in an elevated plus maze.

(L) All groups showed similar time in corners of open field (URB597 × CORT interaction: $F[2,42] = 2.00$, $p > 0.05$).

(M) CORT did not affect time in the open arms of elevated plus maze (main CORT effect: $F[1,42] = 3.88$, $p < 0.05$), but time in open arms was increased by URB597 (main URB597 effect: $F[2,42] = 8.41$, $p < 0.001$).

$^{*}p < 0.05$, $^{**}p < 0.001$, $^{***}p < 0.001$. CORT, corticosterone; EPM, elevated plus maze; HC, home cage; OF, open field; RS, restraint stress; TC, threat conditioning; VEH, vehicle.

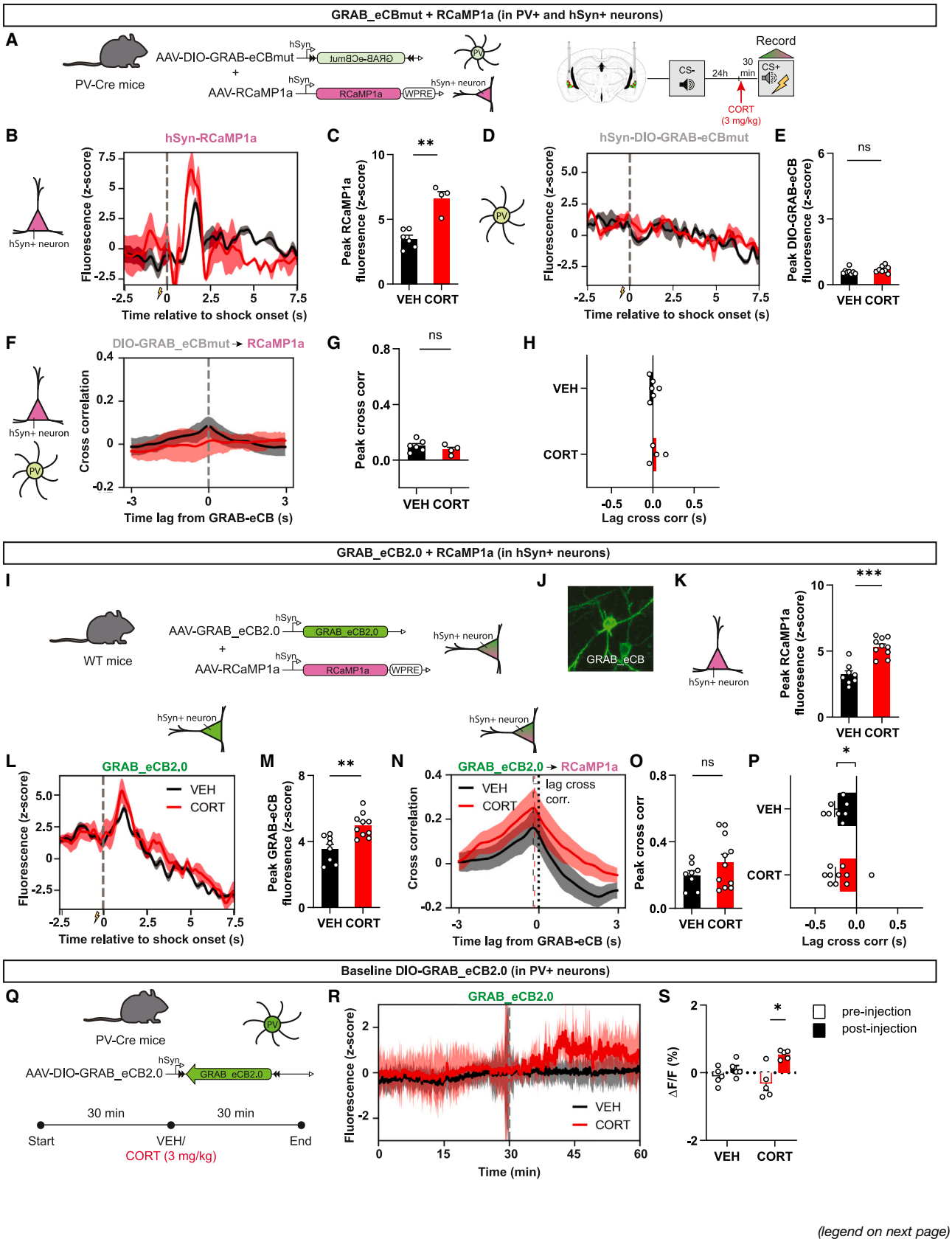

(legend on next page)

Figure S5. Control studies for GRAB-eCB sensors using fiber photometry, related to Figures 5F–5L

(A) (Left) PV-Cre mice were co-microinjected with control GRAB construct AAV-DIO-GRAB_eCBmut that does not change fluorescence with eCB binding, and AAV-RCaMP1a for fiber photometry recordings. (Right) Schematic of dual-color fiber photometry experiment targeting the LA bilaterally.

(B and C) (B) In response to foot shock 3 during training, CORT mice showed larger increase in ΔF/F from jRCaMP1a than VEH mice, (C) as also indicated by a higher RCaMP1a peak ($F[1,8] = 32.72$, $p < 0.001$).

(D and E) As expected, no change in fluorescence in CORT or VEH mice expressing control construct DIO-GRAB-eCBmut in PV+ neurons ($F[1,8] = 0.34$, $p > 0.05$).

(F) As expected, no cross-correlation between signals from DIO-GRAB_eCBmut and RCaMP1a in VEH or CORT mice.

(G and H) (G) No difference between correlation in VEH and CORT mice ($F[1,8] = 1.21$, $p > 0.05$), and (H) lag cross-correlation was not different from 0 (VEH: $F[1,5] = 0.002$, $p < 0.05$; CORT: $F[1,3] = 0.90$, $p > 0.05$).

(I) WT mice were co-microinjected with AAV-hSyn-GRAB_eCB2.0 and AAV-hSyn-RCaMP1a for fiber photometry recordings.

(J) Example of GRAB eCB2.0 expression.

(K) In response to foot shock during training, CORT mice showed larger increase in ΔF/F from hSyn-RCaMP1a than VEH mice ($F[1,16] = 35.40$, $p < 0.0001$).

(L and M) (L) Increase in hSyn-GRAB_eCB fluorescence higher in CORT mice than VEH mice (M) and higher peak GRAB-eCB fluorescence in CORT mice ($F[1,16] = 15.68$, $p < 0.001$).

(N and O) Cross-correlation between hSyn-GRAB_eCB2.0 and hSyn-RCaMP1a showed peak cross-correlation is similar in VEH and CORT mice ($F[1,34] = 1.12$, $p > 0.05$).

(P) In both VEH and CORT mice, peak correlation occurred when the RCaMP1a signal preceded GRAB_eCB signal (VEH: $F[1,7] = 38.07$, $p < 0.001$; CORT: $F[1,9] = 15.29$, $p < 0.001$).

(Q) Baseline recording of PV-GRAB_eCB2.0 with VEH and CORT injection.

(R and S) As expected, increase in baseline PV-GRAB-eCB2.0 binding after CORT injection (injection × CORT interaction: $F[1,16] = 6.00$, $p < 0.05$).

$^{*}p < 0.05$, $^{**}p < 0.001$, $^{***}p < 0.001$. CORT, corticosterone; eCB, endocannabinoids; LA, lateral amygdala; PV, parvalbumin; VEH, vehicle.

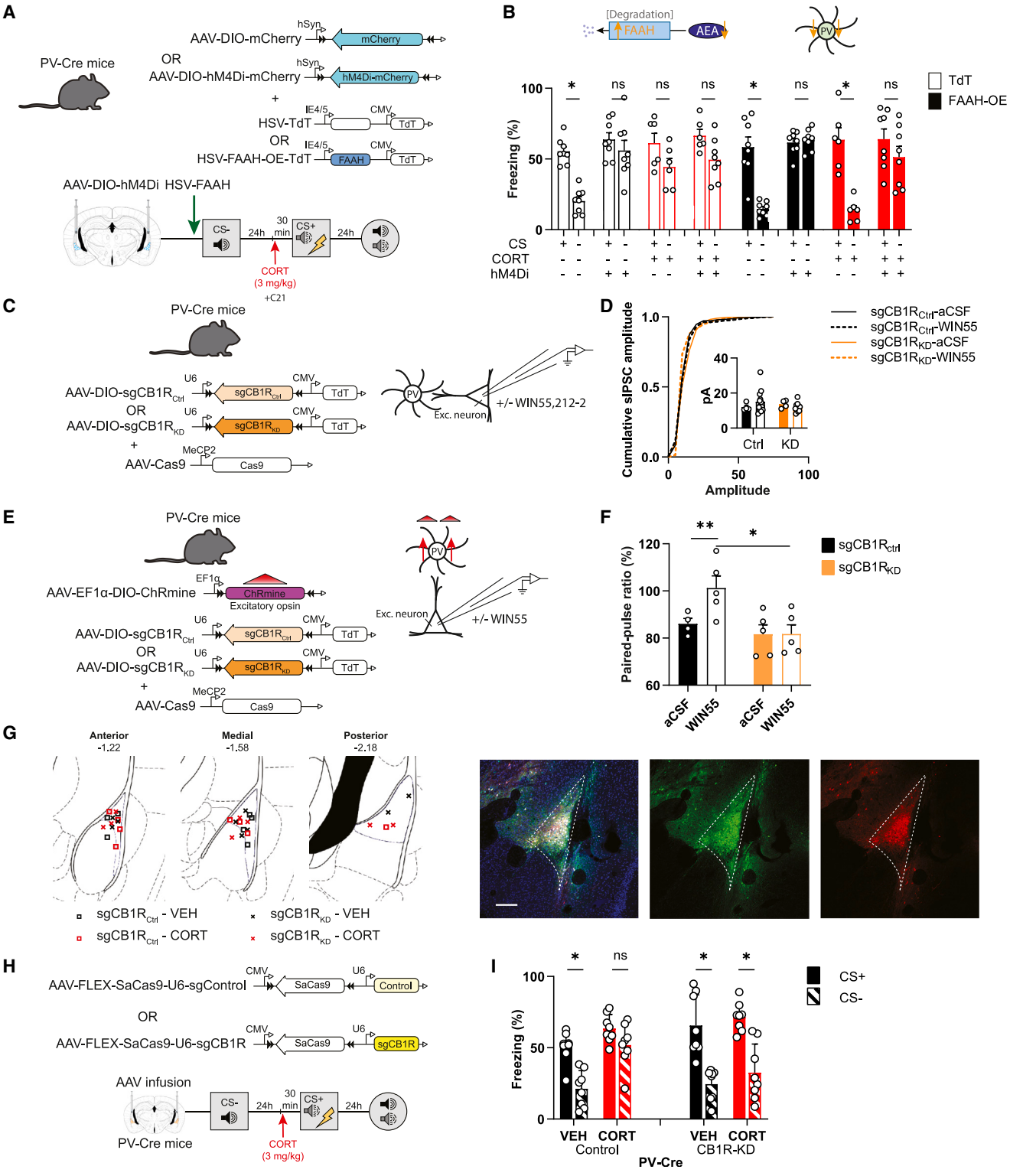

Figure S6. Critical role for LA PV+ neurons and CB1 receptor activation in CORT-induced threat memory generalization, related to Figure 6

(A) PV-Cre mice microinjected with either AAV-DIO-mCherry or AAV-DIO-hM4Di and 18 days later with HSV-TdT or HSV-FAAH-OE-TdT and threat conditioned. (B) Control mice (VEH injection, AAV-DIO-mCherry, HSV-TdT) showed specific threat memory (hM4Di × FAAH × CORT × Tone interaction effect: $F[3,49] = 2.87$, $p < 0.05$, VEH-mCherry-TdT-CS+ vs. VEH mCherry-TdT-CS−: $p < 0.05$), but CORT mice and mice with hM4Di activation of PV+ neurons showed threat memory

(legend continued on next page)

generalization. Expression of FAAH-OE prevented threat memory generalization in CORT mice, but not in CORT mice with hM4Di-induced silencing of PV+ neurons.

(C) AAV-DIO-sgCB1RCtrl or AAV-DIO-sgCB1RKD, and AAV-Cas9 were microinjected into LA of PV-Cre mice. In *ex vivo* brain slices, sIPSCs recorded from excitatory neurons in presence or absence of CB1 receptor agonist WIN55.

(D) Cumulative sIPSC amplitude and average sIPSC amplitude were unaffected by any treatment (Virus × WIN55 interaction: $F[1,6] = 1.65$, $p > 0.05$).

(E) AAV-EF1a-DIO-ChRmine and AAV-Cas9, as well as AAV-DIO-sgCB1RCtrl or AAV-DIO-sgCB1RKD, microinjected in LA of PV-Cre mice. Electrophysiological recordings conducted on excitatory neurons to measure the paired-pulse ratio (PPR) after PV+ neuron activation with optogenetic light pulse, in the presence and absence of WIN55.

(F) In the absence of WIN55, oIPSCs exhibited paired-pulse depression. Paired-pulse depression was attenuated in the presence of WIN55 in sgCB1RCtrl mice (Virus × WIN interaction: $F[1,7] = 7.66$, $p < 0.05$) (sgCB1RCtrl data is the same as presented in Figure 5E). In sgCB1RKD mice, oIPSC paired-pulse depression was not attenuated 4 by WIN55, validating functional knock down of CB1 receptors.

(G) Schematic overview and typical example of viral targeting of LA using our AAV-DIO-sgCB1RCtrl/KD virus, corresponding to data presented in Figure 6G. Scale bar, 250 μm.

(H) Different validated CRISPR construct that also knocked down CB1 receptors, AAV-FLEX-SaCas9-U6 sgControl and AAV-FLEX-SaCas9-U6-sgCB1R, microinjected into LA of PV-Cre mice, and 3 weeks later CORT and VEH mice were threat conditioned.

(I) Knocking down CB1 receptors in La PV+ neurons using these constructs restored CORT-induced memory generalization (CORT × Tone × KD interaction: $F[1,28] = 6.53$, $p < 0.01$).

$^{*}p < 0.05$, $^{**}p < 0.001$, $^{***}p < 0.001$. CB1, cannabinoid receptor 1; CORT, corticosterone; KD, knockdown; LA, lateral amygdala; PV, parvalbumin; VEH, vehicle.

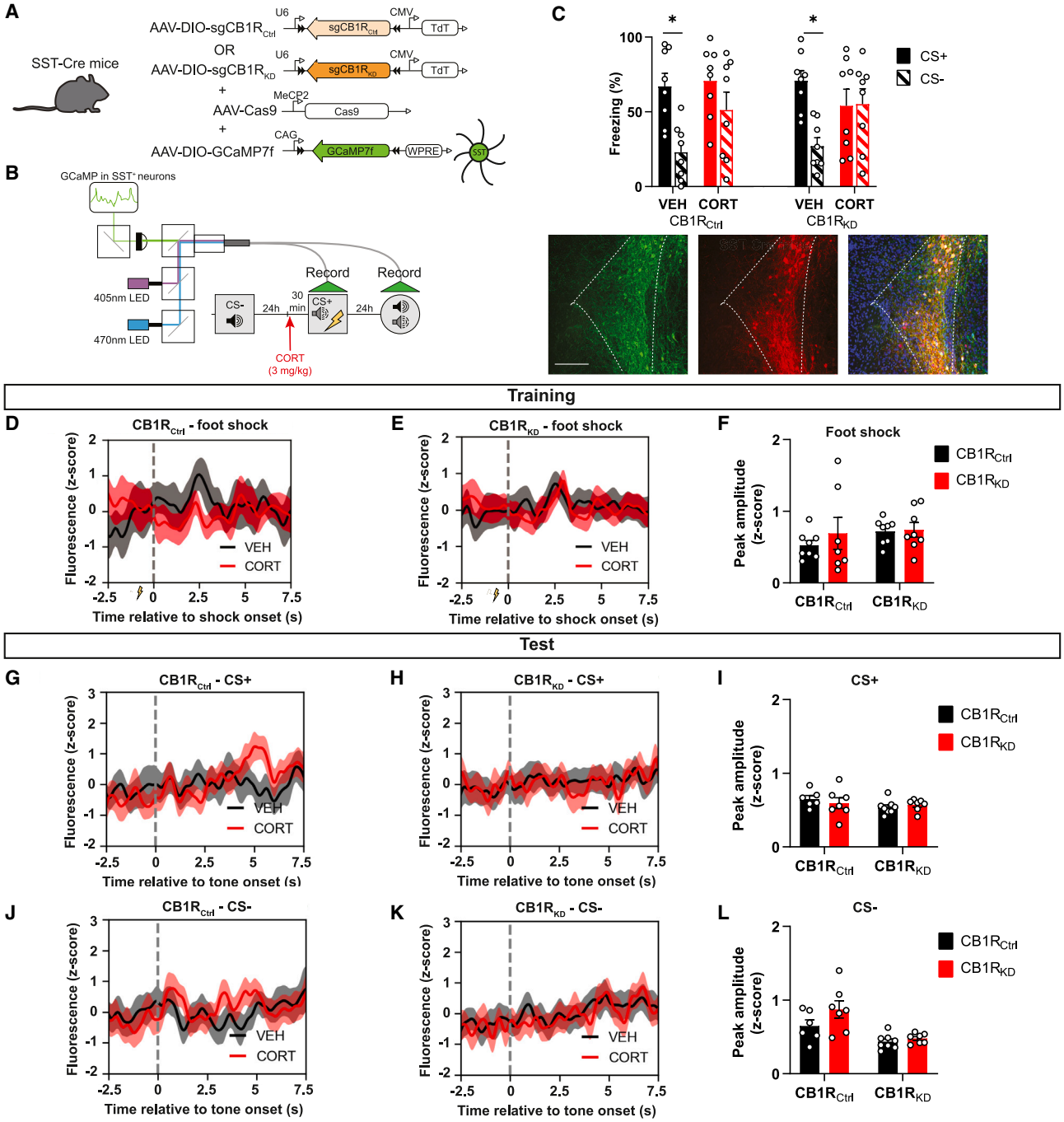

Figure S7. No effect of knocking down CB1 receptors in LA SST+ neurons on CORT-induced threat memory generalization, related to Figure 6

(A) Expression of AAV-DIO-sgCB1RCtrl or AAV-DIO-sgCB1RKD together with DIO GCaMP7f in LA SST+ neurons.

(B and C) CORT mice expressing either the knockdown (sgCB1RKD) or control (sgCB1RCtrl) construct showed threat memory generalization (CORT × KD × Tone interaction: $F(1,28) = 0.52$, $p > 0.05$). Scale bar, 200 μm.

(D–F) (D and E) Neither CORT, nor CB1R knock down in SST+ LA neurons affected the SST-GCaMP7f signal following foot shock during training, and (F) peak amplitude after shock was similar between groups (CORT × KD interaction: $F[1,27] = 0.35$, $p > 0.05$).

(G–L) CORT and CB1R knockdown also did not affect the SST-GCaMP7f signal from SST+ LA neurons following CS+ exposure (CORT × KD interaction: $F[1,24] = 0.81$, $p > 0.05$) (G–I) or following CS− exposure (CORT × KD interaction: $F[1,24] = 1.55$, $p > 0.05$) (J–L).

*$p < 0.05$, **$p < 0.001$. CB1, cannabinoid receptor 1; CORT, corticosterone; SST, somatostatin; VEH, vehicle.